University of Alberta
Printing Department

THE UNIVERSITY OF ALBERTA

DIFFUSIONAL TRANSPORT OF CARBON AND NITROGEN IN IRON UNDER ELECTRIC AND HALL FIELDS

A Thesis

Submitted to the Faculty of Graduate Studies
In Partial Fulfilment of the Requirements
for the Degree of Doctor of Philosophy

DEPARTMENT OF MINING AND METALLURGY

by

Malcolm John Bibby

EDMONTON, ALBERTA

November, 1965

UNIVERSITY OF ALBERTA

FACULTY OF GRADUATE STUDIES

The undersigned certify that they have read and recommend to the Faculty of Graduate Studies for acceptance, a thesis titled

DIFFUSIONAL TRANSPORT OF CARBON AND NITROGEN IN IRON UNDER ELECTRIC AND HALL FIELDS

submitted by MALCOLM JOHN BIBBY

in partial fulfilment of the requirements for the degree of Doctor of Philosophy.

ABSTRACT

The "interstitial mobility" of the solutes nitrogen and carbon in austenite (γ) iron is determined from diffusion experiments carried out under the influence of a direct electric field. Diffusion penetration curves are obtained using microhardness techniques and related to "effective charge" by the Einstein equation. The effective charge of carbon in iron is found to be +8.6 with an estimated error of $\pm$0.9 at 925°C increasing to +13.5 $\pm$1.4 as the temperature is lowered to 842°C. Similarly an "effective charge" of -8.1 $\pm$0.9 is found for nitrogen in (γ) iron at 1000°C increasing to -14.0$\pm$1.5 at atemperature of 922°C. Positive Hall coefficients at 925°C are found for both systems.

The charge of carbon and nitrogen in ferrite (α) iron is determined in a Hall field using ($\gamma \rightleftarrows \alpha$) phase boundary migration techniques. A charge of +4.3 with an estimated error of $\pm$0.9 is found for carbon in α iron. A charge of +5.9 $\pm$1.20 is associated with nitrogen in α iron.

These field charges obtained are discussed in relationship to alloy transport and electronic properties.

ACKNOWLEDGEMENTS

Many thanks to Dr. W.V. Youdelis for his capable direction during the course of the work leading up to this thesis. I consider it very fortunate to have had the opportunity of sharing in his knowledge and guidance during the past two years. I would also like to extend my gratitude to Dr. J. Gordon Parr with whom I was associated during the first months of the project. The congenial association of other staff members Dr. J. Leja, Mr. J.R. Cahoon, M. Sc., and Mr. R.M. Scott is also gratefully acknowledged. The typing assistance of Mrs. F. Klein is very much appreciated. The receipt of a Consolidated Mining and Smelting Company of Canada Scholarship and a Province of Alberta Intersession Bursary together with equipment grants from the Defence Research Board (DRB 9535-16) and the National Research Council (NRC A-836) are gratefully acknowledged.

TABLE OF CONTENTS

LIST OF FIGURES

LIST OF TABLES

INTRODUCTION

When a pure metal or alloy is subjected to an impressed external electric field, in addition to the normal transport of electrons a small but significant transport of all atomic components present also occurs. For example, in a nickel bar subjected to a field at a temperature near its melting point nickel ion cores migrate toward the anode.[1] Copper ions in a copper bar subjected to a field will migrate toward the anode below 900°C; however, as the temperature is raised copper migration decreases until finally the migration is reversed and copper moves toward the cathode.[2,3] Interstitial carbon[4] ions migrate toward the cathode in austenite iron-carbon alloys while interstial nitrogen[5] migrates toward the anode. This type of mass transport has been referred to as electrodiffusion, electromigration, or electrotransport. As might be expected electrotransport occurs in liquid metals and at a much faster rate.[6,7] Liquid migration has been used as a method of separating atomic components -- particularly radioactive isotopes.[7] Under carefully controlled conditions electrotransport can be used as a very powerful purification tool and should find use in semiconductor and superconductor metal preparation.

Electrodiffusion has also some very interesting theoretical aspects. The fact that an alloy component migrates in a field indicates that it exists in a charged state. For instance one might conclude that carbon is positively charged in an iron (γ) lattice since it moves toward the cathode. By

the same reasoning nitrogen might be thought of as carrying a negative charge. Hence, this type of work can be used as an experimental method for determining the nature of the solute-solvent bond. Such information might well be very useful in the development of high temperature, high strength ferrous alloys.

There have been many attempts to relate the observed migration with the charge state of the solute component. A recent and very comprehensive review of the subject has been published by Verhoeven.[8] In general the velocity of the diffusing ion may be related to the "fundamental charge" of the diffusing component by the Einstein Equation[9]

$$U_i = \frac{D_i}{kT} \tag{1}$$

where U_i and D_i are respectively the mobility (velocity per unit force) and the diffusion constant of the migrating ion; k is Boltzman's constant and T is the absolute temperature. An expression for the velocity of diffusing ions may be obtained by substituting $\frac{V_i}{F_i}$ for U_i where F_i is the force on the ion, thus

$$V_i = \frac{D_i}{kT} F_i \tag{2}$$

Frenkel[10] derived this same relationship from kinetic relationships and it holds for all small driving forces regardless of the nature of the force. For a long time F_i was considered to originate from the action of the field on ion cores. It is found, however, that the charge is often far in excess of

that attributable to the ionic state of the atom alone. For instance a charge of +13.4 is obtained from the Einstein equation for iron in carbon at 950°C.[11] The electrotransport of several pure metals have been investigated. In many cases transport is anode directed, e.g. in Al, Ag, Cd and Zn.[12] Using the above model, pure metal components can only be positively charged and the force, and hence migration, cathode directed. Even though the positive ion cores are screened from the external field to some extent by the free electrons, on the basis of this simple model the charge exhibited by a pure metal component at most could only be reduced to 0 but could never be negative. These facts indicate that there must be other forces superimposed on the field force, and their resolved sum total must be larger than the field force.

It is now generally accepted that the charge obtained in direct field electrotransport experiments is an effective charge and contains a positive or negative contribution from "electron" and "hole" carrier momentum transfer. There have been several theories developed in recent years taking account of the carrier lattice interaction. One of the most recent of these theories, which takes into account electron momentum transfer, is that of Fiks,[13] and has been extended by Glinchuck[14] to take account of "hole" momentum transfer. The general expression for the resultant force on a diffusing ion is as follows:

$$F_i = eE \{z - n_e l_e \sigma_e + n_h l_h \sigma_h\} \qquad (3)$$

where n, σ and l are respectively the charge carrier concentration, scattering cross-section, and mean free path. The subscripts e and h refer to electrons and holes respectively. It is difficult to calculate the true charge z of migrating solute ions in the absence of scattering cross-section data. However, by using a two band model for iron and data obtained from the conductivity dependence on temperature and concentration, Frantsevich[15] calculated a charge of +3.7 for carbon in α iron. The weakness in the method of Frantsevich is that it requires approximations and data from numerous independent experiments. Such data do not usually contain sufficient accuracy to calculate a meaningful charge.

The experimental verification of Fiks' theory has met with some diffiuclty. Brown and Barnett[16] show that even in conductors with a positive Hall coefficient, momentum is anode directed, contrary to that expected on the basis of Equation (3). Following the publication of Brown and Barnett there has been considerable discussion concerning the direction of momentum transfer.[17] Verhoeven[8] suggested that holes could interact preferentially with activated ions (those ions with sufficient energy to take part in the diffusion jump process) to cause cathode directed migration while still maintaining an overall anode directed momentum transfer. Fiks[13] has shown from a consideration of the Fermi surface that momentum may be cathode directed in "p" conducting materials. Thus, there is considerable doubt surrounding the scattering

mechanisms of hole carriers in metals. Also there is difficulty in accounting for the large positive effective charge for carbon and the large negative effective charge for nitrogen[5]. Both charges are larger than can be accounted for by field forces arising from the charges of the ion cores. Therefore, it may be reasoned that carriers exert a large cathode directed momentum transfer on carbon ions but a large anode directed momentum transfer on nitrogen ions. Since it is unlikely that the substitution of carbon by nitrogen will change the sign of the Hall coefficient in iron, it is difficult to reconcile the present ideas of momentum transfer.

Part of the present investigation is devoted to a comparison of carbon and nitrogen mobilities obtained for (austenite) iron with measured Hall coefficients. The direct field mobilities are obtained from microharndess measurements made across a diffusion weld zone, while Hall field measurements were made using a standard D.C. probe technique.

Mobility investigations of this type connect two phenomena, diffusion and electrical conductivity. Up until recently the mechanism of each was considered independently because diffusion involves essentially interaction between atoms while conductivity involves carrier interaction with the lattice. Effective mobility on the other hand involves the mechanisms of diffusion and electrical transport, and therefore is a measure of the interaction of carriers with

atomic components.

To separate the field force on the transported ion from the force due to carrier interaction Yu Miller[30] proposed Hall field electromigration investigations. The Hall field mobility measurements have the advantage that there is no charge carrier momentum transfer in the direction of the Hall field. Therefore, mass transfer in the Hall direction should indicate the true charge of the migrating ion. An inherent difficulty with these experiments is that the Hall field generated in metals is relatively small and very sensitive methods for detecting the associated mass transfer are needed. In this investigation a method based on the migration of a phase boundary subjected to a Hall field is introduced and the Hall field mobility of carbon and nitrogen in ferrite so determined are presented. The charge of the migrating ion is then obtained by way of the Einstein equation.

THEORY OF ELECTROTRANSPORT

A. DIRECT FIELD ELECTROTRANSPORT

There have been numerous attempts in recent years to explain the phenomenon of electrotransport. Essentially there are two approaches: those theories based on a thermodynamic model, and those based on a kinetic atomic model. For a comprehensive review of these theories the reader is referred to the paper by Verhoeven.[8] One of the recent of these theories, and the one most in accord with solid state transport is that of Fiks.[13] Many previous theoretical attempts did not consider the interaction of electrons with the lattice, or this interaction was introduced formally as a friction coefficient. An electron/ion friction coefficient is a macroscopic approach leaving much of the detail of the mechanism and physics of the problem yet to be explained. Rather than introduce yet another parameter to explain discrepant results, Fiks considered the actual ion scattering mechanism within the framework of the electron theory of metals. The following is largely a straightforward presentation of Fik's theory.

1. Phenomenological Description of a Moving Ion

When an electric field is impressed on a metal, the charged ion cores are accelerated by the field. The acceleration does not continue indefinitely because of the frictional drag forces resisting motion of the ion. Thus the ion reaches a steady state velocity when the accelerating force becomes equal to the drag force. Usually the

characteristic parameter describing this motion is a mobility and may be defined as

$$U_i = \frac{V_i}{F_i} , \qquad (4)$$

where U_i is mobility, V_i and F_i are respectively velocity and force. If the only accelerating force is that due to the electric field then

$$U_i = \frac{V_i}{q_i e E} ,$$

where q_i is degree of ionicity of the atomic component, e and E are respectively the fundamental unit of charge and electric field.

In general the field force is not the only force acting on the ion. Defect lattice points and vibrating atomic components act as scattering centers for electron and hole carriers and in turn receive momentum.

2. Theoretical Treatment of Ion Scattering

Consider an electron moving with a velocity v and momentum p. As a result of a collision with a scattering center it undergoes a momentum change to p' with a component along the field direction p_x'. Let the probability of an electron being scattered into the momentum interval dp' be $W_i\, dp'$ per unit of volume in real space as a result of scattering centers of the i^{th} type. Considering only one atom of the i^{th} type, the scattering probability is $\frac{1}{n_i} W_i\, dp'$. The momentum change in the field direction as a result of the scattering process is $(p_x' - p_x)$. Therefore, the total

momentum transferred by electrons in the momentum interval dp is equal to the number of electrons in this momentum interval multiplied by the momentum change, i.e.,

$$\frac{2}{h^3} \, f dp \, \frac{1}{n_i} \, W_i \, (p_x - p_x') \, dp \quad ,$$

where the number of electrons in the momentum interval dp is $\frac{2}{h^3} fdp$, and f is the Fermi distribution function. The total momentum transferred in one second is equal to the force exerted on the ion, thus

$$F_{ei} = \frac{2}{h^3} \int_p \int_{p'} \frac{1}{n} \, f(p_x - p_x) \, w_i \, dpdp \, .$$

Rearranging terms

$$F_{ei} = \frac{2}{h^3} \int_p f p_x \, dp \, \frac{1}{n_i} \int_{p'} \left(1 - \frac{p_x'}{p_x}\right) w_i dp \, . \qquad (5)$$

Mott[19] has shown that

$$\frac{1}{\tau} = \int_p \left(1 - \frac{p_x'}{p_x}\right) w_i \, dp \quad , \qquad (6)$$

where τ is the mean free time between collisions. τ can also be expressed in terms of mean free path and electron velocity, viz.,

$$\tau_i = \frac{L_i}{v} = \frac{1}{n_i \sigma_i v} \quad , \qquad (7)$$

where L_i, n_i, σ_i are respectively the mean free path, electron density, and scattering cross section. Thus equation 5 reduces to

$$F_{ei} = \frac{2}{h^3} \int_p f p_x \tau_i v dp \, . \qquad (8)$$

From electron theory

$$\frac{2}{h^3} \, dp = \frac{8\pi m^3 \, v dE}{h^3} \qquad (9)$$

where m, v, and E are respectively electron mass, velocity, and energy. The presence of a field can be treated by a Fermi distribution perturbation. That is the distribution of electrons in the field can be considered the no-field distribution plus a perturbation function. Thus,

$$f = f_o + f_1 \quad . \tag{10}$$

The perturbation function may be determined from the Boltzman transport equation

$$f_1 = \frac{L}{v} v_x \left\{ \frac{\partial f_o}{\partial \mathcal{E}} eE + \frac{\partial f_o}{\partial x} \right\} \quad . \tag{11}$$

In general for a homogeneous conductor there is no change in electron density distribution along its length, i.e.,

$$\frac{\partial f_o}{\partial x} = 0$$

Substituting equation 11 into equation 8 gives

$$F_{ei} = - \frac{8\pi m^3 eE}{3h^3} \int_o^\infty L \tau_i v^3 \frac{\partial f_o}{\partial \mathcal{E}} \, d\mathcal{E} \quad . \tag{12}$$

For a degenerate system

$$\int_o^\infty \frac{\partial f_o}{\partial \mathcal{E}} \, d\mathcal{E} = -1 \quad .$$

Therefore

$$\int_o^\infty L \tau_i v^3 \frac{\partial f_o}{\partial \mathcal{E}} \, d\mathcal{E} = -L(\bar{v}) \tau_i(\bar{v}) \bar{v}^3 \quad , \tag{13}$$

and when substituted into equation 12 gives

$$F_{ei} = \frac{8\pi m^3 v^3}{3h^3} eE \, L(\bar{v}) \tau_i(\bar{v}) \tag{14}$$

$$= n_e eE \, L(v) \tau_i(\bar{v})$$

3. Total Force on a Lattice Ion

If we assume with Fiks that the only carriers in the metal are electrons, then the momentum transfer force is $F_{ei} = n_e e E l_e \sigma_i$. To this force must be added the field force q_i eE, so that the total force on the ion is

$$F_i = eE \{q_i - n_e l_e \sigma_i\} . \qquad (15)$$

This equation is completely general and applies to all charged ions in the lattice.

We may now consider three types of lattice ions i.e. normal lattice ions, activated lattice ions, and impurity lattice ions. Normal lattice ions are ions oscillating about their mean position but held in the lattice by neighbouring bonds. Activated ions, on the other hand, are ions with sufficient vibrational energy to execute a jump process. Impurity ions are defect centers in the lattice.

To find the resultant force on normal lattice ions it is necessary to introduce the idea of dissociation. Electrical neutrality requires that the number of atoms (n_a) in the metal multiplied by the average degree of dissociation ($\bar{q}$) be equal to the number of free electrons, thus

$$\sum_k q_k n_k = \bar{q} n_a = n_e , \qquad (16)$$

$$\bar{q} = \frac{n_e}{n_a} . \qquad (17)$$

Substitution into equation 15 of $\bar{q}$ for q_i, σ_a for σ_i, and $l_e = \frac{1}{n_a \bar{\sigma}_a}$ for the mean free path of electrons, gives for the force on normal lattice ions

$$F_n = eE \left\{ \bar{q} - \frac{n_e \bar{\sigma}_a}{n_a \sigma_a} \right\} = 0. \qquad (18)$$

That is, the resultant force on normal lattice ions is zero and the metal as a whole is in mechanical equilibrium.

Although the resultant force on normal lattice ions is zero this is not necessarily true of activated ions. First of all the charge on an activated ion might be quite different from a normal ion since the electron cloud configuration is different for an ion in the activated state. Secondly, the scattering cross section of an activated ion will be different from the scattering cross section of normal ions. If we designate q_i^* as the charge of an activated ion and σ_i^* as the average scattering cross section of an activated ion, equation 15 becomes

$$F_i^* = eE \left\{ q_i^* - n_e l_e \sigma_i^* \right\}. \qquad (19)$$

Substituting $l_e = \frac{1}{n_i \sigma_i}$ into equation 19 gives

$$F_i^* = eE \frac{1}{\sigma_i} \left\{ q_i^* \sigma_i - q_i \sigma_i^* \right\}. \qquad (20)$$

The direction of force and hence movement of an activated ion is then determined by the magnitude and sign of the quantity

$$(q_i^* \sigma_i - q \sigma_i^*) .$$

Fiks further shows that there is a resultant force on impurity ions in the lattice even though they may not be activated. Equation 15 describes this force. However, Fiks has expressed this force in terms of residual lattice resistivity. According to Matthiessen's rule[19]

$$p(T) = p_o + p_i^{(T)}, \qquad (21)$$

where p_o is the residual resistivity due to static

imperfections in the lattice and $p_i(T)$ is the scattering of electrons by lattice phonons. According to Mott[19] the change in residual resistance with increasing impurity centers is given by

$$p_o{}^i = \frac{mv}{e^2} \; c_i \sigma_i \quad , \tag{22}$$

where c_i is the concentration of impurity ion. The specific resistance of a metal may be expressed as

$$p = \frac{m\bar{v}}{e^2 n l} \quad . \tag{23}$$

On substituting equations 22 and 23 into equation 15

$$\sigma_i n_e l_e = \frac{1}{c_i} \; \Delta \frac{p_o}{p}{}^i$$

and

$$F_i = eE \left(q - \frac{1}{c_i} \Delta \frac{p_o}{p}{}^i \right) \tag{24}$$

Thus the resultant force on an impurity ion is in part determined by the residual resistivity of the impurity ion and the resistance of the metal. It should be emphasized that even though the force on impurity ions is different than zero, these ions will not migrate unless they are activated. In general the force exerted on an activated impurity ion is of the form given by equation 15,

$$F_i{}^* = eE \left(q_i{}^* - n_e l_e \sigma_i{}^* \right), \tag{25}$$

where * values refer to activated impurity ions.

4. Activated Ion Migration

According to the ideas of kinetic theory a migration act is possible only when the ion possess sufficient kinetic energy, as a result of thermal fluctuations, to jump into either a neighboring lattice point or an interstitial position.

If Z_o is the number of jumps per second, then according to Frenkel[10]

$$Z_o = \nu \exp - \frac{U_a}{kT} = \frac{1}{\tau} , \tag{26}$$

where τ is the settled lifetime of an ion, ν is the frequency of oscillation in its potential well, and U_a the activation energy for the transition process. The diffusivity and jump frequency are related by

$$D = \frac{a^2}{6\tau} = \frac{a^2 Z_o}{6} , \tag{27}$$

where the factor 6 in the denominator accounts for jump in one direction and a is the jump distance. If an external field is placed on migrating ions, migration acts in the field direction Z_f are biased according to the relationship

$$Z_f = \frac{Z_o}{6} \exp + \frac{aF_i^*}{2kT}, \tag{28}$$

and the number of migration acts in the reverse direction Z_b is

$$Z_b = \frac{Z_o}{6} \exp - \frac{aF_i^*}{2kT} . \tag{29}$$

The velocity of the ion may be expressed as

$$V_i^* = a(Z_f - Z_b) .$$

Expanding the exponential terms in a series and neglecting second and higher order terms (valid only if $aF << kT$) gives

$$V_i^* = \frac{Z_o \, a^2 F_i^*}{6kT} = \frac{D_i}{kT} F_i^* .$$

Substituting equation 25 for F_i^* gives

$$V_i^* = \frac{D_i}{kT} eE \left\{ q_i^* - n_e l_e \sigma_i^* \right\} \tag{30}$$

The quantity inside the brackets is commonly called effective charge and can be calculated knowing the velocity of

activated impurity ions. It is interesting to note that this theory predicts that the effective charge is independent of field.

5. Hole Contribution to Ion Migration

Fiks[13] considered only electron/ion momentum transferred by electron carriers. Glinchuck,[14] in another publication stated that the energy of an electron moving on a periodic potential may be considered

$$E = \frac{p^2}{2\mu} \quad , \tag{31}$$

where p is the momentum and μ is the effective mass of the electron. The effective mass of electrons can either be positive or negative. Thus electron/ion collision momentum can be either anode or cathode directed depending on the sign of the electron mass. Alternatively "defect electrons" i.e. electrons with a quantum mechanical negative effective mass may be considered as positively charged particles with a positive effective mass (generally referred to as "holes"). The justification for this has been shown by Seitz.[21]

This introduces yet another force acting on lattice ions. By the same reasoning as used by Fiks for electrons, an additional force $F^{11} = n_h l_h \sigma_h eE$ is added to the ions, where l_h, n_h and σ_h are respectively mean free path, concentration and scattering cross section for holes. Modifying equation (15) to take account of the hole contribution gives for the total force acting on an ion in a conductor

$$F_i = eE \{q_i - n_e l_e \sigma_e + n_h l_h \sigma_h\} . \tag{33}$$

Accordingly, equation 30 should be modified as follows:

$$V_i^* = \frac{D}{kT} eE \left\{ q_i^* - n_e l_e \sigma_e^* + n_h l_h \sigma_h^* \right\}, \quad (34)$$

and equation 20 should read

$$F_i^* = eE \left\{ q_i^* - \frac{n_e}{n_a} \frac{\sigma_e^*}{\sigma_e} + \frac{n_h}{n_a} \frac{\sigma_h^*}{\sigma_h} \right\}. \quad (35)$$

Fiks[18] has shown that the periodic potential of the lattice very significantly affects the magnitude of the transfer. Electrons or holes either closely bound to the lattice or relatively free of the lattice do not impart momentum to the lattice. However, in the case of intermediate interaction the momentum transfer mechanism becomes significant, with momentum being transferred either toward the anode or cathode depending upon the curvature of the Fermi surface.

B. OTHER THEORIES

One of the earliest published investigations in electrotransport was that of Skaupy.[22] He proposed that impurity ions might well have a different "effective charge" than the solvent ions and hence experience a different field force. In addition, Skaupy introduced the idea of electron/ion friction and that the friction force is equal to the field force - a consequence of mechanical equilibrium. Impurity ions that increase the electrical conductivity experience a larger frictional force than the solvent ion and "vice versa". This general rule is basically in agreement with experiments on the motion of ions in mercury.[23]

Schwarz[25] recognized that beside the field force there was an additional superimposed force felt by the ions, introduced through a hydrostatic force caused by the electric field. Klemm[26,27] in 1953, returned essentially to the idea of mutual friction forces introduced by Skaupy. Various friction coefficients are introduced to account for the electron/ion interaction force. The force equation from the theory of Klemm is very similar to that of Fiks, viz,

$$F_i = eE\ K \left\{ Z_i^* - \bar{Z} \frac{r_i^*}{r_i} \right\},$$

where r_i and r_i^* are the electron/ion friction coefficients for the normal and activated ions, $\bar{Z}$ and Z_i^* are the average ion valence and activated ion valence respectively and K is a constant. Klemm's treatment is based on generalized transport phenomena within the framework of irreversible thermodynamics. Mangelsdorf,[28] starting from the assumption that the frictional force is proportional to the electron flux, developed the following relationship for the force on an ion in the lattice

$$F = eE \left\{ Z_i - \bar{Z} \frac{\delta_i}{\bar{\delta}} \right\},$$

where δ_i and $\bar{\delta}$ are the momentum transfer coefficients between the electrons and ions. If δ_i and $\bar{\delta}$ are identified with the scattering cross section in equation 35 the theory of Mangelsdorf is consistent with the theory of Fiks. Both the theory of Mangelsdorf and of Klemm, however, are based on the introduction of macroscopic friction coefficients

without any examination of the origin of these coefficients. In this regard Fik's theory of ion scattering is more fundamental.

The above theories along with several other similar theoretical attempts in the last decade are considered in detail in the review article by Verhoeven.[8]

C. SUPERIMPOSED CHEMICAL AND ELECTRIC FIELD DIFFUSION

There are several methods of determining the velocity and hence effective charge of impurity ions. One of these methods involves superimposing field motion and chemical diffusion. Experimentally the sample comprises two effectively semi-infinite diffusion couples arranged in a sandwich fashion. These couples are then subjected to a field at a predetermined annealing temperature. The mass flow into one diffusion couple half is a result of both chemical diffusion and electric field flow, while the mass flow into the other couple half constitutes the chemical diffusion flow minus the direct field flow. Thus one-half the total mass flow into both diffusion couples is due to chemical diffusion flow and one-half the difference between the two flows is due to electrotransport. This type of experiment has a two-fold purpose. The chemical flow can be used to determine the diffusion constant while the electric field flow is used to determine the velocity and hence charge of diffusing impurity ions.

This method, however, requires considerable chemichal analysis and is very difficult since diffusion takes place over very small distances. The following theory provides another method of determining ion velocity without the need of detailed couple analysis.

The motion of an ion moving in an electric field superimposed on a chemical diffusion field is described to a good approximation by the linear partial differential equation[29]

$$\frac{\partial c}{\partial t} = D \frac{\partial^2 c}{\partial x^2} - v \frac{\partial c}{\partial x} \qquad (36)$$

where c, t, x and v are concentration, time, distance and ion velocity due to the electric field and D is the inter-diffusion constant. This assumes that both v and D are independent of concentration. The solution of this equation for the boundary conditions corresponding to a semi-infinite diffusion couple is given by

$$c = \frac{c_o}{2}\left(1 - \text{erf}\ \frac{x-vt}{2\sqrt{Dt}}\right), \qquad (37)$$

where the couple comprises two sections one section pure solvent and the other section containing impurity ion of concentration c_o. This solution has some interesting features. For instance, consider the motion of a plane of constant composition in the diffusion zone. To find an expression for the velocity of the plane it is necessary to consider the exact differential equation

$$dc = \left(\frac{\partial c}{\partial x}\right)_t dx + \left(\frac{\partial c}{\partial t}\right)_x dt.$$

For dc = 0 (plane of invarient composition)

$$\frac{dx}{dt} = \frac{\left(\frac{\partial c}{\partial t}\right)_x}{\left(\frac{\partial c}{\partial x}\right)_t} . \qquad (38)$$

But $$\left(\frac{\partial c}{\partial x}\right)_t = \frac{c_o}{2} \frac{2}{\sqrt{\pi}} \left\{\exp -\left(\frac{x-v t}{2\sqrt{Dt}}\right)^2\right\} \frac{1}{2\sqrt{Dt}}, \tag{39}$$

and $$\left(\frac{\partial c}{\partial t}\right)_x = \frac{c_o}{2} \frac{2}{\sqrt{\pi}} \left\{\exp-\left(\frac{x-vt}{2\sqrt{Dt}}\right)^2\right\} \left\{\frac{x}{2\sqrt{D}} (-1/2) \frac{1}{t^{3/2}} - \left(\frac{1}{2} \frac{x}{2D} \frac{1}{t^{1/2}}\right)\right\}. \tag{40}$$

Substituting 39 and 40 into 38 gives

$$\frac{dx}{dt} = \frac{x}{2t} + \frac{v}{2}, \tag{41}$$

which is a linear differential equation whose solution is

$$x]_c = k^1\sqrt{Dt} + vt. \tag{42}$$

Physically this implies that the chemical potential gradient and field electric forces operate independently and are additive. This non-interaction of forces permits the calculation of the effective charge from diffusion data. For example, consider single-phase diffusion couples annealed under field conditions as in Figure 1.

If the ion is being carried along the field direction, then from equation 42

$$x_2 = k^1\sqrt{Dt} + vt \tag{43}$$

$$x_1 = k^1\sqrt{Dt} - vt \tag{44}$$

subtracting 43 from 44 gives the velocity of the diffusing ion. Thus

$$\frac{x_1 - x_2}{2t} = v \tag{45}$$

Equation 45 shows that by measuring the position of planes of equal concentration in the sandwich couples the field velocity of the diffusing ion can be found. Such measurements are possible in heat treated iron-carbon and

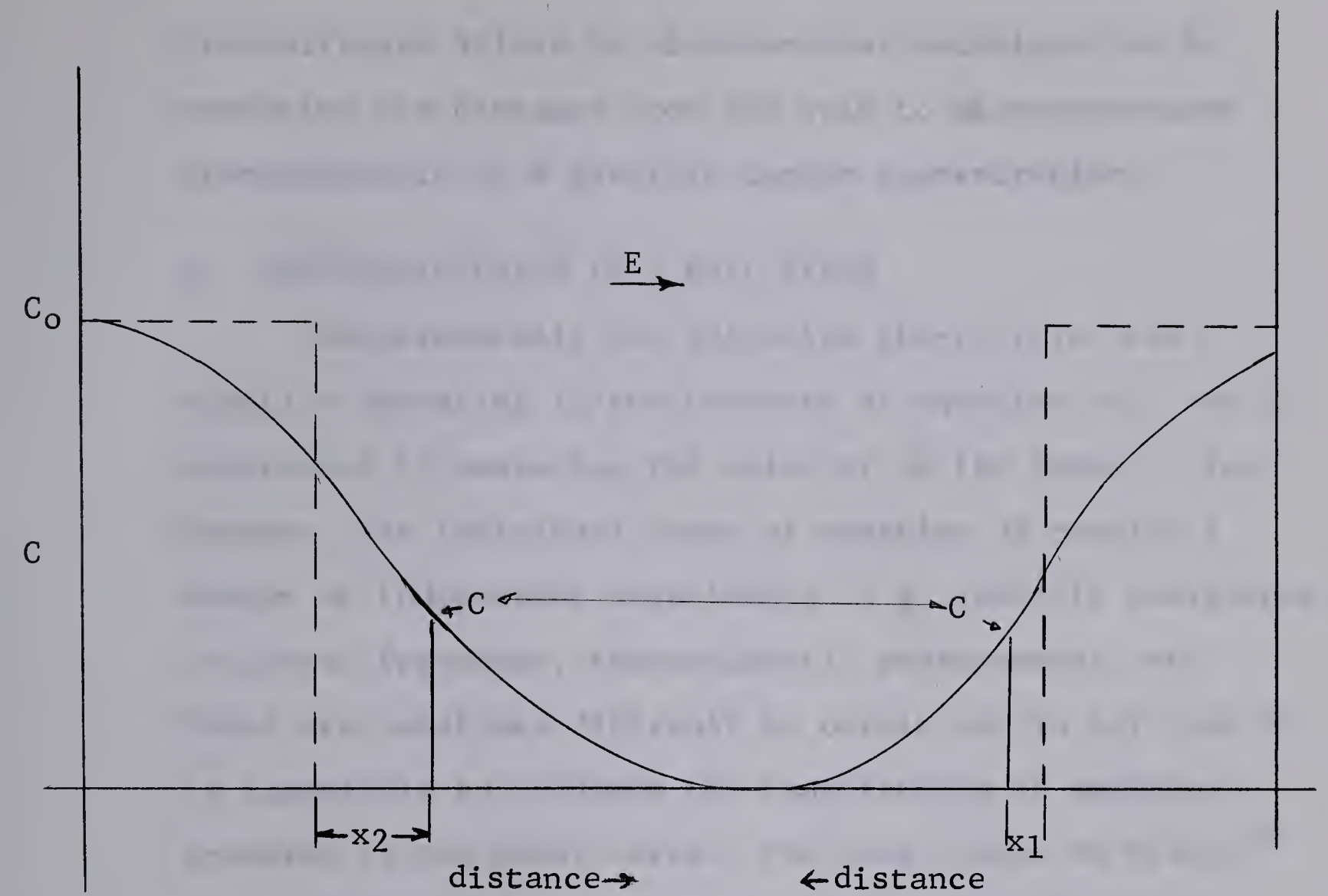

Figure 1. Penetration Profile after Diffusion anneal in an External Force Field.

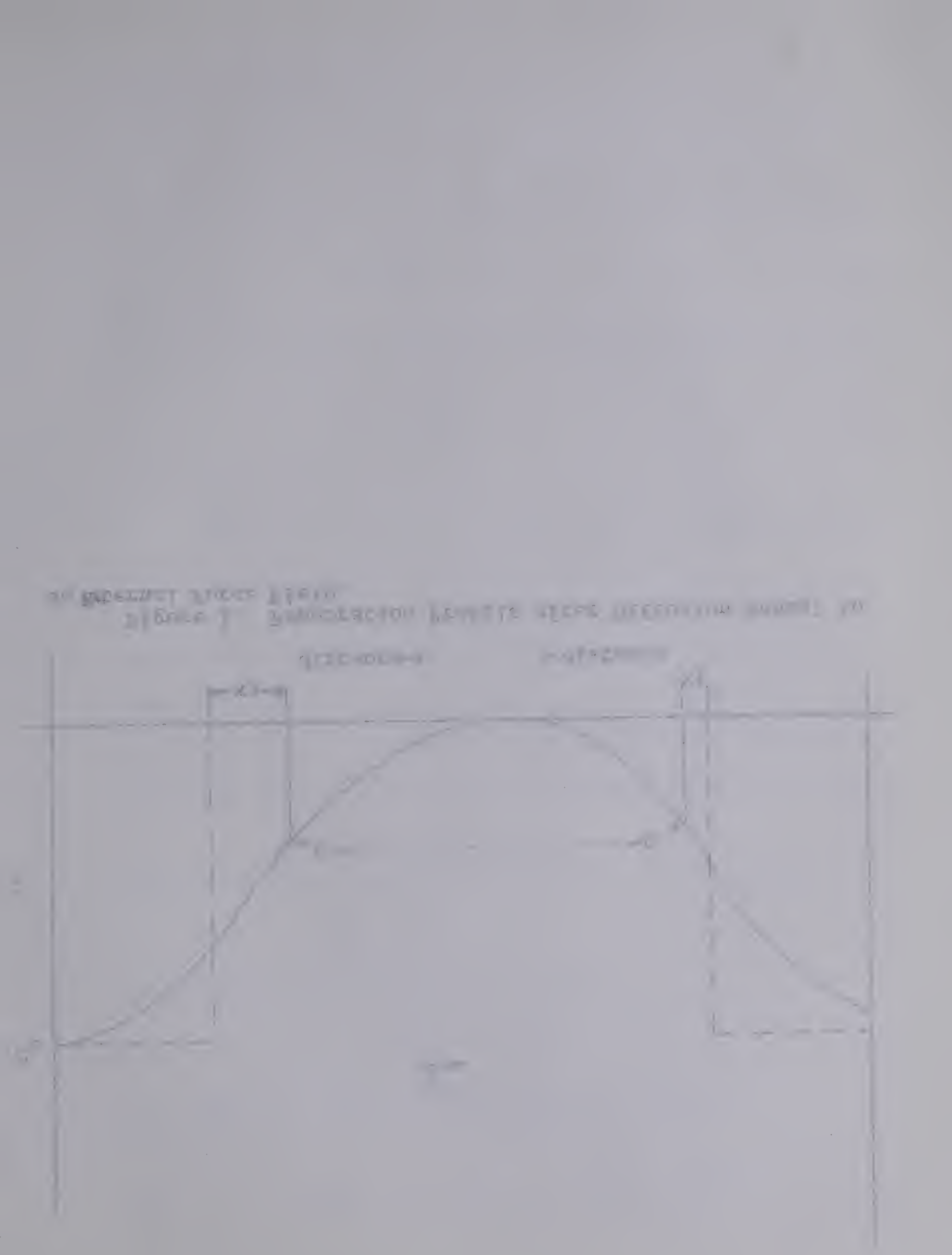

iron-nitrogen alloys by microhardness techniques or by measuring the distance from the weld to microstructures characteristic of a specific carbon concentration.

D. ELECTRODIFFUSION IN A HALL FIELD

Experimentally the effective charge (i.e. the quantity appearing in the brackets of equation 34), can be determined by measuring the velocity of the impurity ion. However, the individual terms of equation 34 require a number of independent experiments, e.g. specific resistance, cyclotron frequency, thermoelectric measurements, etc. These are sometimes difficult to obtain and in any case it is impossible to estimate the contribution of momentum transfer to the total force. For this reason Yu Miller[30] has suggested and carried out migration experiments in Hall fields, where the momentum transfer is perpendicular to the generated Hall field and migration along the Hall field is exclusively a result of the direct field force on the ion. By finding the velocity of the ion in the Hall field the true charge of activated alloy ions can be determined. In the following the Hall field transport equation is derived.

When a magnetic field is applied at right angles to the direction of current flow, an electric field is set up in a direction perpendicular to both the current direction and the magnetic field direction. The physical significance of this is apparent when the current is considered as a

stream of electrons flowing through the solid. Moving electrons as a result of the field will be subjected to a Lorentz force (B x v)e. In free space the electrons would be deflected in a direction perpendicular to B and v. However, the current inside a solid will be constrained within the bounds of the solid. The first few electrons to be deflected will set up a field which will counter-balance the Lorentz force. As a result the current can flow as before and the resulting electric field is given by

$$(B_z \times v_x)e = eE_y$$

where Ey is the Hall field.

A theory for ion migration in the Hall field has been developed by Fiks.[31] The carriers in a conductor are subjected to a Lorentz force in a magnetic field which gives rise to a pressure gradient ∇p, within the conductor collinear with the Hall field. An ion moving in a pressure gradient then feels a force $\nabla p\ v_i$ where v_i is the volume of the ion. The ion will also be acted on by the Hall field giving rise to a force $Z_i eE_y$. Since the current generated in this direction is negligible, the contribution of momentum transfer is assumed to be negligible. Thus,

$$F_i = -\nabla p v_i + z_i eE_y. \tag{46}$$

In order to evaluate $-\nabla p v_i$ consider a unit volume of liquid metal subjected to an electric field along the x direction and magnetic field in the z direction. The

force on the element of liquid is given by

$$f_y = - \nabla p + \frac{1}{c} \left[j \times H \right] . \tag{47}$$

If mechanical equilibrium is assumed,

$$- \nabla p = \frac{1}{c} \left[j \times H \right] . \tag{48}$$

Substituting equation 48 into 46 gives

$$F_i = \frac{1}{c} \left[j \times H \right] v_i + Z_i \, eE_y \tag{49}$$

Substituting $j = nev$ and $E_y = \frac{1}{c} \left[v \times H \right]$ into 49 gives

$$F_i = eE_y \left\{ Z_i - nv_i \right\} , \tag{50}$$

The number of electrons is related to the number of ions by $Z_{io} N_{io} = n$ where Z_{io} is the ionization of the solvent ions and n_{io} is the number of solvent ions. Substituting this into equation 50 and noting that $\frac{1}{n_{io}} = v_{io}$ we obtain

$$F_i = eE_y v_i \left\{ \frac{Z_i}{v_i} - \frac{Z_{io}}{v_{io}} \right\} . \tag{51}$$

Therefore the force on a charged ion subjected to electric and magnetic fields is determined by the charges and volumes of impurity and solvent ions. In the case where $v_{io} \gg v_i$, F_i may be approximated to $Z_i eE_y$. Substituting this into the generalized Einstein equation gives an expression relating the velocity of an activated ion in a Hall field with its charge.

The above treatment is also applicable to solids. However, in the case of solids the pressure gradient of electromagnetic origin in the electron gas (j x H) is not as

effective in causing individual ion motion because of the rigidity of the lattice. This fact would further tend to eliminate the significance of the $+v_p v_i$ term and the approximation $F_i = Z_i e E_y$ is even a better one.

Miller and Gurov[32] considered the magnitude of the Lorentz force on the ions as a result of migration in the electric field along the x axis. This force is negligible compared to the field force because of the very small velocity of the moving ions.

E. PHASE BOUNDARY MIGRATION AND ELECTRIC FIELD DIFFUSION

Since Hall fields in metal systems are usually very small ($\sim 10^{-4}$ v/cm. in conductors) very sensitive methods of determining ion movement are necessary. Radioactive tracer techniques are useful for some alloy systems. A method of enhanced phase boundary migration under Hall fields is another possible means of detecting small solute movements. A review of diffusional phase boundary migration in the solid state is given by D.D. Van Horn.[33] The consequences of placing an electric field across a phase boundary under certain limited conditions will be considered here.

Consider a phase diagram in a temperature range which exhibits two single-phase regions separated by a two-phase region, of which the iron-carbon diagram in the temperature range from 738°C to 910°C (Figure 2) is typical.

The penetration curves associated with a diffusion couple in this region are shown in Figure 3a. A phase

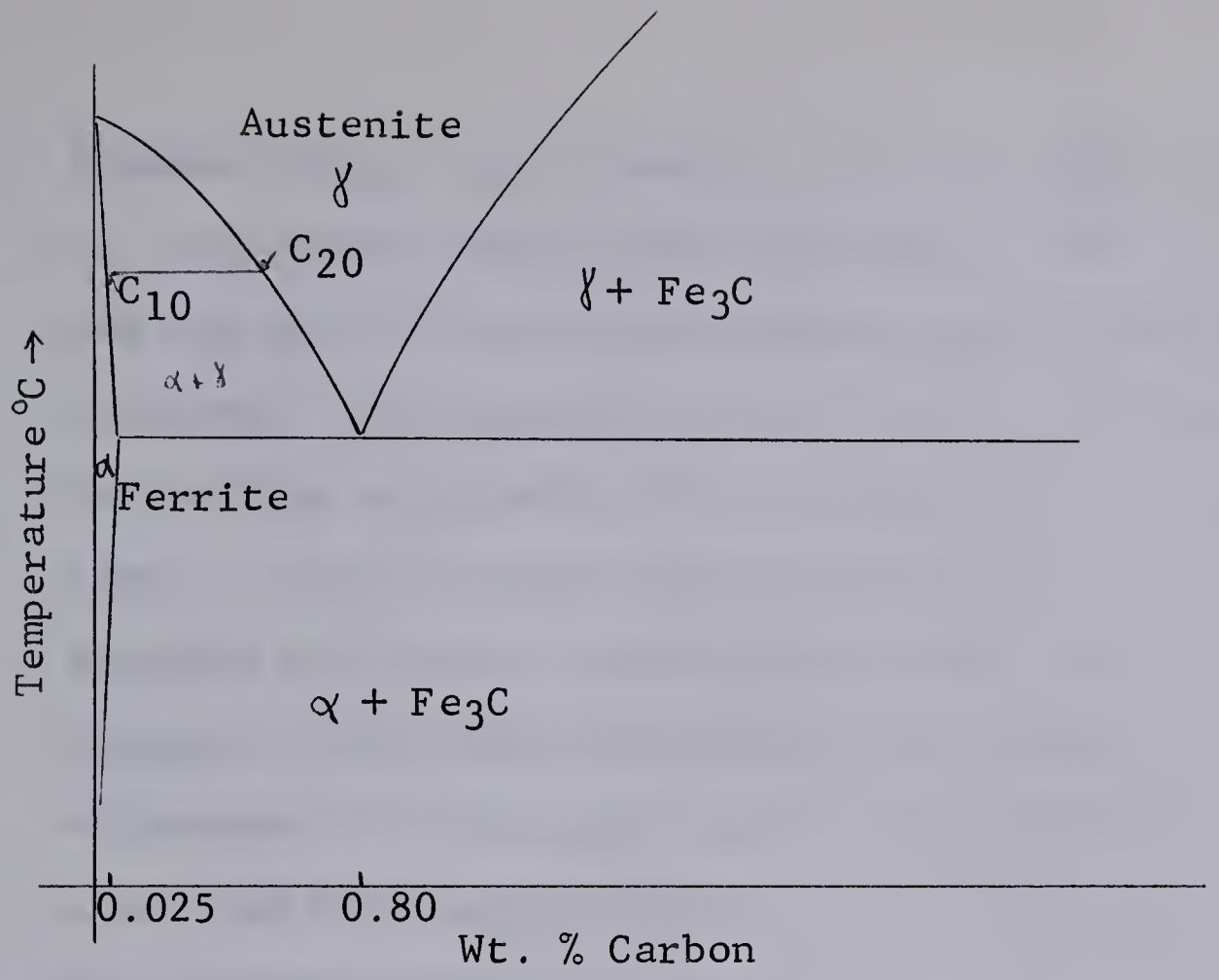

Figure 2. Iron-carbon Phase Diagram showing Austenite (γ) and Ferrite (α) Regions.

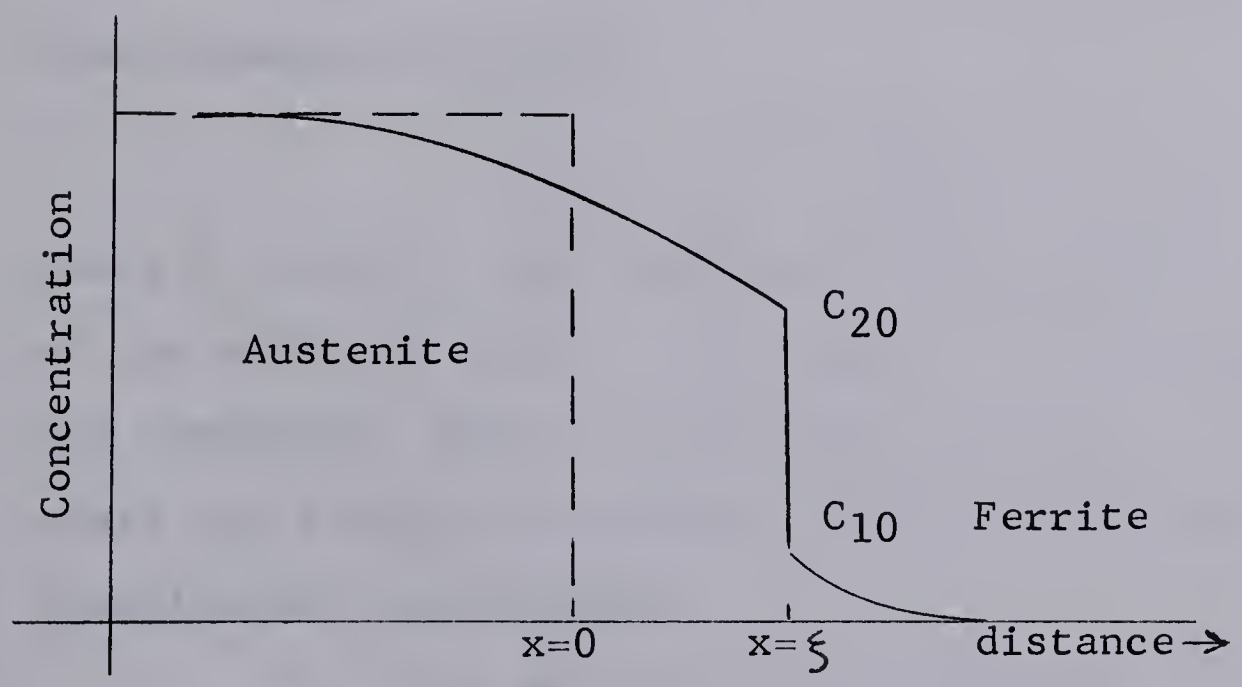

Figure 3(a) Concentration-Penetration Distribution of Diffusion Couple annealed in Two-phase Region.

boundary (C_{20} - C_{10}) separates the two phases (in the case of iron-carbon alloys these two phases are γ and α). C_{20} and C_{10} are the equilibrium phase diagram concentrations as indicated. The migration of the phase boundary is controlled by the flux supplied to the boundary from the high concentration side of the couple and by the flux leaving the boundary on the low concentration side. No two-phase region appears. Most phase boundaries are observed to move as the squareroot of time, and this $\sqrt{t}$ time dependence is taken to mean that the boundary motion is diffusion controlled and not reaction controlled ($\gamma \rightleftarrows \alpha$).

The penetration curves appearing in the single-phase regions under this condition are considered to constitute part of a semi-infinite diffusion penetration profile. These two parts are matched at the phase boundary by a mass flow balance as follows:

$$- D_\gamma \frac{\partial c_\gamma}{\partial x}\Big|_{x=\xi} + D_\alpha \frac{\partial c_\alpha}{\partial x}\Big|_{x=\xi} = \delta \frac{\partial \xi}{\partial t} , \qquad (52)$$

where D_γ and D_α are respectively the diffusion constants of the solute in phase γ and phase α . The following boundary conditions define the diffusion system: $\delta = C_{20} - C_{10}$, where C_{20} and C_{10} are respectively the austenite and ferrite equilibrium concentrations.

$C_\alpha = C_{10}$ at $x = \xi$, $C_\gamma = C_{20}$ at $x = \xi$,

$C_\alpha = 0$ at $x = \infty$, and $C_\gamma = C$ at the high solute end of the diffusion couple. Appendix G contains the phenomenological diffusion theory for these conditions

developed by Von Horn.[53]

Consider the case wherein the diffusion couple is not semi-infinite but is terminated at a finite distance. After annealing for a sufficiently long time (at say 750°C as in Figure 2) the diffusion gradients appearing in the single-phase region disappear and the concentration profile of Figure 3(b) results. This is a consequence of the fact that the system is in chemical equilibrium. The result is a diffusion couple with one homogeneous section at C_{20} and the other homogeneous section at C_{10}, separated by a phase boundary. This method has been employed successfully by Kirkaldy and Purdy[34] to design diffusion couples in the iron-carbon system and has the advantage that there is no weld. The presence of a weld and weld oxides can cause serious error in diffusion experiments.

If an electric field (direct or Hall) is placed across the couple, it will cause a movement of impurity ions in both phases and result in a boundary movement. Impurity ion velocity in phase 2 will cause a flux of ion $J_\gamma = C_{20} V_\gamma$ and in phase 1, $J_\alpha = C_{10} V_\alpha$. The difference in these fluxes multiplied by time represents the area swept out on a concentration-distance plot as shown in Figure 3(c). Applying a mass balance at the boundary,

$$J_\gamma t - J_\alpha t = (C_{20} - C_{10}) x,$$

and

$$C_{20} V_\gamma t - C_\alpha V_\alpha t = (C_{20} - C_{10}) x.$$

But

$$\frac{v_\gamma}{D_\gamma} = \frac{q_\gamma eE}{kT} \quad \text{and} \quad \frac{v_\alpha}{D_\alpha} = \frac{q_\alpha eE}{kT}.$$

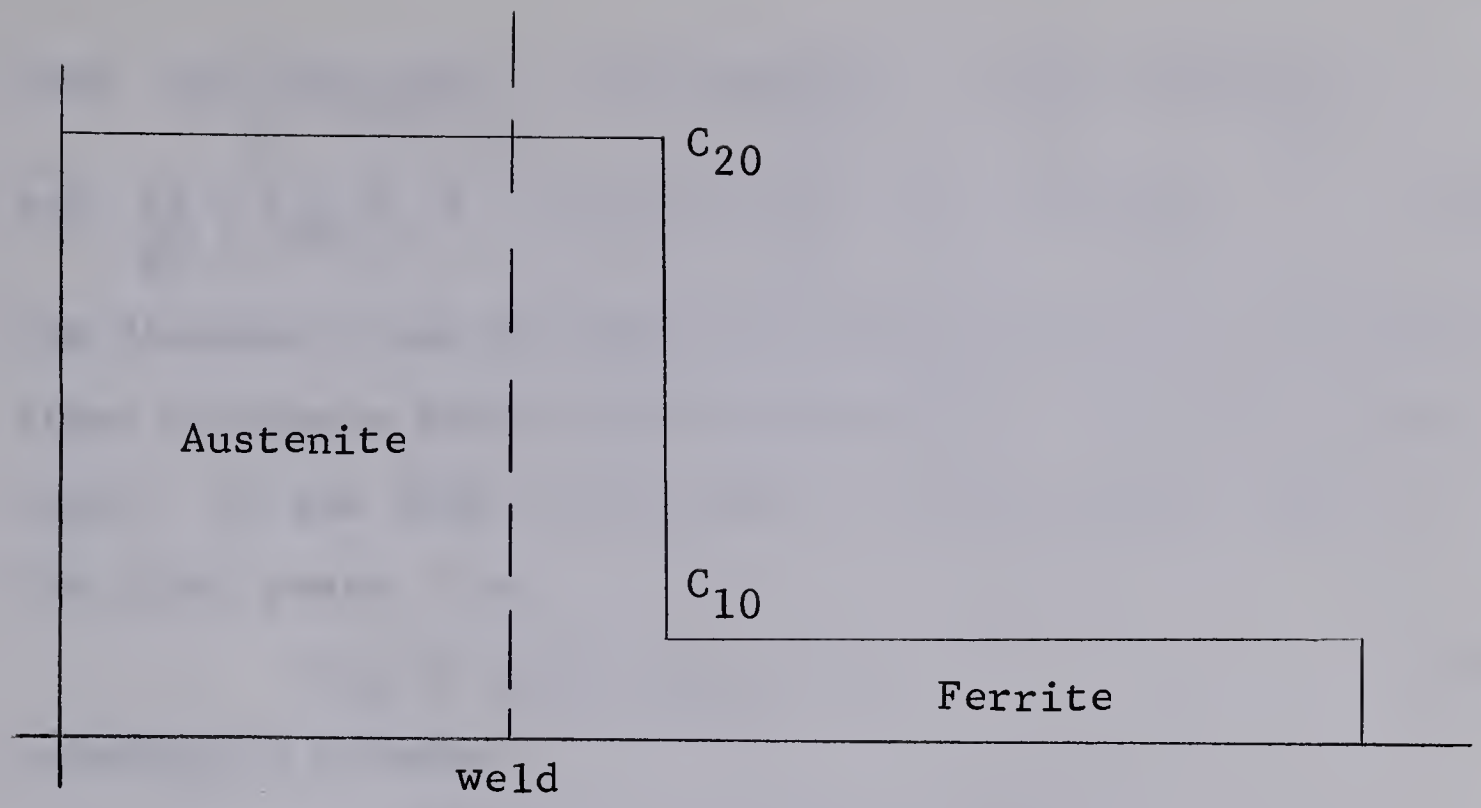

Figure 3(b) Concentration Profile of Diffusion Couple equilibrated in a Two-phase Temperature Range.

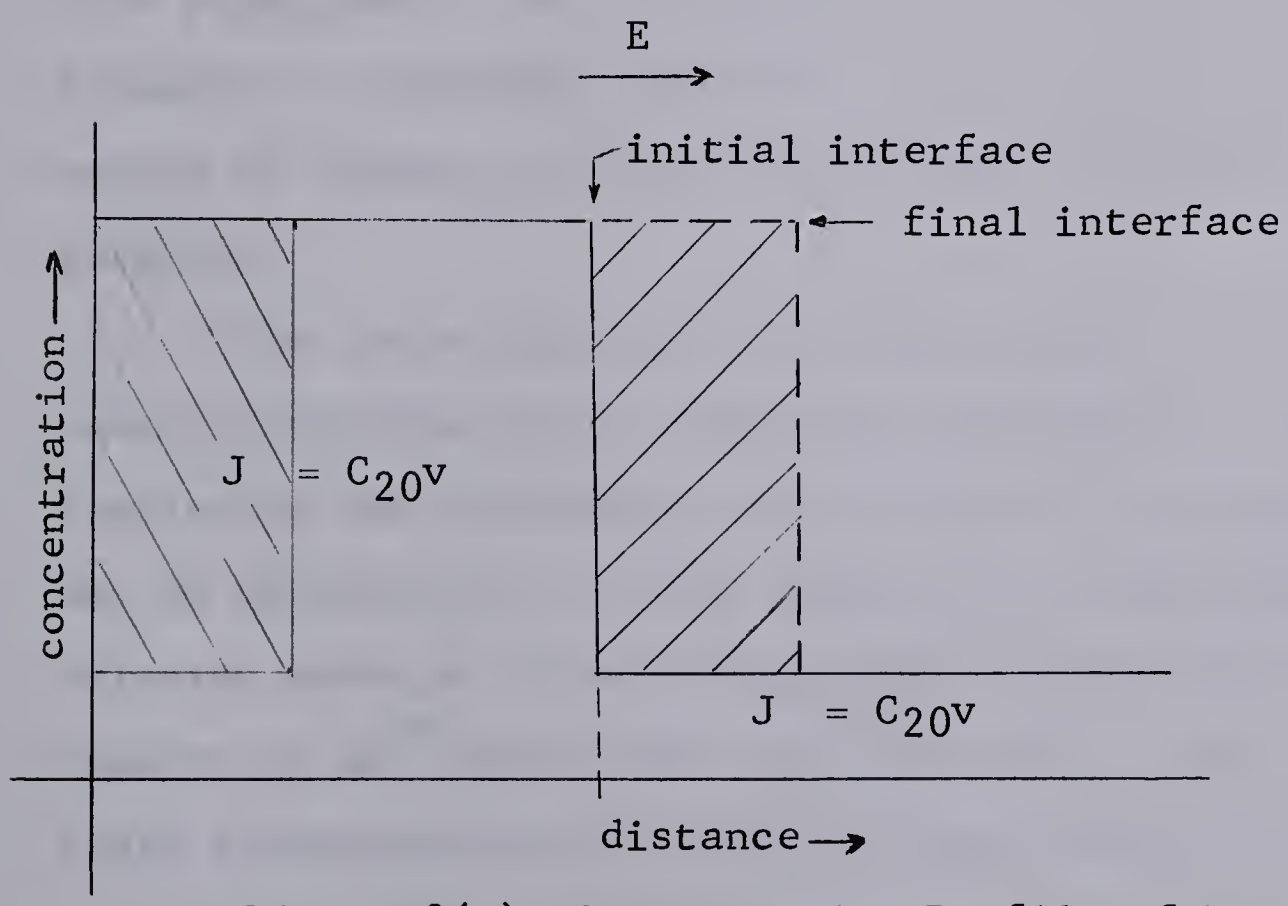

Figure 3(c) Concentration Profile of Equilibrated Diffusion Couple annealed under Electric Field.

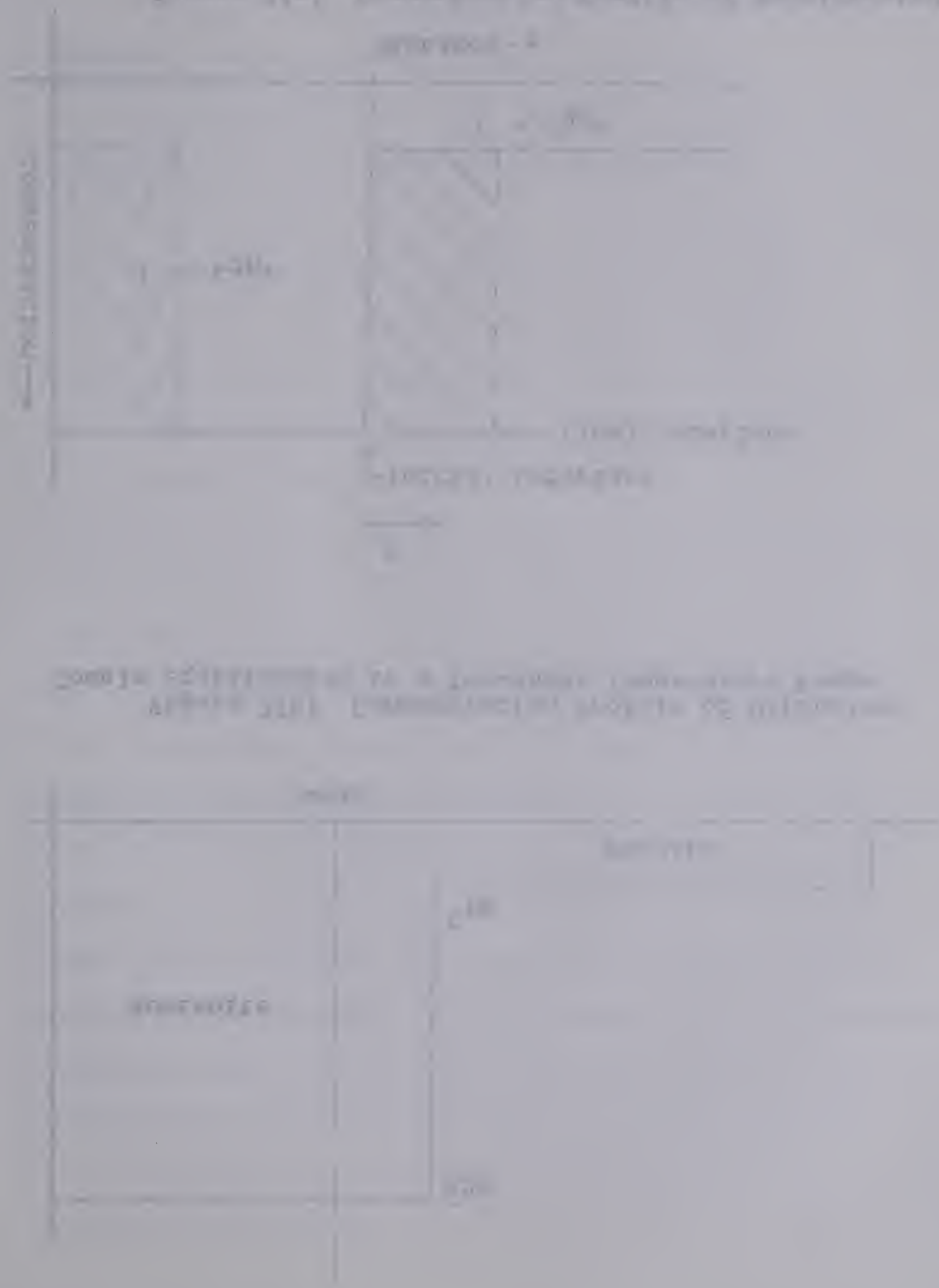

Thus $C_{20}\left\{\frac{D_\gamma q_\gamma eE}{T}\right\} - C_{10}\left\{\frac{D_\alpha q_\alpha eE}{kT}\right\} = (C_{20} - C_{10})\frac{x}{t}$,

and $\frac{eE}{kT}\left[C_{20}\, q_\gamma\, D_\gamma - C_{10}\, q_\alpha\, D_\alpha\right] = (C_{20} - C_{10})\frac{x}{t}$. (53)

The distance x can be measured metallographically from some fixed reference point and the expression in brackets calculated. If the flux in one phase is much greater than in the other phase, i.e.,

$$C_{20}\, D_\gamma\, q_\gamma \ll C_{10}\, q_\alpha\, D_\alpha \tag{54}$$

equation 53 becomes

$$-\frac{eE}{kT}\left\{C_{10} D_\alpha\, q_\alpha\right\} = (C_{20} - C_{10})\frac{x}{t} ,$$

and

$$q_\alpha = -\left\{\frac{C_{20} - C_{10}}{C_{10}}\right\}\frac{xkT}{eED_\alpha t} . \tag{55}$$

This relationship can be shown to be true for the Hall field transport of nitrogen and carbon in iron and provides a method of finding the Hall field charge of these solutes in ferrite.

The above equations are valid however, only when the phase transformation is diffusion controlled and not controlled by the nucleation rate of any of the phases. This may be determined by noting whether the phase boundary velocity under a concentration gradient has $\sqrt{t}$ dependence. Grozier et al[35] have shown that both the $\alpha\rightarrow\gamma$ and the $\gamma\rightarrow\alpha$ phase transformations in iron-nitrogen alloys are diffusion controlled. The $\gamma\rightarrow\alpha$ transformation in iron carbon alloys has been shown to be diffusion controlled by Smith.[36] Kirkaldy and Purdy performed a $\alpha\rightarrow\gamma$ migration experiment at

792°C and found that it also obeyed a $\sqrt{t}$ time dependence. Only one temperature determination has been made for the $\alpha \rightarrow \gamma$ transformation and it is necessary to investigate other temperatures of interest before equation 55 can safely be used.

HISTORICAL REVIEW OF ELECTROTRANSPORT

In the following review some of the more pertinent historical aspects of electrodiffusion in solid metals are presented. For a more complete treatment of the subject the reader is directed to the excellent review paper of Verhoeven.[8]

Electrotransport may be conveniently divided into three groupings i.e. self transport in pure metals, transport in substitutional alloys and interstitial transport. Wever[1,2] studied the self-transport of various metals. In nickel bars a mass transport to the anode was found, while for iron there was mass transport to the cathode. In copper, transport was observed to be anode directed below 900°C and cathode directed above 1000°C. In nickel, which is an n-conducting metal Wever concluded that the momentum transfer force is larger than the field force. In iron both the field force and the momentum transfer force act in the cathode direction because iron is a p-conducting material. Consequently a large positive effective charge is observed.

This interpretation does not, however, appear to hold in general. Kuzsmenko and Kharhov[37,38] investigated several pure metals and found anode directed mobility even in Zn, Cd and Sn which have positive Hall coefficients, and therefore Wever's interpretation is somewhat oversimplified. All conductors are probably mixed conductors, that is charge is carried by both holes and electrons. A positive Hall

coefficient indicates only that a conductor has more holes than it does electron carriers and the momentum transferred to a moving impurity ion depends not only on the density of carriers but also on their mobility and amount of momentum transfered by each carrier. It is conceivable that in a predominently hole conducting material such as zinc, carrier momentum could be anode directed if, for instance, the scattering cross section of activated zinc for electrons is greater than for holes.

Several solid solution alloys have also been investigated. Seith and Wever[39] investigated γ and β phase migration in copper-aluminum alloys. Aluminum migrated to the anode in the β phase where conduction is n-type, whereas in γ where conduction is predominantly p-type, it migrated to the cathode. Similar results were obtained in the copper-tin and silver-zinc systems. Extensive investigations in this field have been carried out by Frantsevich et al and by Kuzmenko and co-workers. A tabulation of their results may be found in the review paper of Verhoeven.[8]

Electrotransport in interstitial alloys is usually much faster than in solid solution alloys because diffusion coefficients are in the order of 100 times greater. For this reason interstitial alloys have been investigated somewhat more than solid solution alloys. Oxygen in both body centered cubic Ti[40](β) and Zr[41](β) migrates toward the anode. In Pd, hydrogen migrates toward the cathode[42]. Since Palladium has a negative Hall coefficient, this implies that the

electric field force predominates.

A considerable number of papers have been published on the migration of carbon in γ iron.[43,44,45,46,47,48] The results are consistent regarding the direction of transport but there is considerable discrepancy in the reported magnitude of the charge.

Darken and Dayal[45] determined the mobility of carbon in iron by finding the amount of carbon depletion in the anode zone and the amount of carbon accumulation in the cathode zone of an initially uniform iron-carbon alloy. A combustion analysis technique was used for carbon analysis. They find an average charge of +3.7 for carbon at temperatures ranging from 1000°C to 1200°C; however, there was no account of electron-ion momentum exchange in their analysis. Hume-Rothery[49] has criticized Darken and Dayal's interpretation of the results, pointing out that the ionization potential for the first four electrons of carbon is 147 electron volts, and that iron is a poor acceptor of electrons. Thus he concluded that strong electronegative elements such as carbon would tend to retain their electrons. Alternatively, Hume-Rothery suggested that iron-carbon bonds were of a resonating-covalent type giving rise to positive and negative carbon ions. The large negative ions remain stationary in the lattice while the comparatively small positive ions migrate. The high temperature required for electromigration serves a two-fold purpose. First, when the vibrational

frequency is increased, an ion is more likely to migrate. Secondly, the homopolar bonds between iron and carbon are disrupted giving rise to the resonating bond.

Many authors have since, generally corroborated the results of Darken and Dayal. For instance, Frantsevich et al[46] find carbon migration to be cathode directed. Radioactive tracer methods were employed by following the displacement of deposited carbon in an iron wire annealed under a field at temperatures as low as 530°C. The effective charge of carbon was found to increase with decreasing temperatures.[48] At 950°C an effective charge of +13.4 was associated with carbon migration and it was suggested that hole ion momentum transfer was responsible for the high charge obtained. The motion of iron atoms in the same samples was also followed. In relatively pure iron (free of carbon) iron migrated toward the cathode, but in iron-carbon alloys, some iron migrated toward the anode. This suggests that carbon donates electrons to unfilled iron energy levels giving them a negative charge. The thermal motion of lattice ions gives rise to a diffusion of conduction electrons between different s-states and between 4s and 3d-states. The probability of these migrations is enhanced near an impurity center where conduction bands are said to be deformed. Such ideas contradict the concepts of Hume-Rothery since migration is observed over a very wide temperature range, not just at high temperatures where the homopolar bond, suggested by

Hume-Rothery is unstable. These authors also found that the tracer zone completely disappeared from the anode end. This eliminates the possibility of negative or unionized carbon atoms. The authors concluded that the mass transport was a result of a combination of the direct field force on the ions and a momentum transfer force.

Using the theory of Fiks[13] and a two-band electronic model for iron, Frantsevich and Smolin[50] developed a method of determining the true charges of activated impurity ions. The method depends on an examination of the temperature and concentration dependence of electrical conductivity. Results of experiments using this method indicate a true charge of +3.7 associated with carbon in austenite.

Extensive results on the migration of carbon in pure iron ferrite and alloy ferrite have been reported by Babakova.[51] Unfortunately the results are analyzed without taking into account momentum transfer and by using a kinetic theory based on transport numbers. Kalinovich[48] recalculated Babakova's results using the Einstein equation and found an effective charge of +49 associated with migrating carbon in ferrite. This indicates that the hole momentum transfer force on carbon in ferrite is somewhat larger than the momentum transfer force in austenite. Yu Miller[30] investigated the Hall field migration of radioactive carbon in ferrite and found cathode directed transport. However, the method of Miller was not amenable to charge calculation.

In contrast to carbon in austenite, nitrogen in austenite migrates toward the anode. Seith and Daur[52] metallographically detected large anode directed transport indicating a very high negative charge. The unpublished work of Li[53] confirms the direction of transport. Such migration is difficult to rationalize on a momentum transfer model since it is unlikely that the substitution of nitrogen for carbon in the lattice would result in a change of the Hall coefficient. There is no account of any investigation relating migration and charge of nitrogen in ferrite.

EXPERIMENTAL

A. PREPARATION OF ALLOYS

The alloys were prepared by gas carburizing and gas nitriding Armco iron (see Appendix A for a complete analysis). A chromel-A resistance heated tube furnace was used to maintain the carburizing anneal temperatures. The furnace comprises a vitroseil tube used to contain the samples and gas atmosphere, a shielded chromel-alumel thermocouple coated with zirconium cement, and a Honeywell temperature control unit. The temperature was controlled to $\pm 5^{\circ}C$ with this unit. Figure 4 shows a schematic diagramof the furnace assembly. Armco wire samples 0.050 inches in diameter were suspended in an alundum boat and placed in the tube furnace. Methane gas was passed through the furnace and through an oil filled jar that acted as a flow indicator. The bubble formation rate in the jar indicated the gas flow. Varying the time at temperature and rate of gas flow produced samples of varying carbon content. This was usually estimated by assuming the surface of the sample to be saturated with carbon and then applying Van Horn's formula for carbon penetration i.e. $\xi = 2\gamma \sqrt{Dt}$. For example a time of 45 minutes at $875^{\circ}C$ is required to produce a sample of 0.5 wt. % carbon after annealing to homogenize the sample.

This treatment leaves the wire with a very heavy border of pearlite as shown in Figure 5, which is typical of

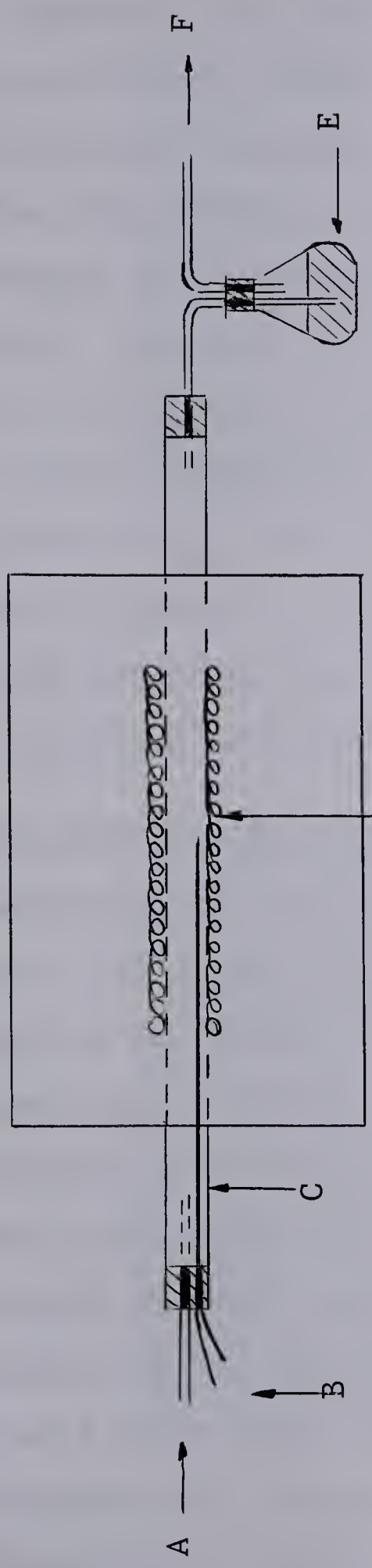

A Gas Inlet
B Chromel-Alumel Thermocouple - to controller
C Vitreosil Tube
D Heating Element
E Oil Bubble Chamer
F Gas Outlet

Figure 4. Resistance Heated Tube Furnace

the microstructures of the wire cross-section. A phase boundary separates the carburized austenite region from the uncarburized ferrite interior region. Further high temperature annealing was necessary to homogenize the cross-section. The samples were mechanically cleaned of excess surface carbon, suspended in an alundum boat and again placed in the tube furnace. An argon gas atmosphere was maintained around the sample and the temperature of the furnace raised to 1050°C. Complete homogeneity was accomplished after ten hours as indicated by the typical cross-section microstructure shown in Figure 6. The homogeneity was further confirmed by taking microhardness measurements across the diameter of the water quenched specimen.

B. PREPARATION OF DIFFUSION COUPLES

Carburized or nitrided Armco iron wire 0.050 inches in diameter, and Armco iron as received, were given a cross-section polish and lapped with Linde B polishing grit. A metallographic examination ensured that only sound alloys free of defects were being used. After the metallographic examination, the samples were repolished with Linde B powder and thoroughly cleaned in water and alcohol. Each sample was carefully removed from the polishing mount and secured by means of a screw clamp in a small spot welder. The welder (Rocky Mountain 506) was essentially a low voltage, high current transformer, capable of delivering about 100 amps for very short times. Figure 7 shows the welder with two

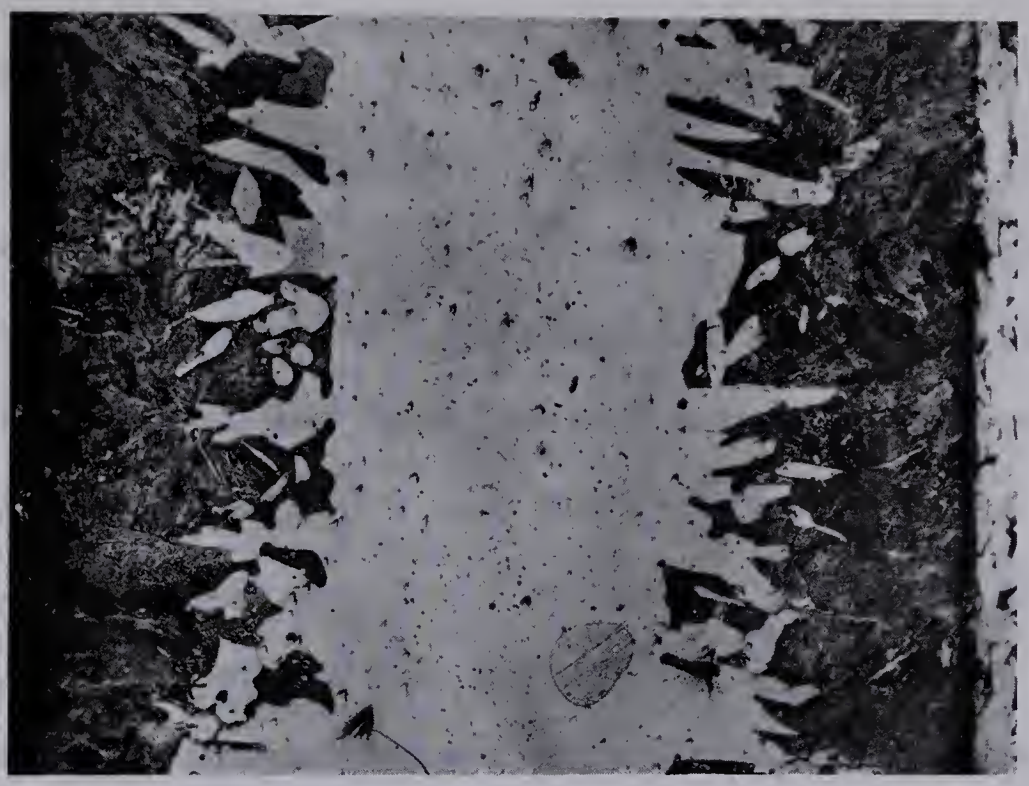

Figure 5 - Cross-section of gas carborated sample x 100.

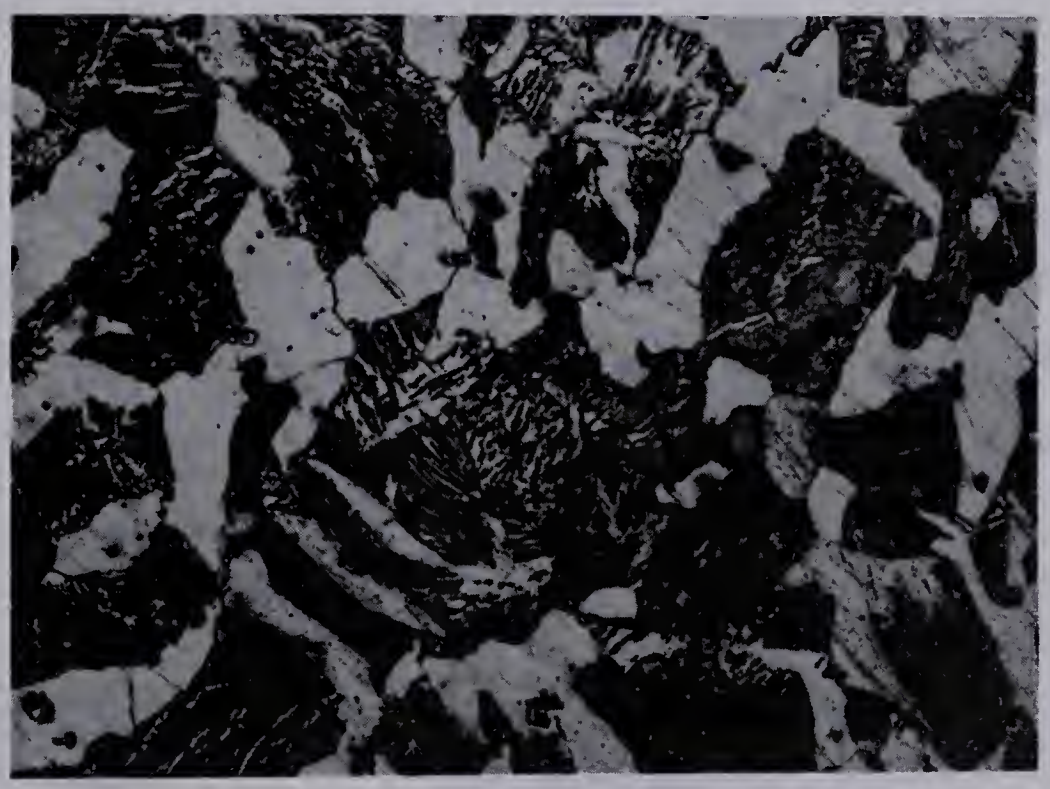

Figure 6 - Homogenized cross-section after ten hours at 1050 C. x 250.

wire specimens being welded. The welding operation involves removing the electrodes and replacing them with the alloy wire and Armco wire. Extreme care was taken to ensure that both sample faces were parallel and a slight spring pressure applied. A large current was then passed through the samples resulting in a butt weld. Since the entire operation is essentially instantaneous, one can reasonably expect very little volume diffusion of solute across the weld. Very sharp clean welds were produced by this method as indicated by the iron-iron weld shown in Figure 8. On direct electro-diffusion experiments sandwich diffusion couples were prepared by welding two unalloyed Armco sections to a small alloyed centersection.

Since the samples were required to withstand long high temperature anneals they were electroplated with copper using a cyanide plating technique[54] to prevent oxidation and decarburization. Any scale resulting from the welding operation was removed mechanically. The couple was clamped to the cathode of a 2-volt battery power supply with a pure copper bar comprising the anode. The electrolyte contained the following:

CuCn	120 g/litre
K Cn	135 g/litre
NaOH	35 g/litre
NaHCN	15 g/litre

Also inserted in the circuit was a variable resistor to control the current density of the plating bath. A schematic

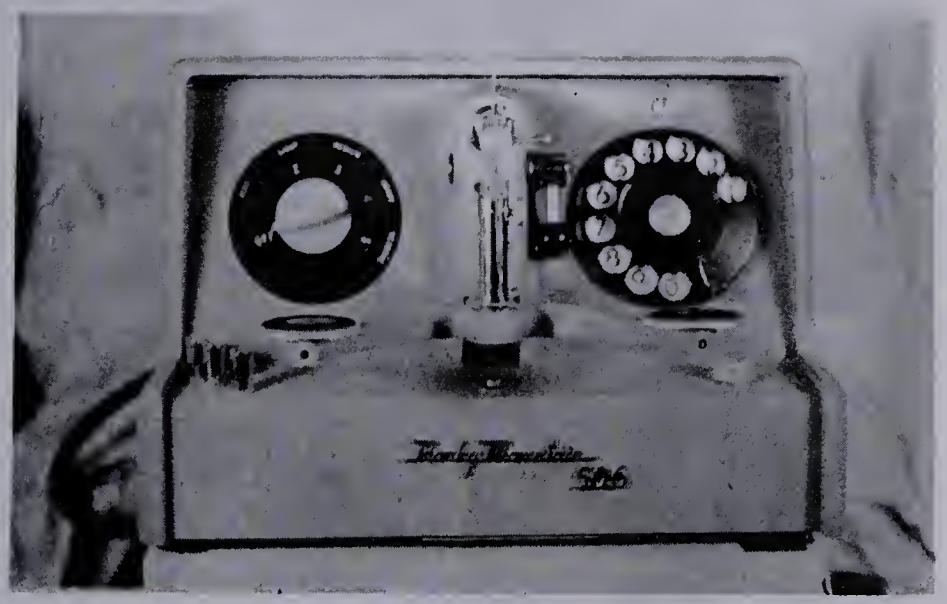

Figure 7 - Diffusion couple welding assembly.

Figure 8 - Armco Iron - welded to Armco Iron illustrating soundness of weld. x 400

diagram of the plating assembly is shown in Figure 9. Very low current densities ($\sim$ 0.5 milliamps/cm^2) appeared to give the best copper coating, with about 24 hours giving a coat thickness of $\underline{\sim}$ 0.001 inches. In each case the coating was examined under the binoculars (30 x magnification) for porosity.

After the coating operation the diffusion couples were transferred back to the spot welder where thermocouple and voltage probe wires were attached. This was accomplished by clamping the diffusion couple and wires between the electrodes of the welder and passing a current through the assembly for a few seconds. Usually the thermocouple wires were attached a few millimeters outside the diffusion zone in the unalloyed Armco iron section of the couple and the voltage probe placed about a centimeter toward the other end. A three wire thermocouple balanced by a bridge circuit was necessary because of extraneous resistance voltages picked up across the thermocouple bead due to the current passing through the sample. The three wires comprise two chromel wires surrounding an alumel wire. Voltage probe wires were alumel wires and field voltage was measured between a probe wire and the center thermocouple wire. This arrangement is shown in Figure 10.

C. DIRECT FIELD ELECTRODIFFUSION

An assembled sandwich type diffusion couple was mounted between two large water cooled electrodes. The

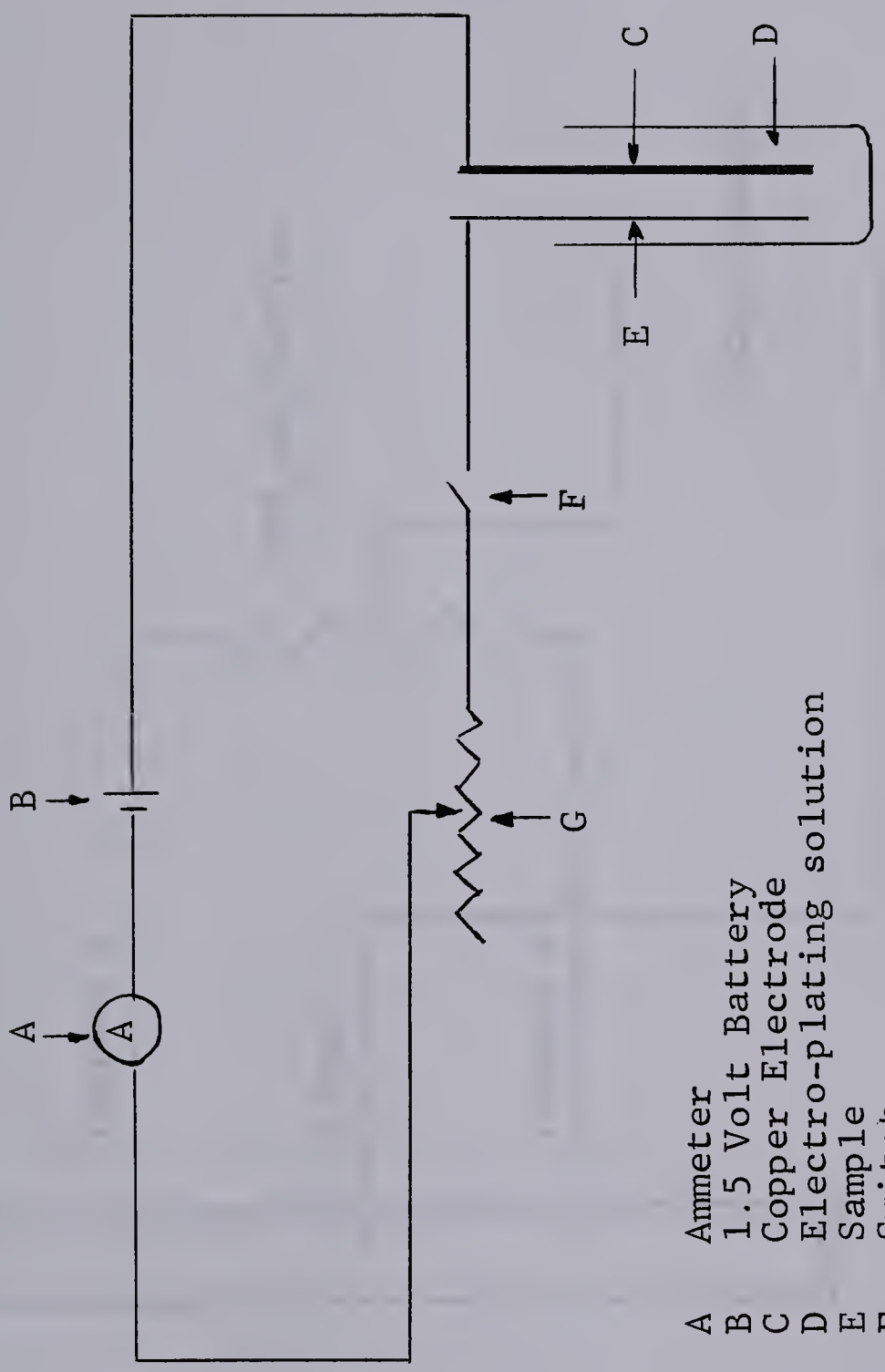

A Ammeter
B 1.5 Volt Battery
C Copper Electrode
D Electro-plating solution
E Sample
F Switch
G Variable Resistor

Figure 9. Diagram of Copper Plating Apparatus

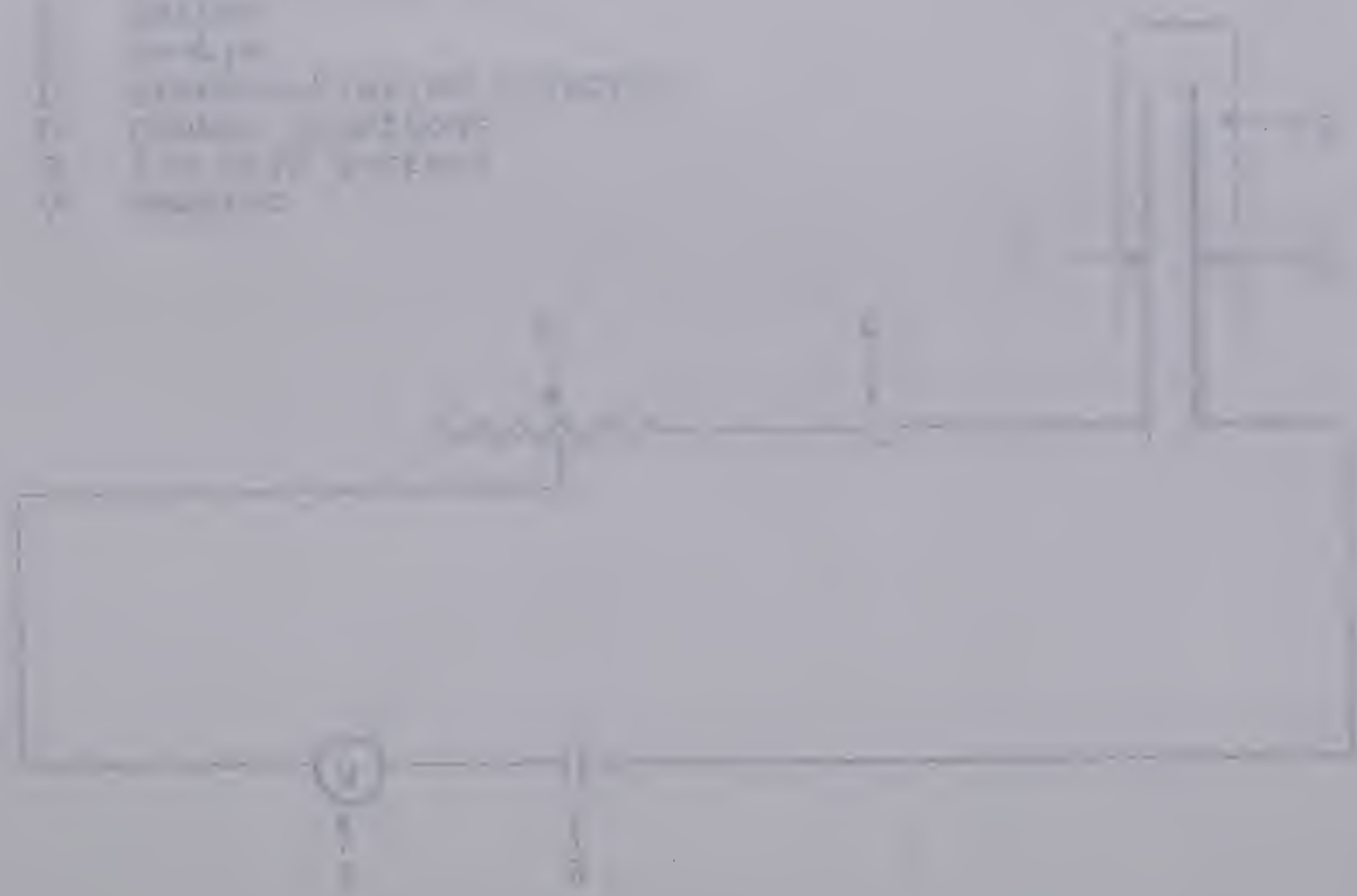

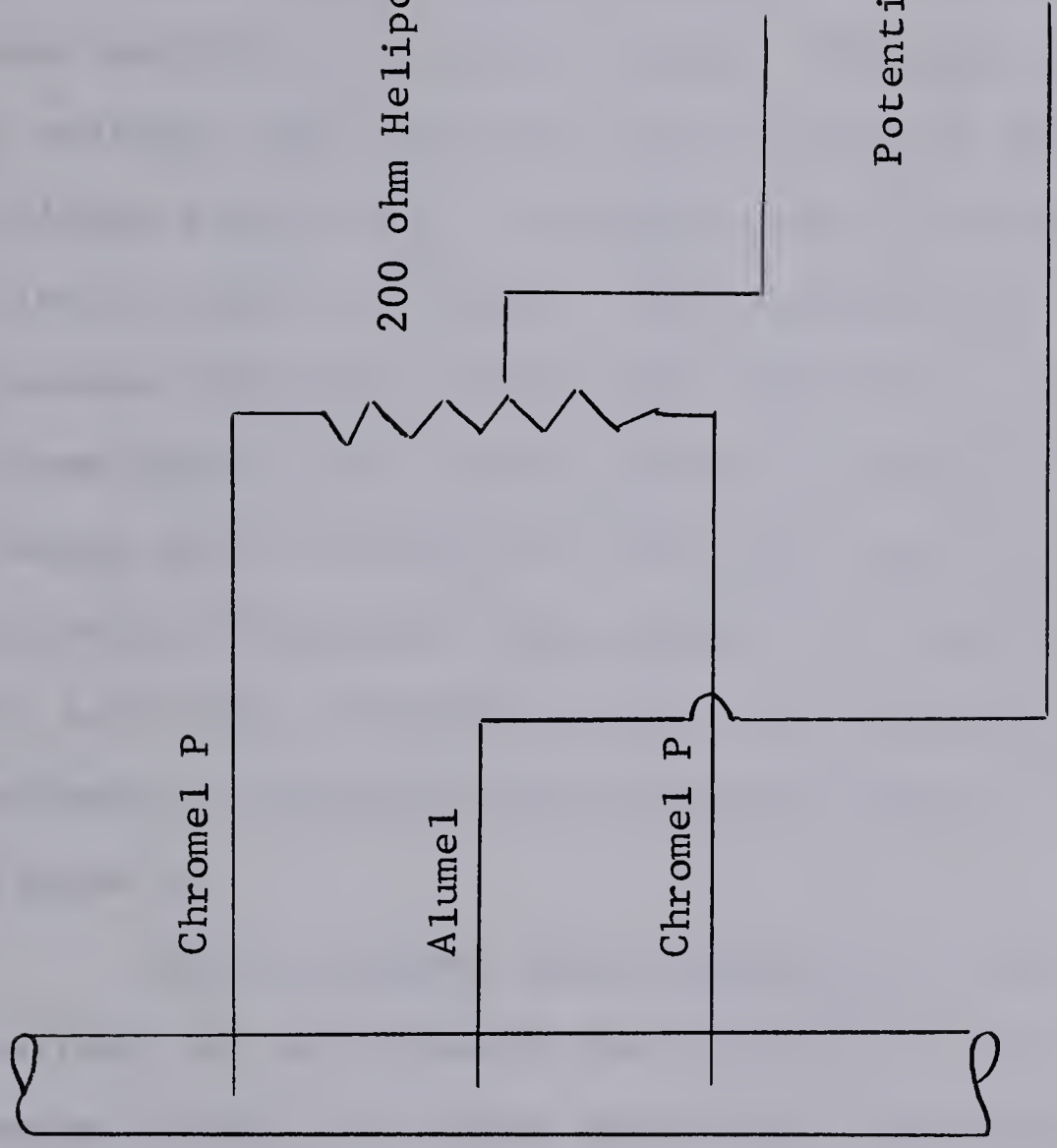

Figure 10. Thermocouple Balancing circuit (after Boedtker and Duwez)

electrodes extending through a brass vacuum base plate were insulated from the base plate by rubber O-rings. An eighteen inch Bell jar vacuum sealed to the base plate by an L-ring surrounded the electrodes. An Edwards four inch vacuum pump backed by a Duo Seal 120 c.f.m. mechanical pump, served to maintain a vacuum within the system. A small D.C.-N.J.E. power supply capable of 0-30 volts and 0-20 amps. was employed as a field source. The power supply contained a voltage stabilizer that was capable of maintaining the voltage within 0.1%. Current control adjustment was sensitive to about 0.01 amps. Also inserted in the circuit between the power source and diffusion couple was a double throw-double pole current reversing switch. The thermocouple wires attached to the sample were fed through glass to metal electrical seals inserted in the vacuum base plate to a 200 ohm variable resistor and a potentiometer. A schematic diagram of the electrode circuit is shown in Figure 11.

After assembly and evacuation of the system, a small current was fed through the electrode circuit. A potentiometer reading was taken across the thermocouple probes, the current reversed and the potentiometer reading again taken. The variable resistor was adjusted so that the two readings coincided. The potentiometer reading at this point measured the true temperature since all extraneous voltages were counterbalanced.[55] Power from the N.J.E. power source was

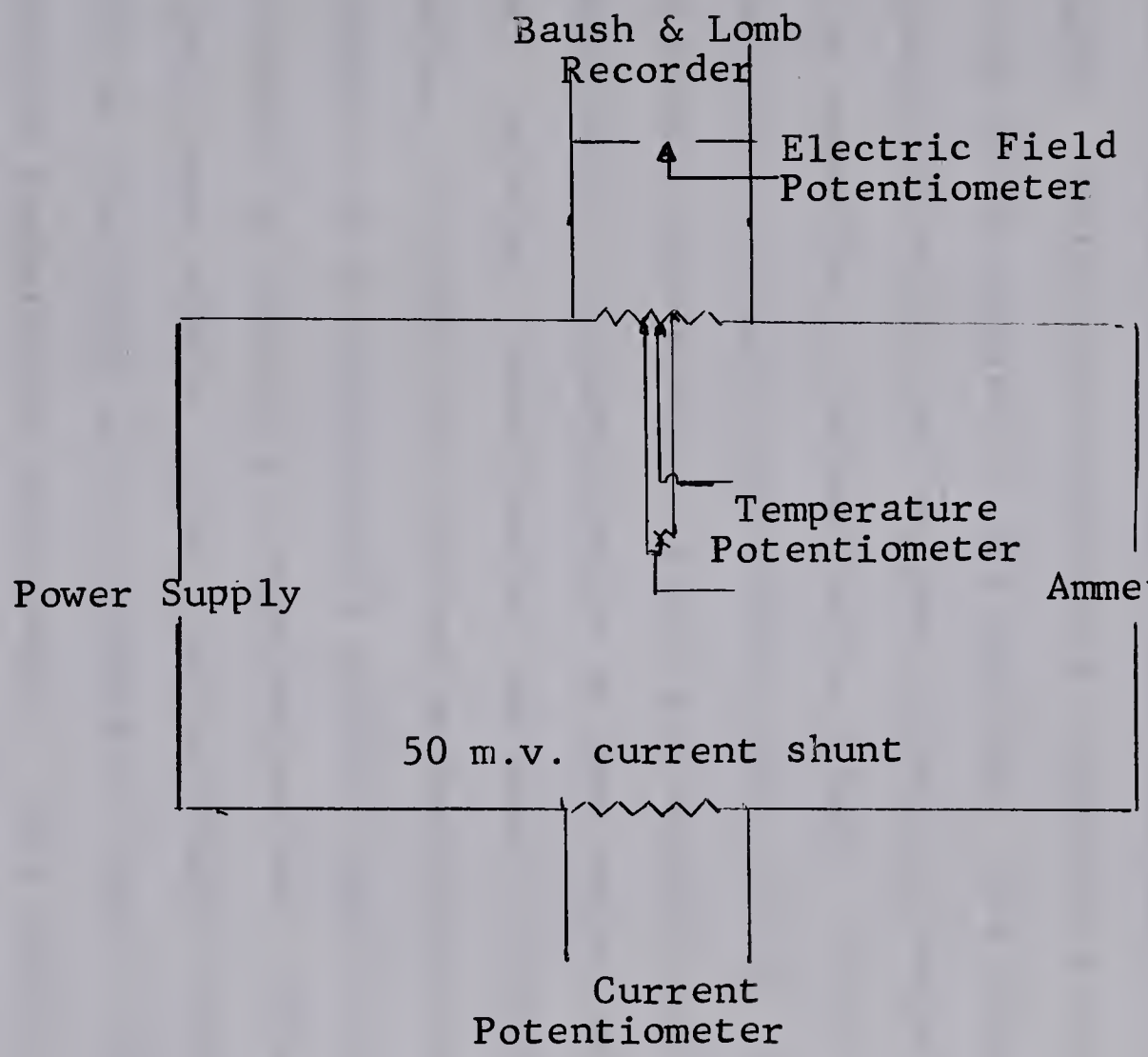

Figure 11 Schematic Diagram of Electrodiffusion Assembly

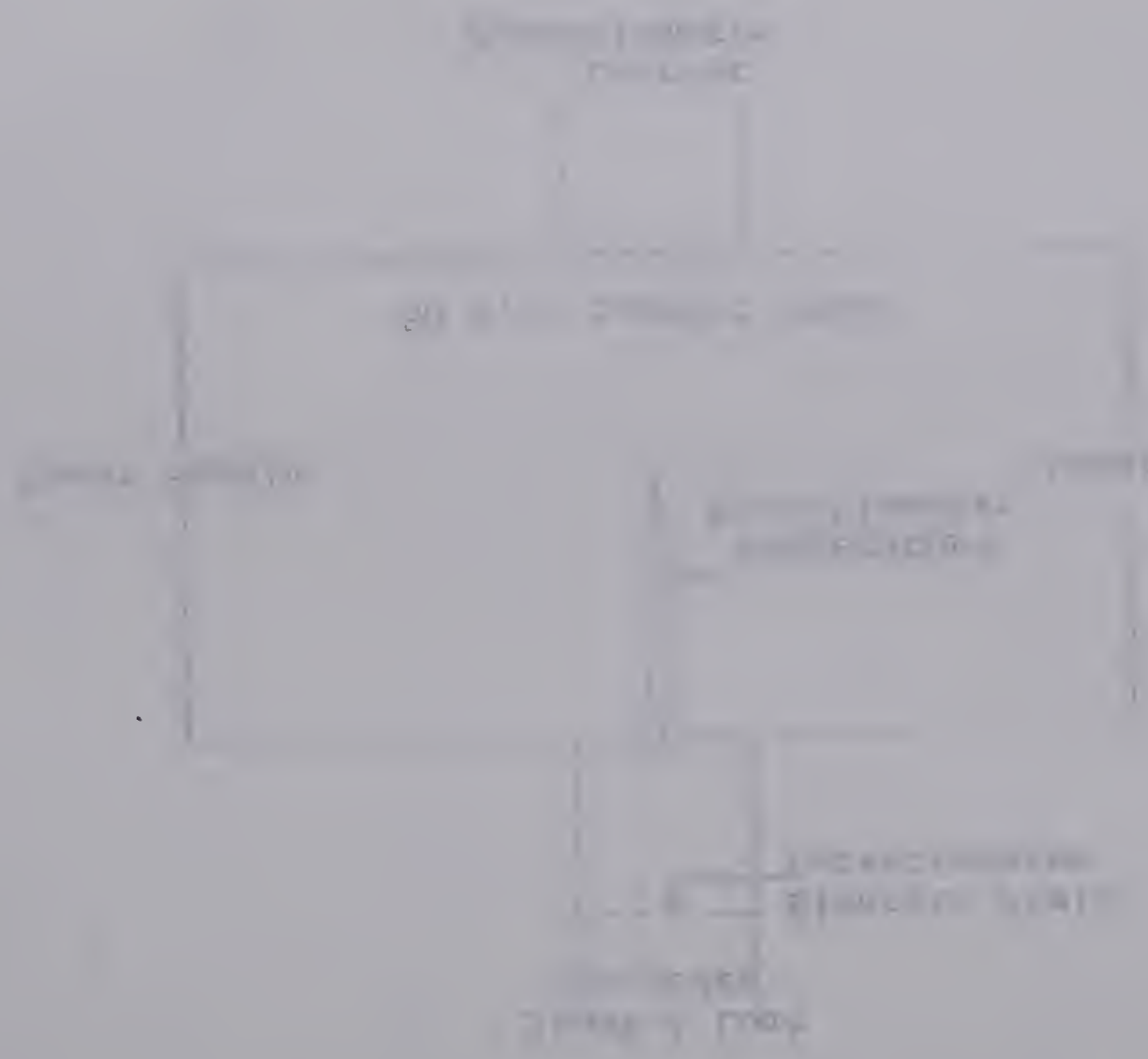

increased until the specimen reached the annealing temperature, and was then maintained for a predetermined length of time. Electric field measurements were obtained by potentiometer readings across the center wire of the three wire thermocouple and voltage probe. The potentiometer could be read directly to 0.010 mv and estimated to 0.005 mv. Voltages from 10 volts to 10^{-5} volts were measurable on this instrument. During the experiments temperature was controlled by the field applied to the specimen. The temperature occasionally drifted from the mean annealing temperature and had to be corrected by adjusting the field. A six inch chart recorder with a voltage range from 0.001 v/cm to .05 v/cm was used to record both electric field and current readings so that experimental characteristics of the entire run could be examined. Another potentiometer was used to monitor the temperature. Current was obtained by measuring the potential drop across a 50 mv standardized current shunt with the same potentiometer by adjusting a selector switch. This potentiometer was a very stable, versatile instrument reading directly to 0.005 mv. resulting in an accuracy of about $0.05^{o}C$ of thermocouple temperature measurement. This error is far less than errors introduced by compositional variation in the thermocouple and errors in balancing the thermocouple bridge circuit. The millivolt reading from the standardized shunt resistor was read to approximately 0.005 millivolts which

gives a current sensitivity of 0.05 amps. After the anneal the couples were removed to a soaking furnace of similar design as shown in Figure 4, soaked at 1000°C for 10 minutes, and then quenched into a water bath located directly below the furnace.

D. ANALYSIS

1. Determination of Microhardness Calibration Curve

Samples from the carburizing treatment were chosen at random and annealed at 1000°C for 10 minutes. A Wheelco controller ensured that the temperature remained within ±5°C of the anneal temperature. After the anneal the samples were water quenched, sprayed with ethanol, dried and mounted in bakelite. They were then polished, lapped and etched lightly with a 4% nital etchant. Nital etching revealed a typical martensite structure as shown in Figure 12. Microhardness measurements were then taken across the wire diameter in several directions. The Reichert model MIHEP-2760 microhardness tester mounted on the Riechert Model MEF microscope was employed in all hardness measurements. Precise positioning of the impression is realized on this instrument by use of a common mount for the front lens of the objective and the Vickers test diamond. Complete details of the structure and use of this tester are available in the literature.[56]

The usual procedure is to convert microhardness diagonal measurements into hardness numbers. However,

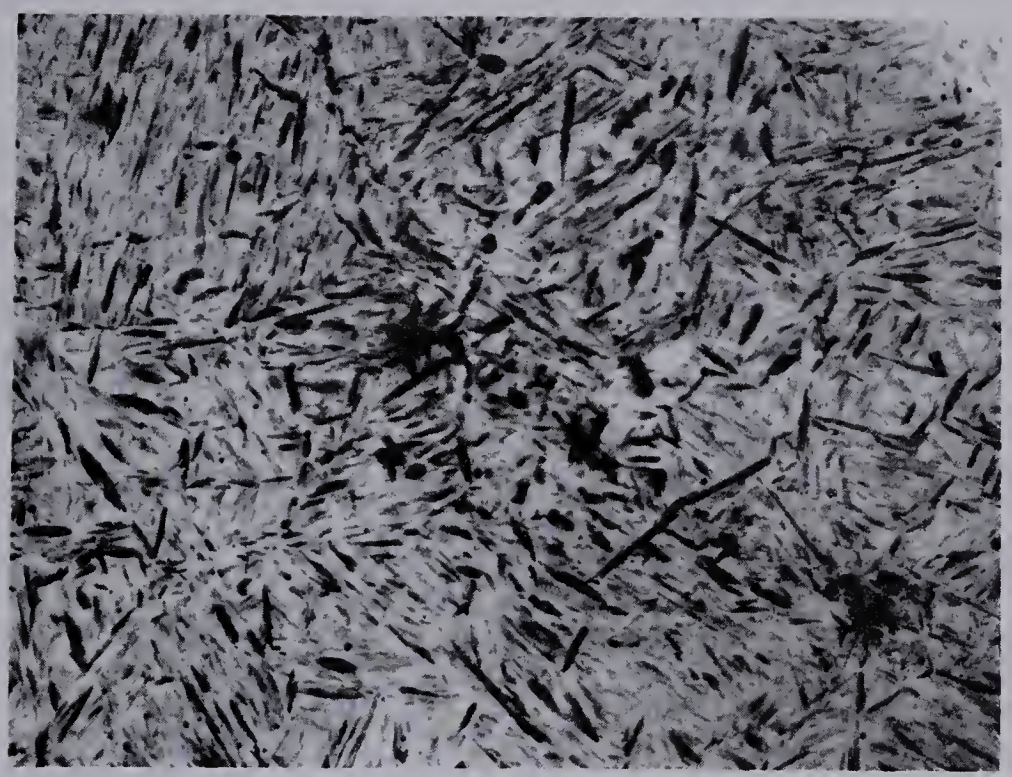

Figure 12 - Martensite structure typical of water quenched iron-carbon alloys.

hardness numbers can only be used accurately when comparing materials of different hardness based on indentations of the same diameter. This requires the calibration of hardness numbers as a function of load for the entire solute range considered. This is not practical for analytical purposes and recourse must be made to a method of comparing the hardness readings on the basis of constant load. Microhardness measurements were found to be very sensitive to carbon content at a load of 35.5 grams where readings ($\sim$100) were obtained on the quenched samples. Some of the samples were then analyzed by the vacuum fusion method for carbon content. Thus, a plot of microhardness indentation diameter as a function of carbon concentration was obtained which proved to be a powerful microanalytical tool.

A similar calibration curve was established for nitrogen in iron except that the heat treatment involved an anneal at 900^{o}C for 10 minutes.

For the purpose of illustrating the use of the microhardness method in solid solution analysis, the calibration curve of silicon in iron was determined. Iron silicon alloys up to 6 wt% silicon were prepared from silicon 99.97% pure and Armco-iron. Silicon powder was weighed and packed into a 1/2 inch Armco round bar. This was then placed in an alundum boat and melted in a Philips high frequency unit. The edges and ends of the ingot were cropped off to minimize segregation. They were mounted in bakelite and hardness

measurements taken. The ingots were then wet analyzed for silicon content. The results are contained in Appendix B.

2. Microhardness Traverse Across the Diffusion Zone

The quenched diffusion couples resulting from electrodiffusion experiments were mounted and prepared in the same way the calibration specimens were prepared. Hardness readings were taken on both unetched and etched specimens and were found to compare very favorably. It was concluded that extreme care in surface preparation was not necessary as for instance, in copper-aluminum alloys.[74]

The first step in making microhardness measurements on a sandwich couple was to align the couple with the weld interfaces exactly parallel to one direction of stage travel. The indentations were accurately placed perpendicular to the weld by traversing with a micrometer mechanism. Indentations were placed every 0.05 mm. apart along the direction of diffusion using the weld interface as a reference. Four such traverses were made about 0.15 mm. apart. The length of the traverse varied depending upon the length of diffusion anneal. A 2 mm. diffusion length zone appeared to be the maximum. Often the velocity of the solute ion could be determined without recourse to the calibration curve. On the other hand for a Grube analysis it was necessary to convert these readings by using the calibration curve and plotting solute concentration curves.

E. PHASE BOUNDARY MOTION IN A HALL FIELD

The diffusion couples used in Hall field electromigration differed from those used for direct electrotransport. 0.050" Armco wire was passed through a rolling mill until its section was reduced to 0.020" x 0.090". Rolled sections about 8" long were cleaned of any lubricant with carbon tetrachloride and dried in ethanol. They were suspended on alundum blocks in the carburizing tube furnace and carburized at 850°C. Rough estimates from the equation of Van Horn (Appendix G) showed that an annealing time of about 15 minutes was adequate. In actual fact about 10 minutes was required for sufficient carbon penetration.

Argon was then substituted for the carburizing atmosphere and the samples given a 24-hour anneal at 755°C. Figure 13 shows the concentration profile of the sample before and after homogenization. The final specimen contained a heavy pearlite border of carbon with the concentrations C_{20} and C_{10} determined through the use of a phase diagram. Some of the samples were quenched and cross-sectional microhardness measurements taken to check the homogeneity. The remaining alloy couples were copper coated and thermocouple wire attached to the copper coated surface. The longitudinal probe was also attached to measure the electric field along the couple.

Prepared samples were then clamped between the current poles of the apparatus described in Section C. In addition

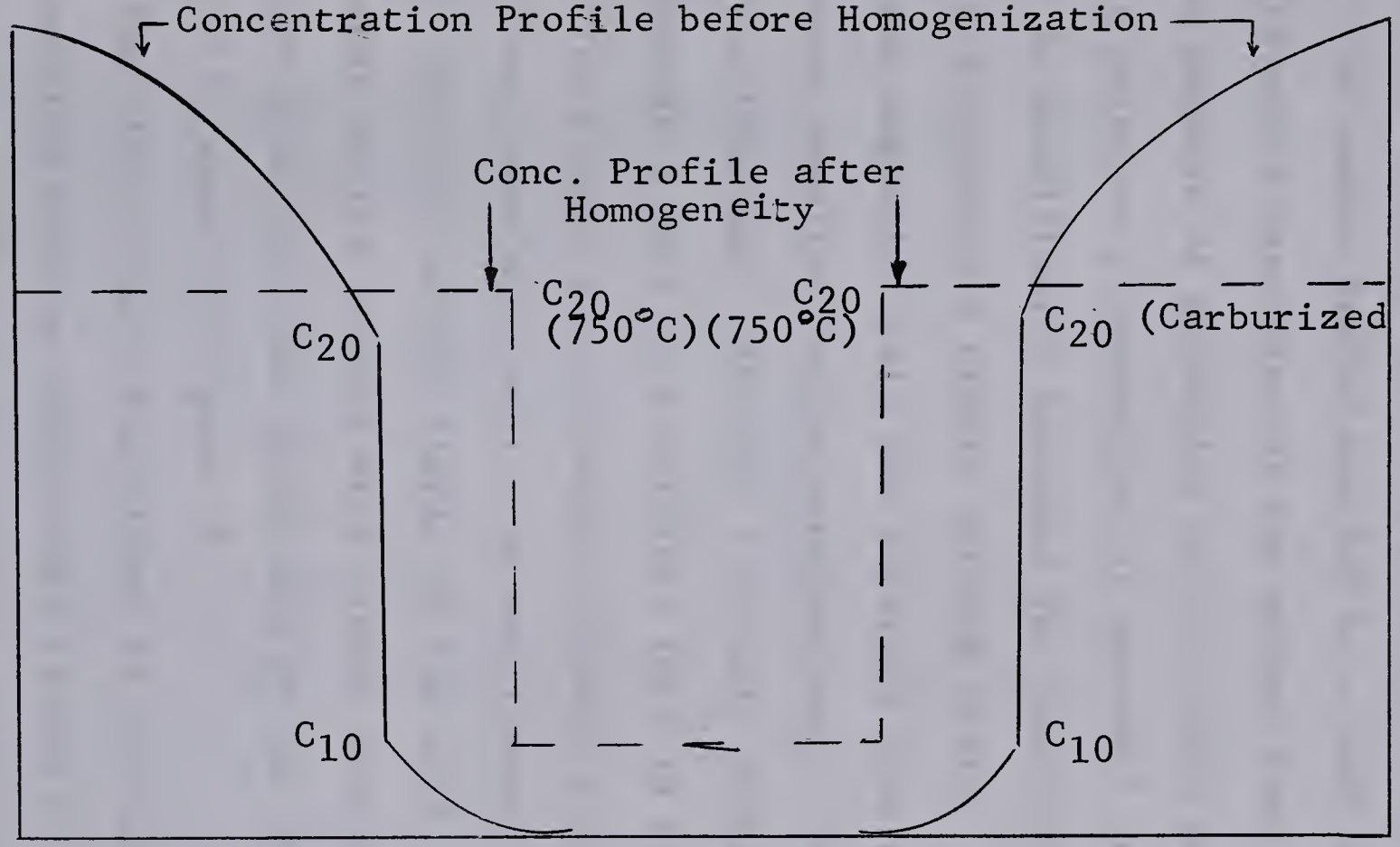

Figure 13. Hall Field Diffusion Couple before and after Homogenization Treatment

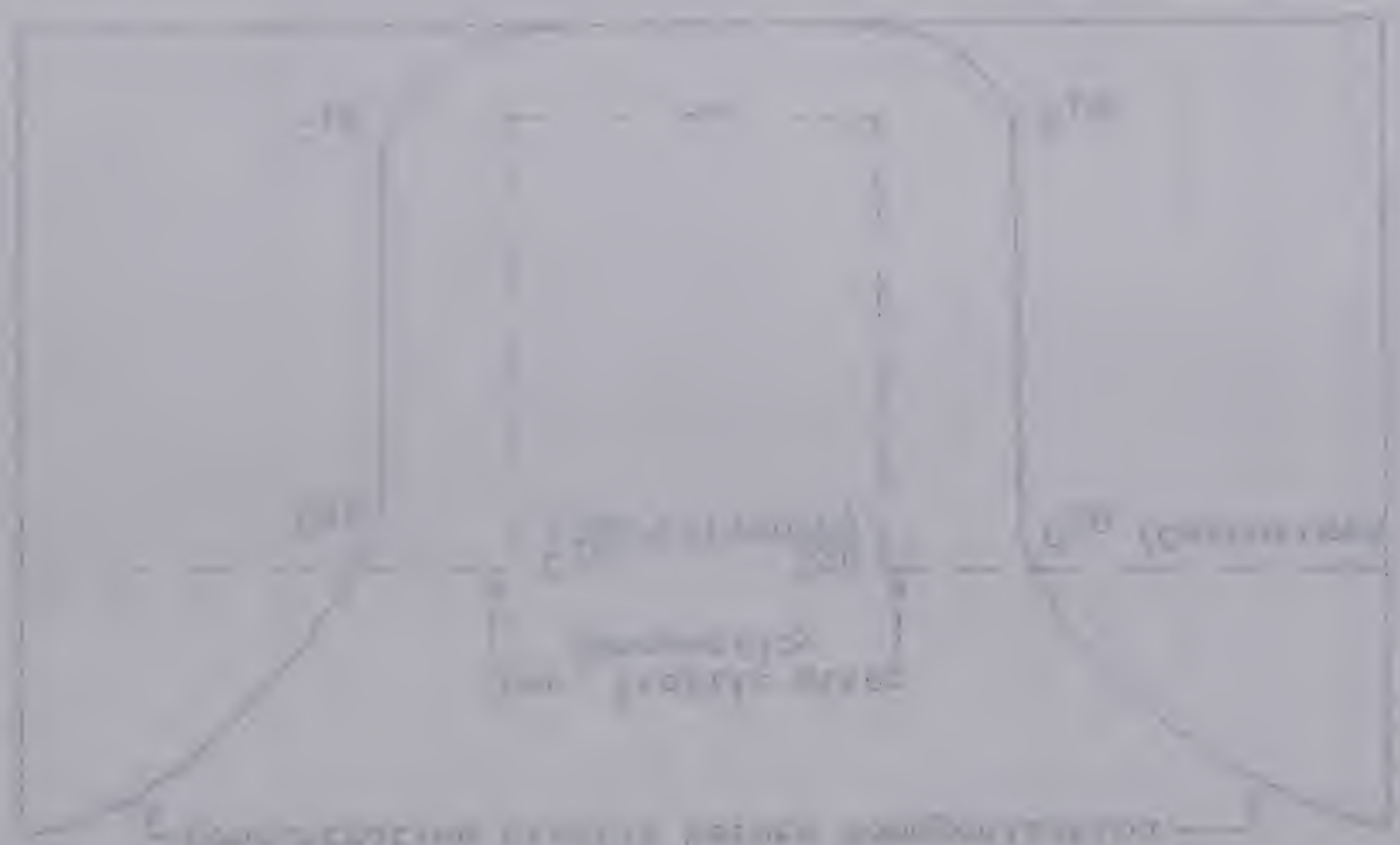

the poles of an Alpha Scientic Electromagnet AL 7500 were positioned such that the magnetic field was perpendicular to the direction of current flow (see Figures 14 and 15). Water cooling coils and current leads were admitted through the base plate of the vacuum system and led to a heat sensing device that prevented operation of the magnet when overheated. The magnet was capable of producing up to 22,000 gauss by using one-inch poles at a separation of one-half inch. The electromagnet is specifically designed for suseptibility measurements and produces a highly uniform field. The magnitude of the magnetic field was obtained from a current calibration curve supplied by the manufacturer. The magnet was powered by a 0-20 amp. 110-volt D.C. unit operated by an A.C. source through a bank of rectifiers (BYY 16 silicon rectifiers). The ripple was minimized through a series of capacitors and an inductance coil. An oscilloscope trace indicated less than 5% current ripple in the unit. Two large brass water cooled jackets were placed over the magnet poles to protect them from heat generated by the sample. The entire assembly is shown in Figure 16.

After the alloy couple was placed in the field, the system was evacuated and the temperature raised to 755 $^{\circ}$C by increasing the power. The temperature circuit was balanced at the operating temperature. The direct electric field, temperature and current were all obtained by potentiometers in the same way described for direct electrodiffusion

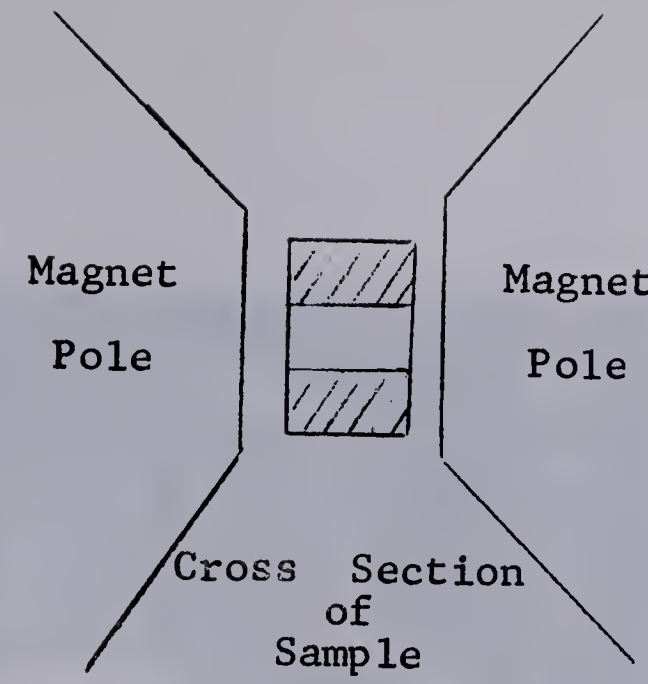

Figure 14 - Cross sectional diagram illustrating Hall Field diffusion couple position.

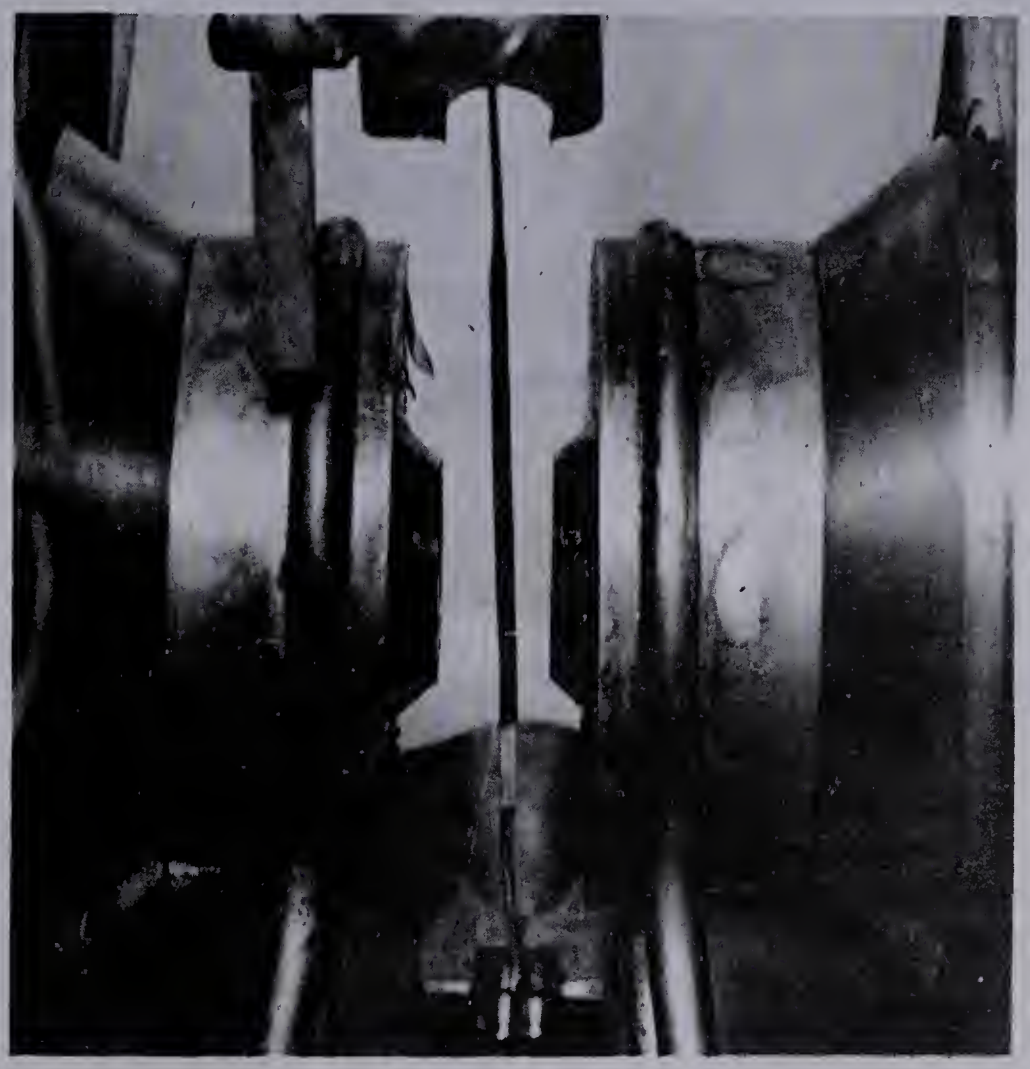

Figure 15 - Pole Magnet - Diffusion Couple Electrodiffusion arrangement.

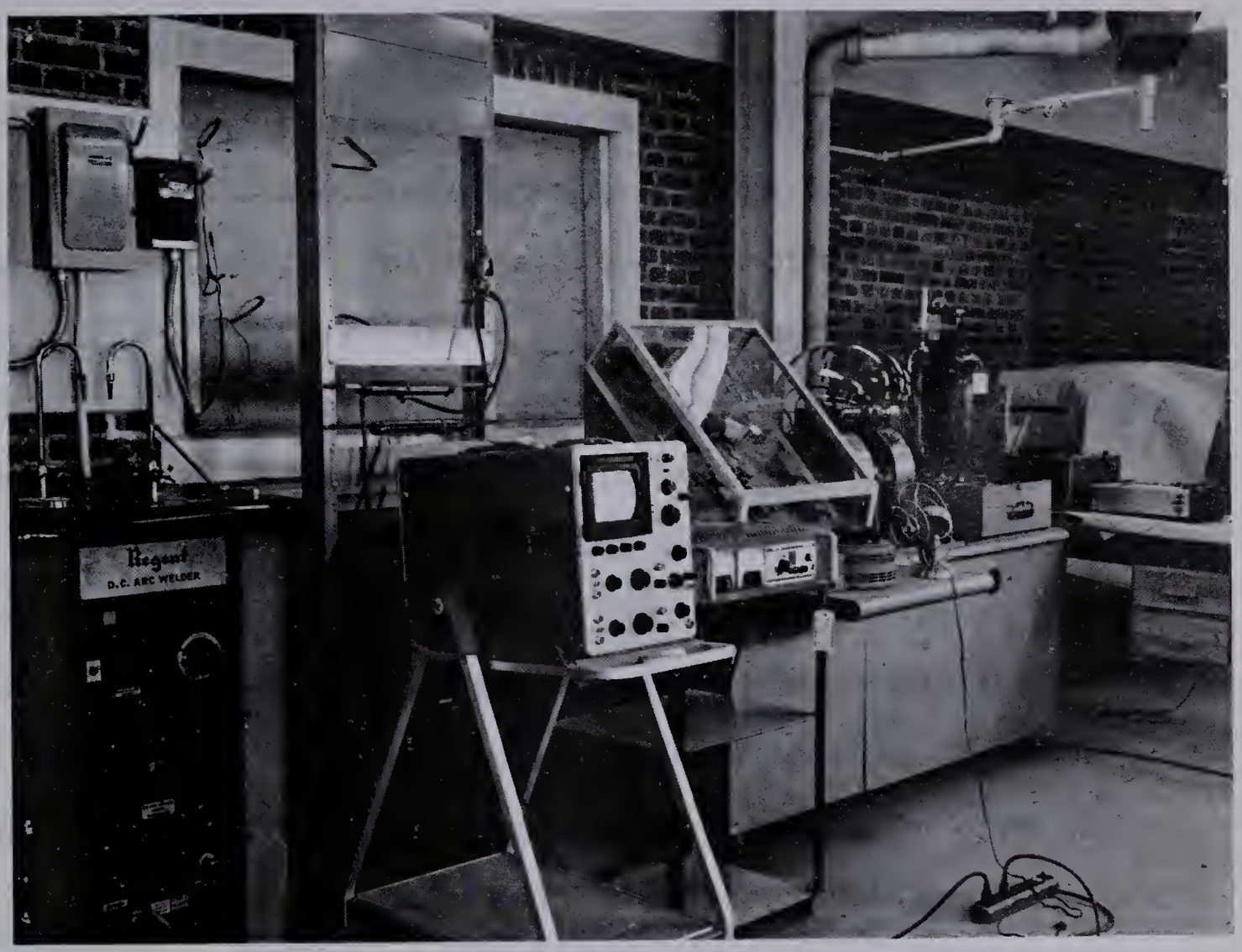

Figure 16 - Hall field electrodiffusion apparatus.

experiments. The direct electric field was recorded with a Bausch and Lomb recorder and the current characteristics were examined by a Tektronix 502 oscilloscope.

In addition to transport along the Hall field there is also considerable transport along the direction of the applied electric field. Since this mass transport is of no interest in these experiments, the directions of both the magnetic and electric fields were reversed every half-hour to reverse the mass flow and eliminate longitudinal gradients. Anneal times in the order of 24 hours were employed.

At the end of the anneal the couples were removed, mounted in bakelite and polished and etched in nital. The distance of boundary migration was measured on the Tukon Filar unit scale. A sensitivity of 0.33 microns could be measured on this instrument using a magnification of x 425.

The magnitude of the Hall field was obtained from the measured magnetic field, current density and from the (anomolous) Hall coefficient measured independently. This, along with the measured boundary migration allowed a calculation of carbon mobility and hence the "Hall field charge" of carbon.

The mobility of nitrogen in α iron was determined by the same method except that the homogenizing and anneal temperature employed was 735^{o}C.

F. MEASUREMENT OF HALL FIELD

The diffusion couple specimen size being very small ($\sim$ 0.020 inches) necessitated the use of special techniques to obtain an accurate Hall field. Foner et al[58] have shown that in ferromagnetic substances the Hall field can be represented by

$$E_H = \left[R_o H + 4\pi\alpha M R_1\right] J,$$

where R_o and R_1 are Hall coefficients, α is a field parameter, M is magnetization and J is current density. The quantity inside of the brackets is characteristic of the field intensity and temperature of the material. In all electrodiffusion and Hall field measurements a magnetic intensity of 18,000 gauss was employed. The Hall field at this magnetic field intensity was measured over a considerable temperature range on larger specimens that permitted such measurements. With these data obtained, the Hall field in an electrodiffusion sample could be determined by simply taking the current density ratio of the former Hall field (see Appendix E).

Alloys for this purpose were rolled from one-half inch Armco bar stock to a cross-section of 1 cm. by 0.095 cm. Eight-inch sections of rolled strip were placed in the carburizing tube furnace and carburized to a predetermined level of carbon; in the case of α iron 0.03 wt% carbon. Higher carbon content specimens were prepared for austenite Hall field determinations. These alloys were annealed and then examined for homogeneity. A three-wire thermocouple was

positioned along with an electric field voltage probe about 1 cm. from the thermocouple. Two Hall probes were also attached as indicated in Figure 17. This assembly was mounted between the poles of the magnet, clamped into place, and the system evacuated. Current was supplied by a Regent generator-rectifier unit. This unit was capable of providing up to a maximum of 400 D.C. amps. with a ripple of $\pm$5%. The current served as both an electric field source and a source of power for resistive heating of the sample. Current was, therefore, supplied to the specimen until the desired temperature was reached and then the magnetic field raised to 18,000 gauss. Simultaneous readings of temperature, electric field, magnetic field and Hall field were taken. The electric field was then reversed and the same readings taken. Reversing the magnetic field provided two more readings. The average of these four readings gave the Hall field at that temperature. These four readings were necessary in order that thermoelectric and thermomagnetic potentials be eliminated. The method is standard for measuring Hall fields and is fully described by Putley[59]

G. PHASE BOUNDARY DIFFUSION ANNEAL

Equation 55, relating the charge of the solute ion to the migration of the phase boundary, is valid only if the transformation involved is essentially volume diffusion controlled. This was checked for the $\alpha \rightarrow \gamma$ transformation in the temperature range between 738°C and 910°C. Carburized and

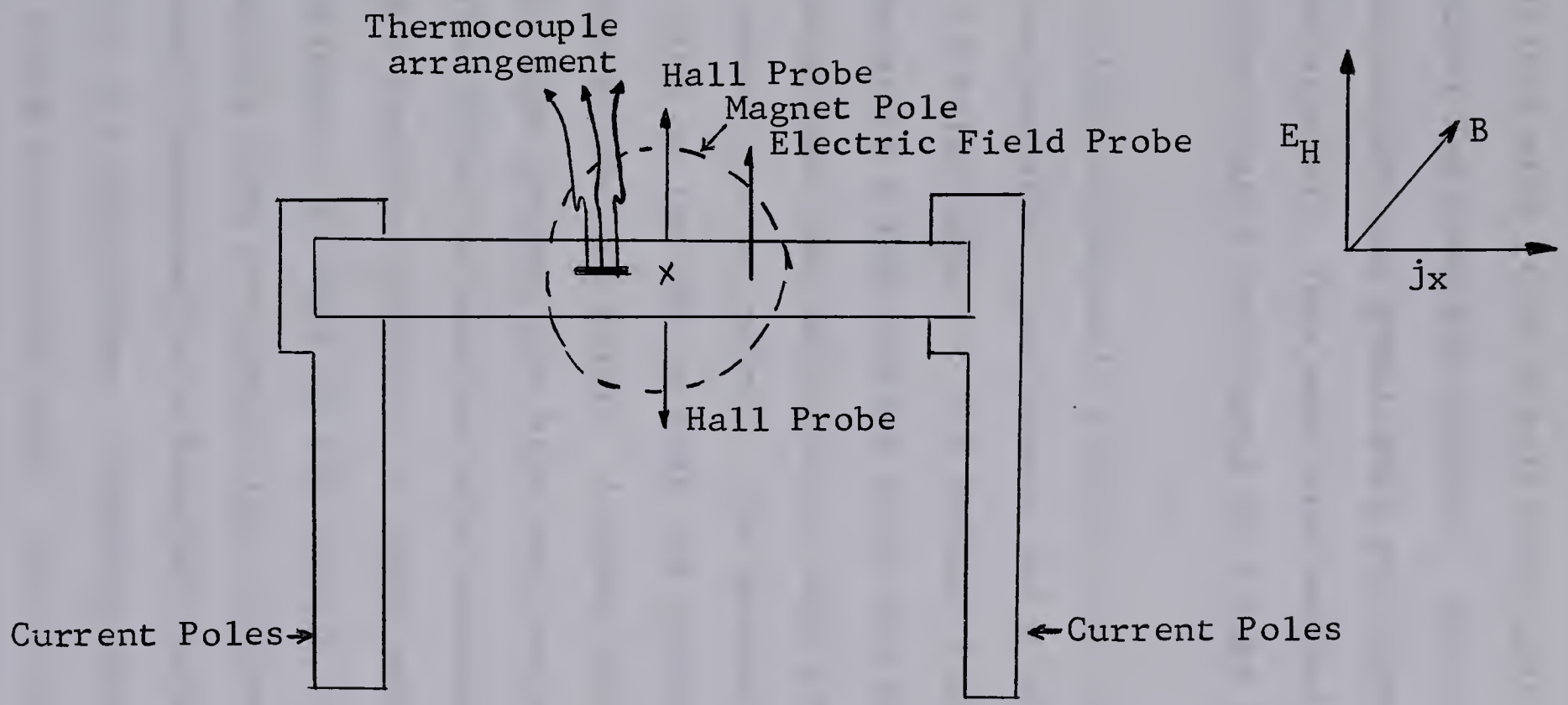

Figure 17. Schematic Diagram of Hall Field Measurement Assembly

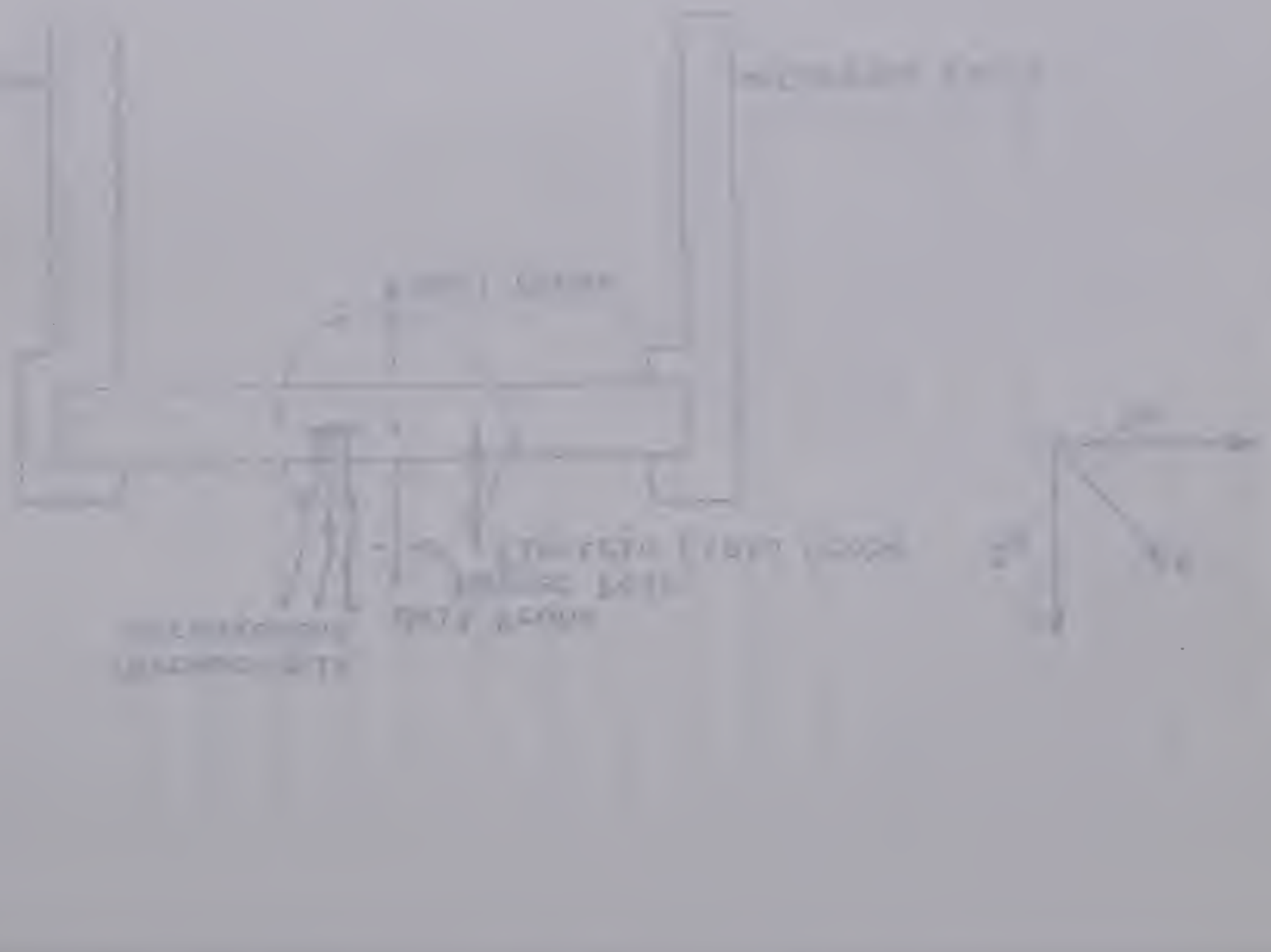

unalloyed circular sections of Armco iron (0.050 inch diameter) were polished with Linde B polishing grit, etched with nital and examined for possible defects. If no defects were found the cross-section was repolished and thoroughly cleaned with water and alcohol. They were then welded, cleaned mechanically, copper coated and placed in a tube furnace for annealing.

A high-low assembly powered the furnace, which consisted of two variable transformers and a relay. One transformer was set to relay power to the furnace sufficient to maintain the temperature a few degrees below the set point, while the other transformer was adjusted to hold the temperature a few degrees above the set point. The Honeywell controller selected the high or low set so that the temperature was maintained very close to the set point. A power differential of about 50 watts was kept between the high and low set.

The diffusion couples were suspended in an alundum boat and a positive pressure of argon maintained throughout the experiment. As well as the control thermocouple temperature readings from the controller, another chromel-alumel thermocouple connected to a Honeywell potentiometer was used to monitor the temperature. Readings were taken every 1/2 hour to check the control unit. Four annealing temperatures were used: 752°C, 809°C, 842°C and 870°C. In every case the temperature was maintained to within $\pm 2^{\circ}$C. of the predetermined anneal temperature. At successive time intervals the couples

were removed from the furnace, mounted in a bakelite mold, polished and etched with nital. The distance from the original weld to the phase boundary was measured by the calibrated filar unit scale of a Tukon microscope. After each determination, the couple was re-coated with copper and annealed in the tube furnace. The migration distance was plotted as a function of the square root of time.

RESULTS

A. MICROHARDNESS CALIBRATION CURVES

The effect of the solutes, carbon and nitrogen on the hardness of iron, is given in Figures 18 and 19, respectively. The results are not reported in terms of microhardness numbers but rather indentation diagonal lengths as length-units are more convenient in the present investigation. Conversion to microhardness units Kgm/mm^2 may be made by the relationship

$$H_m = \frac{VP}{d^2} \quad ,$$

where H_m is the diamond pyramid number, V is a constant that depends upon the geometry of the indentor, 1854.4 in the case of the indentor used in this investigation, P is the load (35.5 grams) and d is the indentation diagonal length in millimeters. Soaking temperatures within $\pm 100^{\circ}C$. of the mean annealing temperature were found to have little or no effect on the calibration curves for carbon and nitrogen solutes. Also investigated, was the effect of soaking time on hardness and soaking times up to 2 hours were found to have little effect on hardness values between 0.1 wt% and 0.6 wt% solute. Below 0.1 wt% solute, martensite colonies appeared among the ferrite grains giving some scatter to the indentation values.

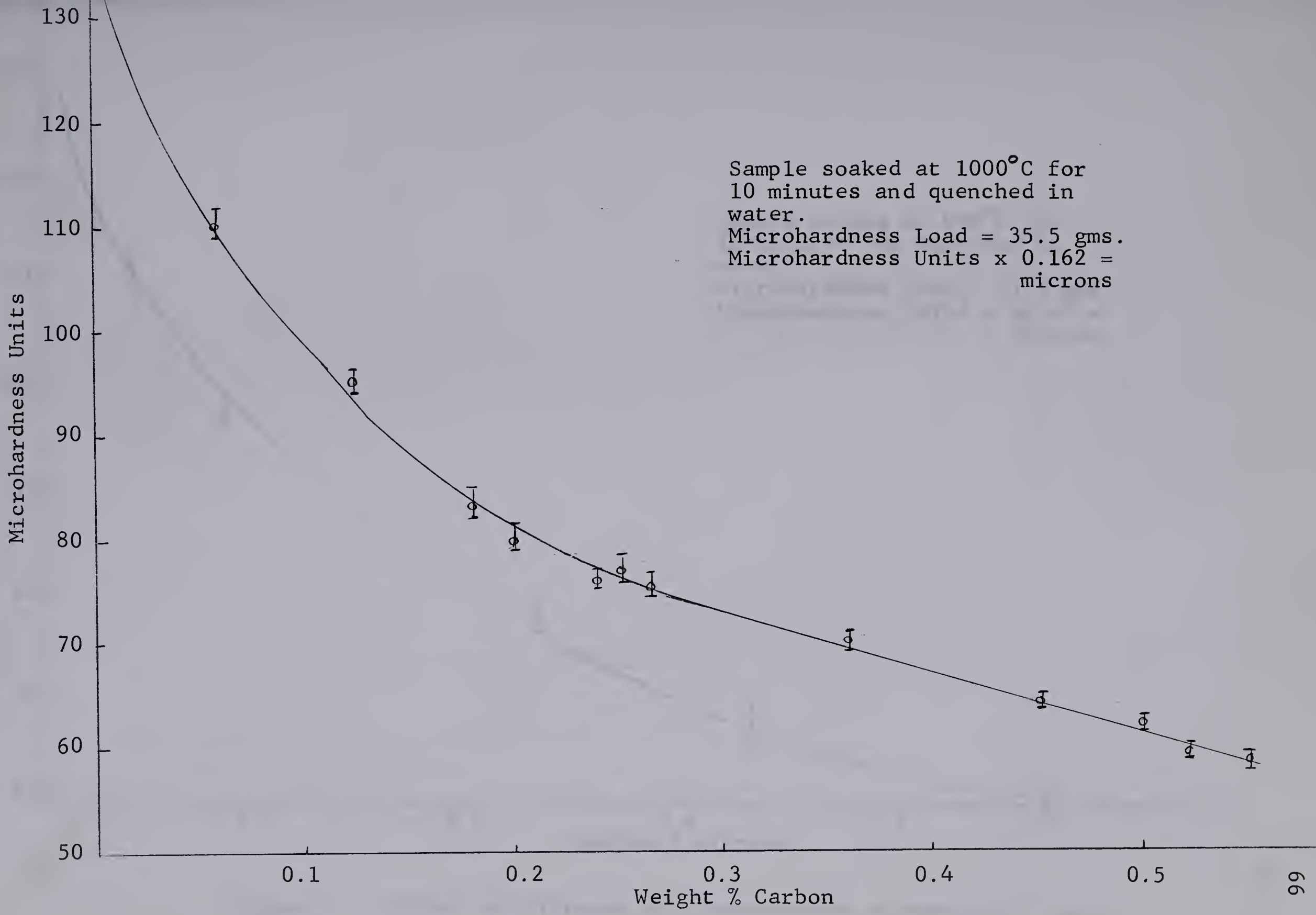

Figure 18. Effect of Carbon on the Microhardness of Martensite

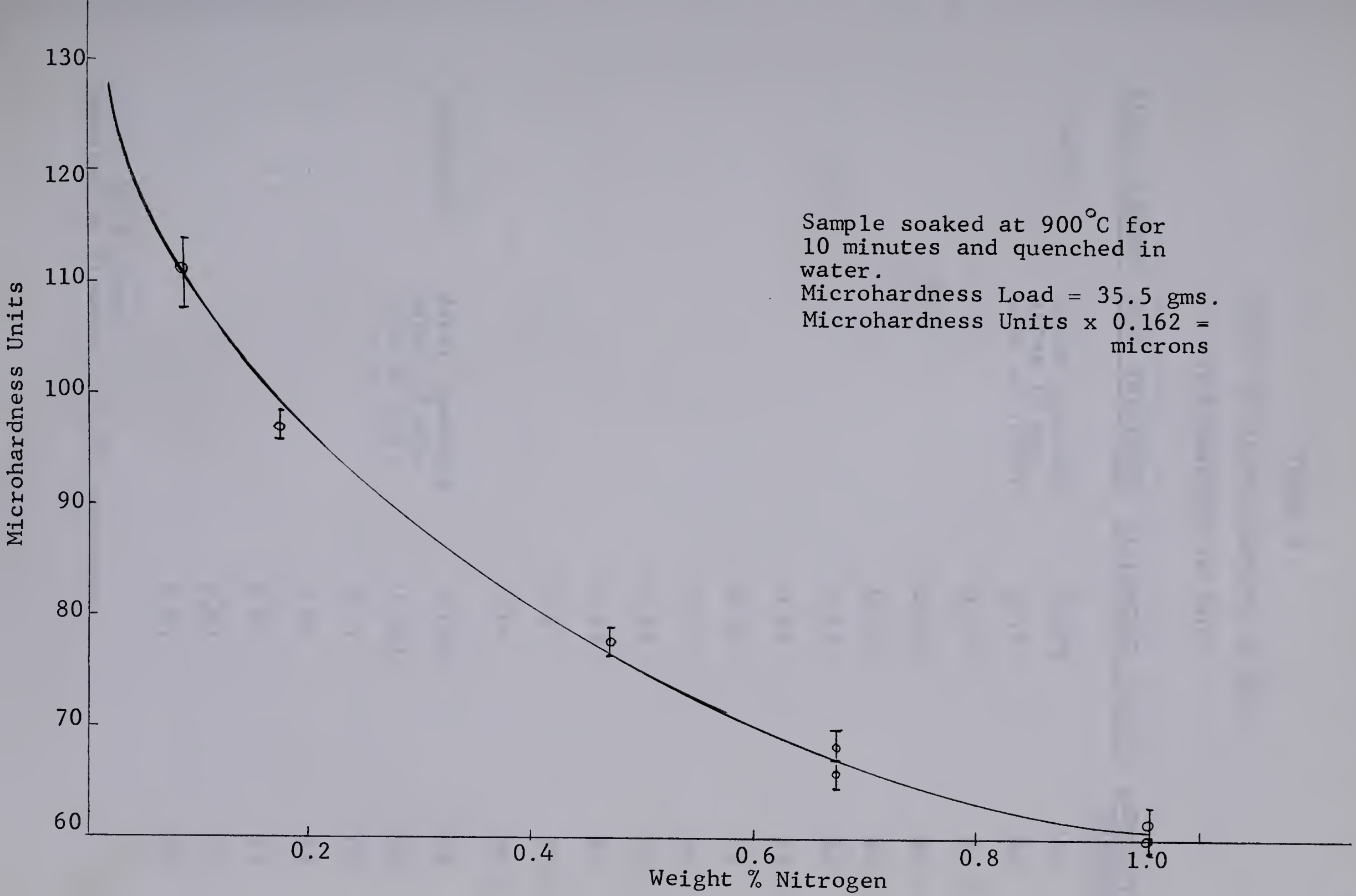

Figure 19. Effect of Nitrogen on Microhardness of Martensite Iron

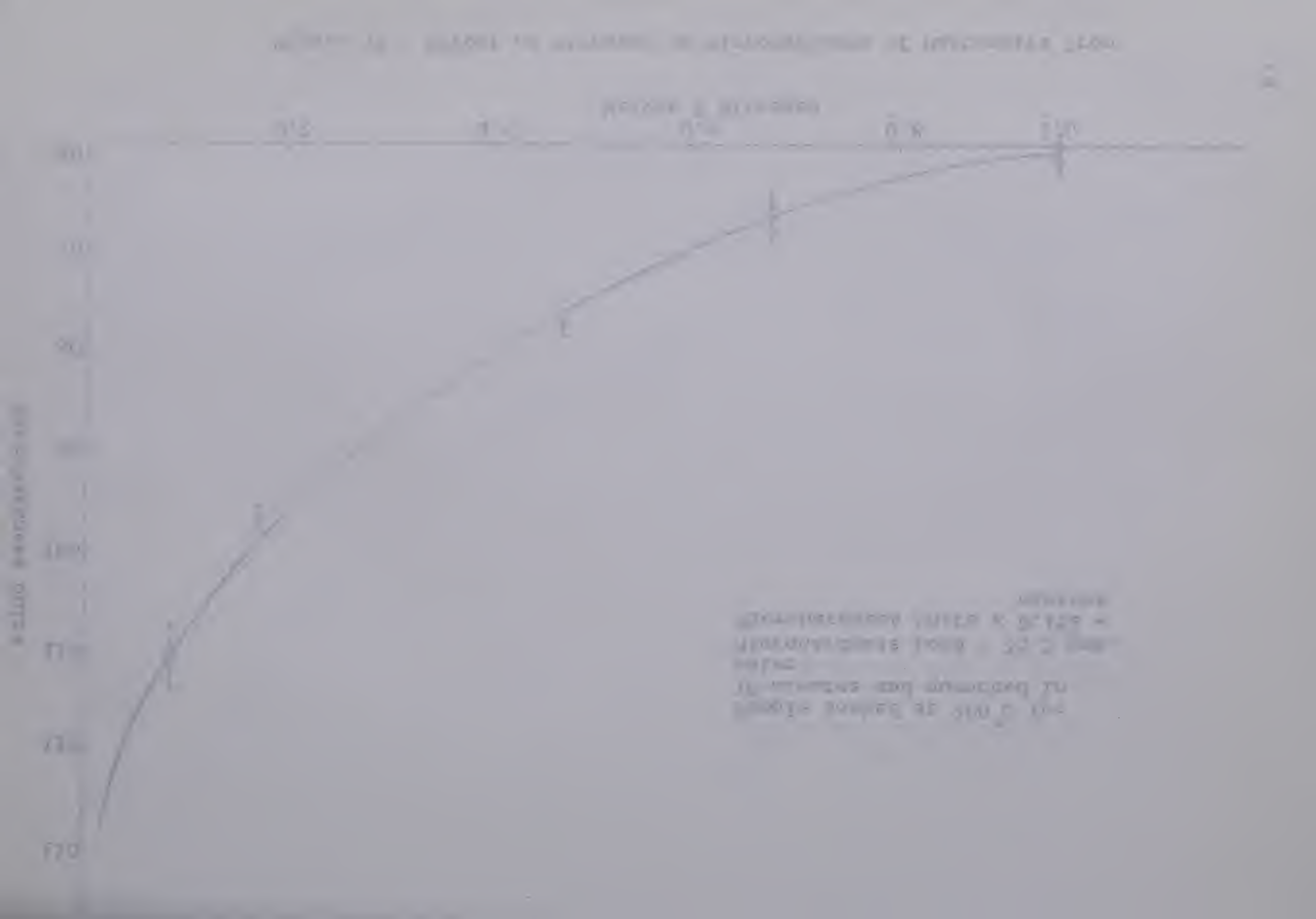

TABLE I

EFFECT OF ALLOY ELEMENTS ON THE

MICROHARDNESS OF IRON

ALLOY ELEMENT	HEAT TREATMENT	WT.PERCENT SOLUTE	INDENTATION DIAMETER
CARBON	Water quenched after 10 minutes at 1000°C	0.009	142
		0.17	86
		0.19	85.5
		0.19	86.5
		0.23	80
		0.25	80
		0.26	83.5
		0.36	72
		0.45	66
		0.50	62.5
		0.53	60
		0.55	59.5
		0.64	56.5
NITROGEN	Water quenched after 10 minutes at 950°C	0.000	142
		0.080	118
		0.17	102
		0.46	83
		0.67	73
		0.67	74
		0.95	65

Load - 35.5 grams
Indentation diameter x 0.162 = microns

B. DIRECT ELECTRIC FIELD MOBILITY

The penetration curves for combined chemical diffusion and electrodiffusion are given in Figures 20 to 22. There are two penetration curves for each sandwich diffusion couple, one curve representing diffusional flow enhanced by electromigration and the other representing diffusional flow decreased by electromigration. These traverses are parallel to both the direction of diffusion and electromigration. The weld interfaces were located metallographically and the indentation measurements referenced to the weld. Table II summarizes the results of calculations giving the charge of nitrogen in iron at various temperatures. The mobility (velocity per unit field) appears in Column 3 and is used to obtain the effective charge appearing in Column 5. C, in the footnotes, refers to the initial alloy concentration in the diffusion couple. Published diffusion constants contained in the footnotes were used in the charge calculations since the diffusion constants obtained by the "Grube method" in Column 4 do not possess sufficient accuracy to warrant use. These diffusion constants were nevertheless determined as approximate check on the experimental soundness of the techniques used (see Appendix C).

Similar results for the migration of carbon in austenite are shown in Figures 23 to 25. The results are summarized in Table III. Microhardness data for the penetration curves are tabulated in Appendix D.

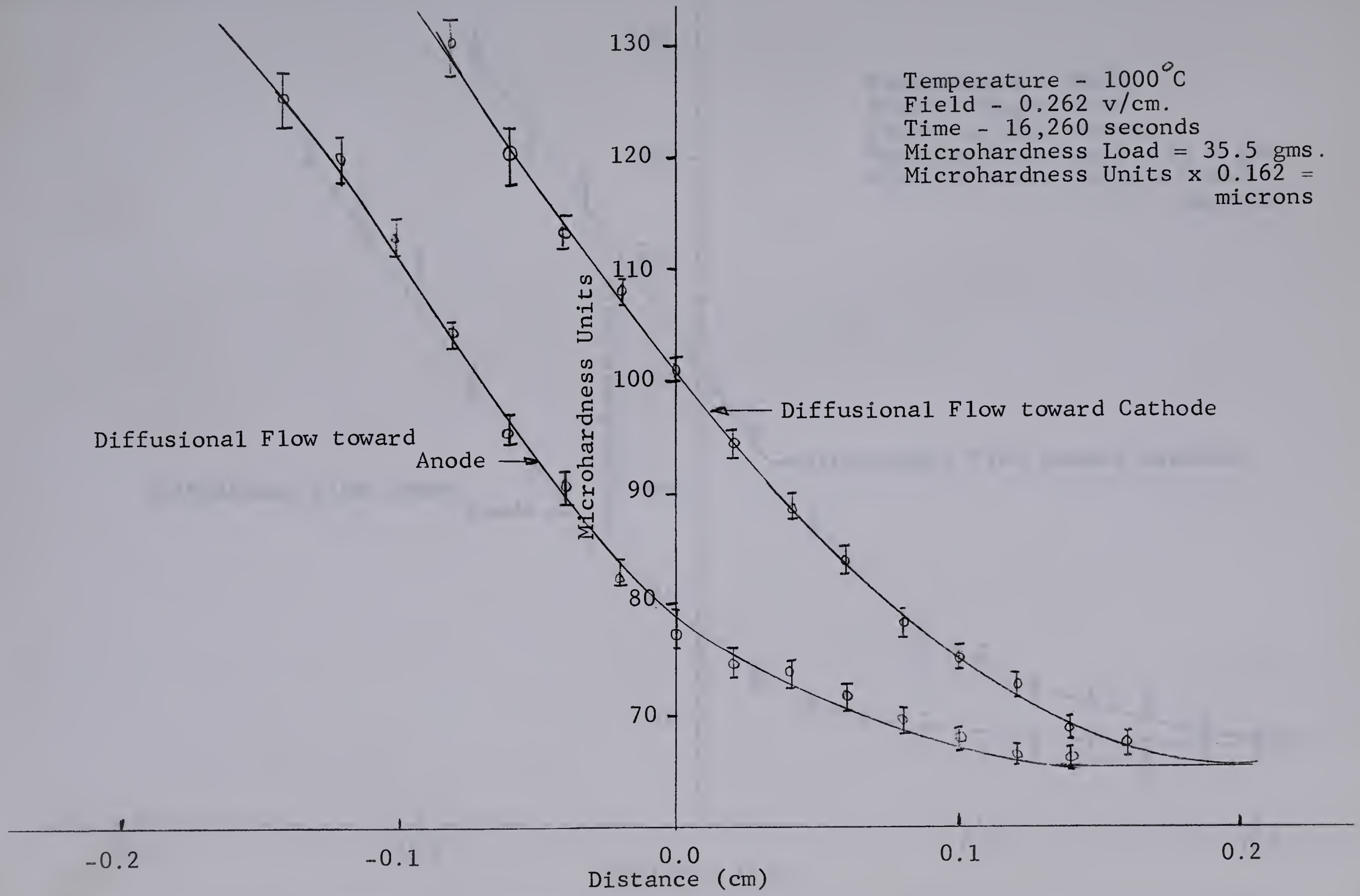

Figure 20. Nitrogen Penetration Curve Represented in Microhardness Units (1000°C)

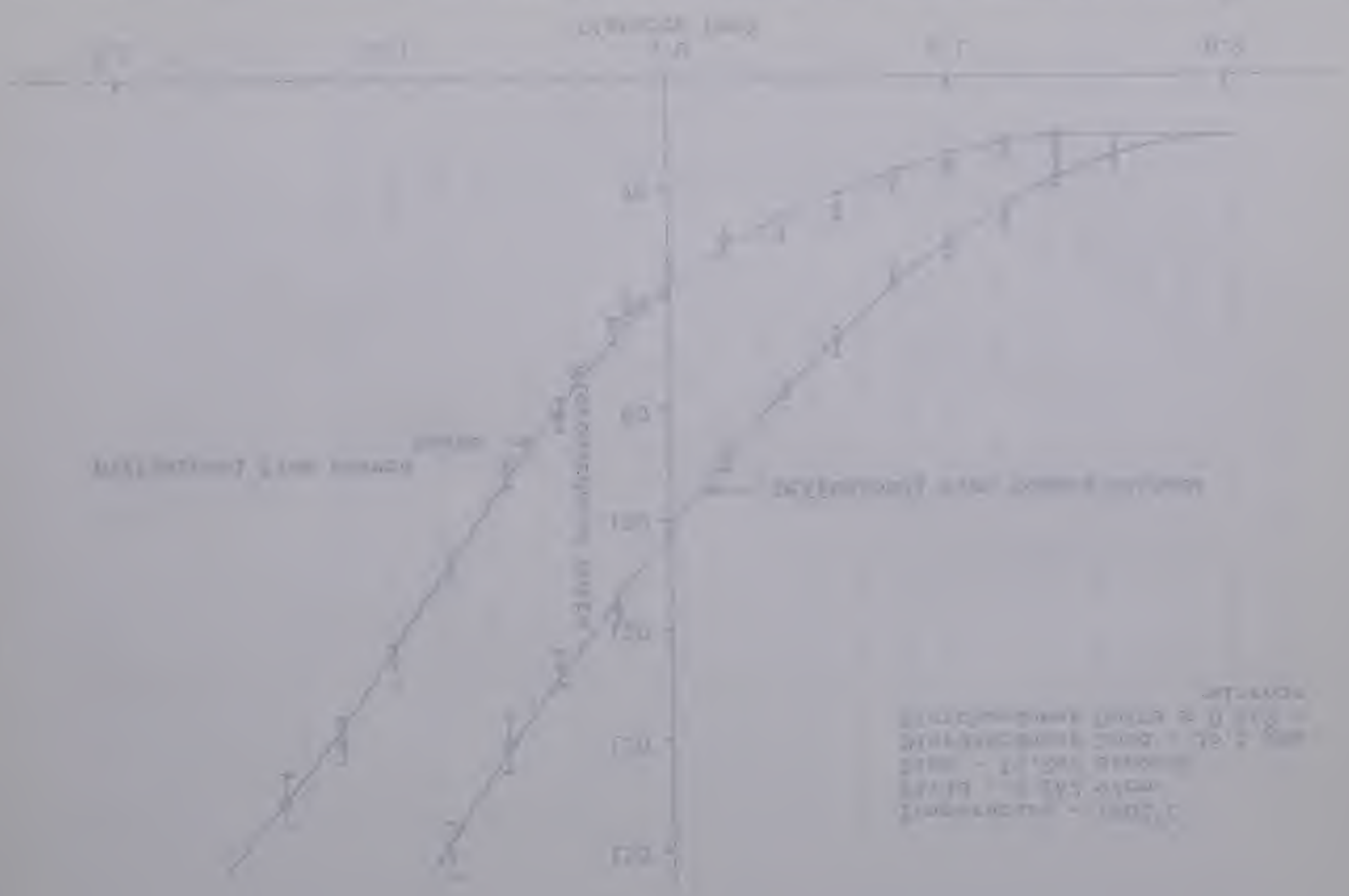

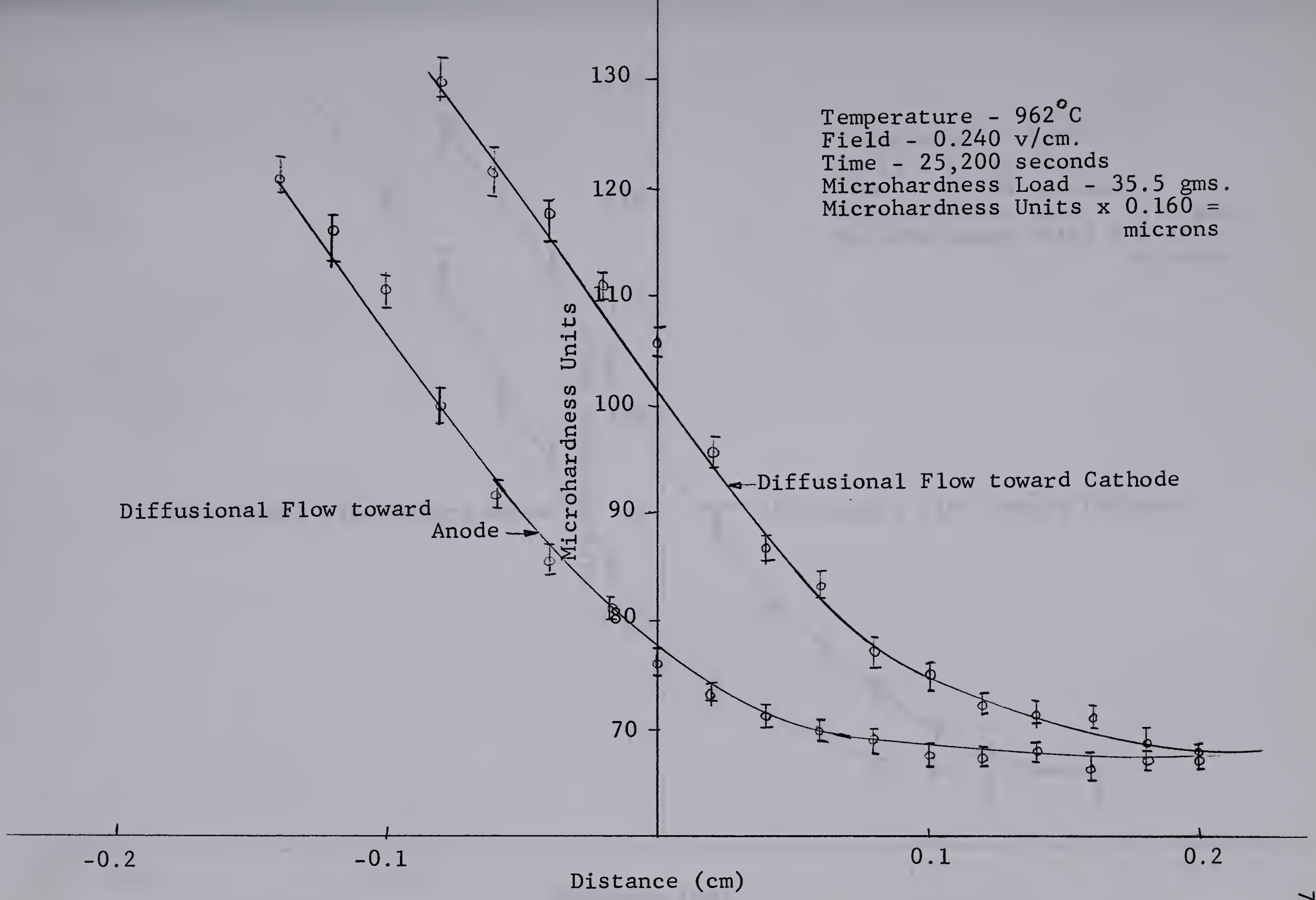

Figure 21. Nitrogen Penetration Curve Represented in Microhardness Units(962°C)

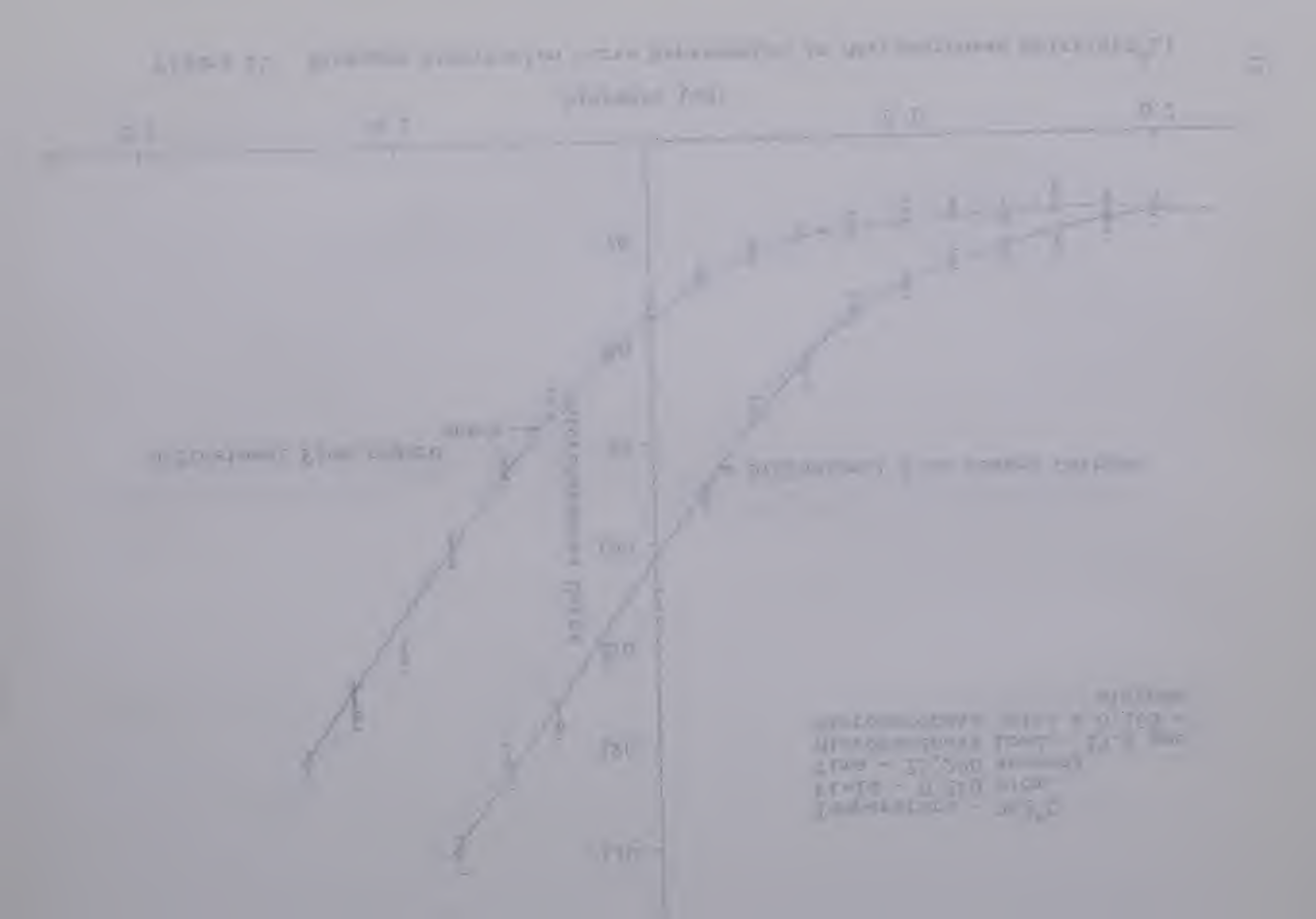

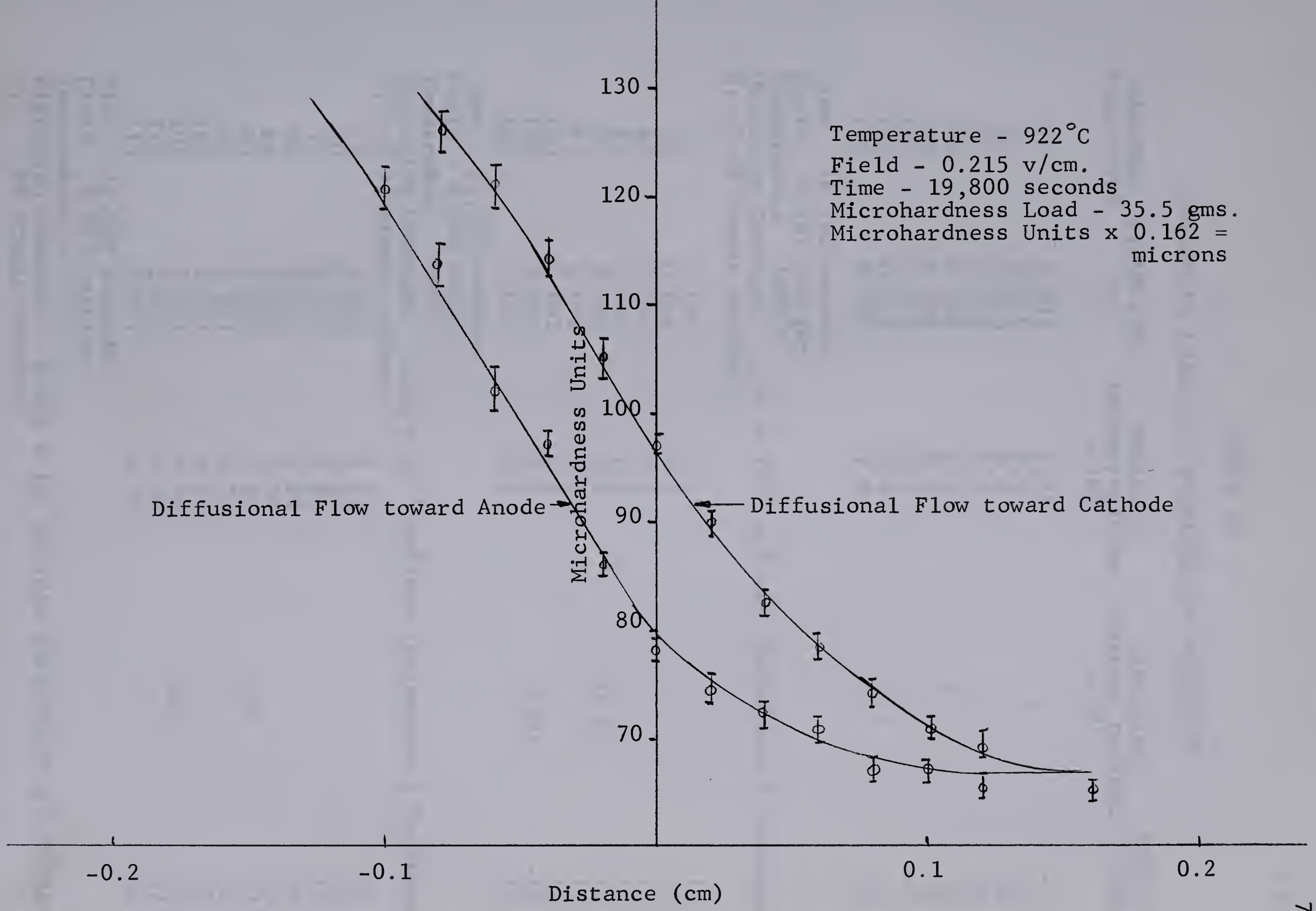

Figure 22. Nitrogen Penetration Curve Represented in Microhardness Units(922 C)

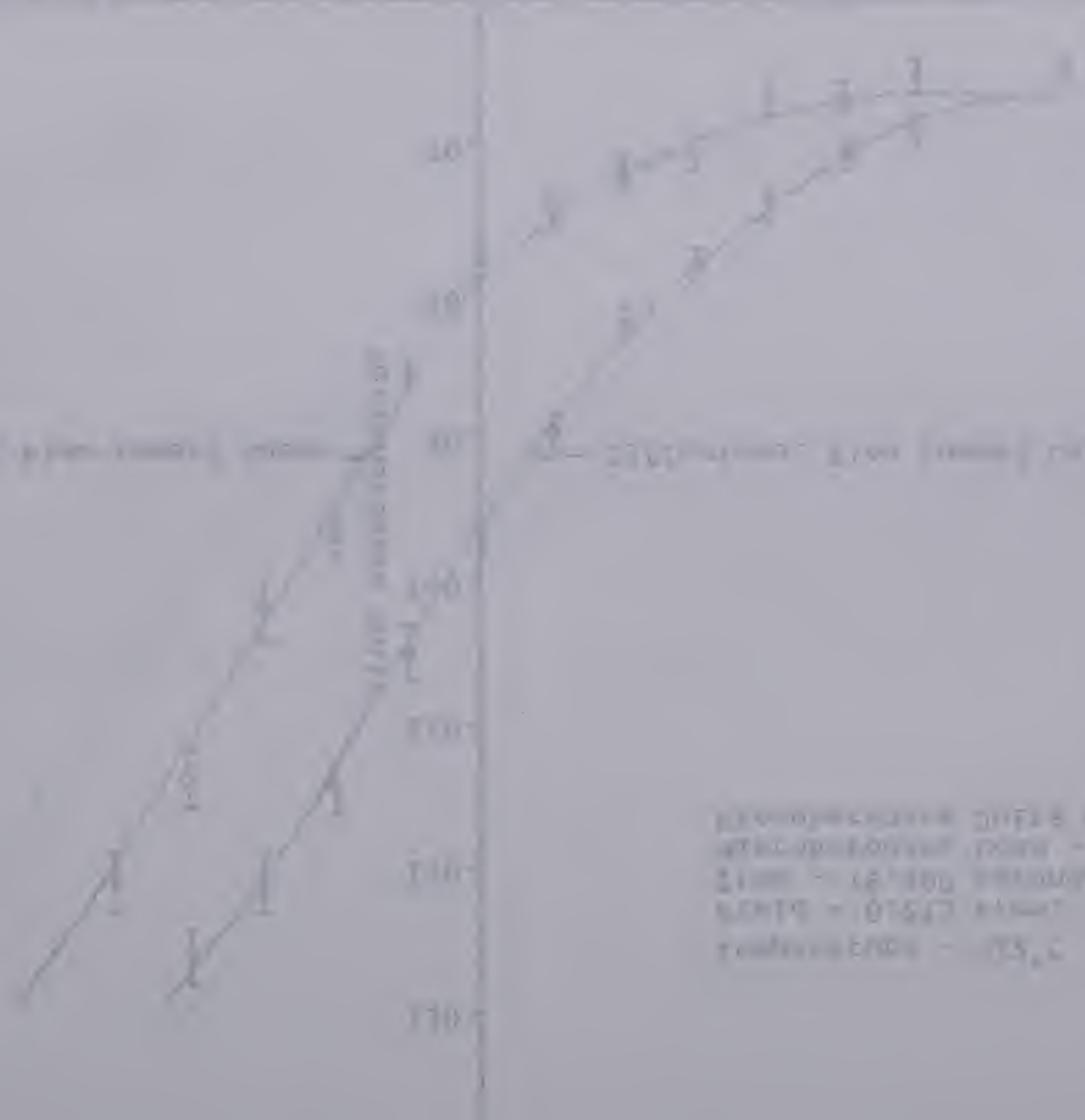

TABLE II

EFFECTIVE CHARGE OF NITROGEN IN AUSTENITE

HARDNESS DIAG.UNITS	FIELD DIST. cm.	MOBILITY Cm/sec/volt/cm x 10^6	DIFFUSION Constant cm^2/sec x 10^7	EFFECTIVE CHARGE
70	0.031	7.25		-7
75	0.040	9.4		-9
80	0.040	9.4		-9
85	0.038	9.0		-8.6
90	0.036	8.4	1	-8.1
95	0.036	8.4		-8.1
100	0.035	8.2		-7.9
110	0.032	7.4	1.3	-7.2
115	0.030	7.0		-6.8

Time - 16,260 seconds.
Field - 0.262 volt/cm.
Temperature - 1000°C.
Diffusion Constant - 1.14×10^{-7} cm^2/sec.(Grieveson & Turkdagon).
C_1 -2.92 Atomic percent.

70	0.048	7.9		-12.8
75	0.046	7.7		-12.5
80	0.044	7.3		-11.9
85	0.042	7.3		-11.9
90	0.042	6.8	0.75	-11.2
95	0.042	6.8		-11.2
100	0.042	6.8		-11.2
105	0.040	6.6	0.60	-10.8
110	0.040	6.6		-10.8

Time - 25,200 seconds.
Field - 0.240 volt/cm.
Temperature - 962°C.
Diffusion Constant - 0.65×10^{-7} cm^2/sec.(Grieveson & Turkdagon).
C_1 - 2.92 Atomic percent.

65	0.025	5.85		-15.4
70	0.025	5.85		-15.4
75	0.025	5.85		-15.4
80	0.024	5.60		-14.7
85	0.022	5.20		-13.5
90	0.022	5.20	0.3	-13.5
95	0.021	4.70		-12.8
100	0.021	4.70		-12.8
105	0.021	4.70	0.45	-12.8
110	0.021	4.70		-12.8
115	0.021	4.70		-12.8

Time - 19,800 seconds.
Field - 5.215 volt/cm.
Temperature - 922°C.
Diffusion Constant - $0.392 \times 10^{-7} cm^2/sec$.(Grieveson & Turkdagon).
C_1 - 2.92 Atomic percent.

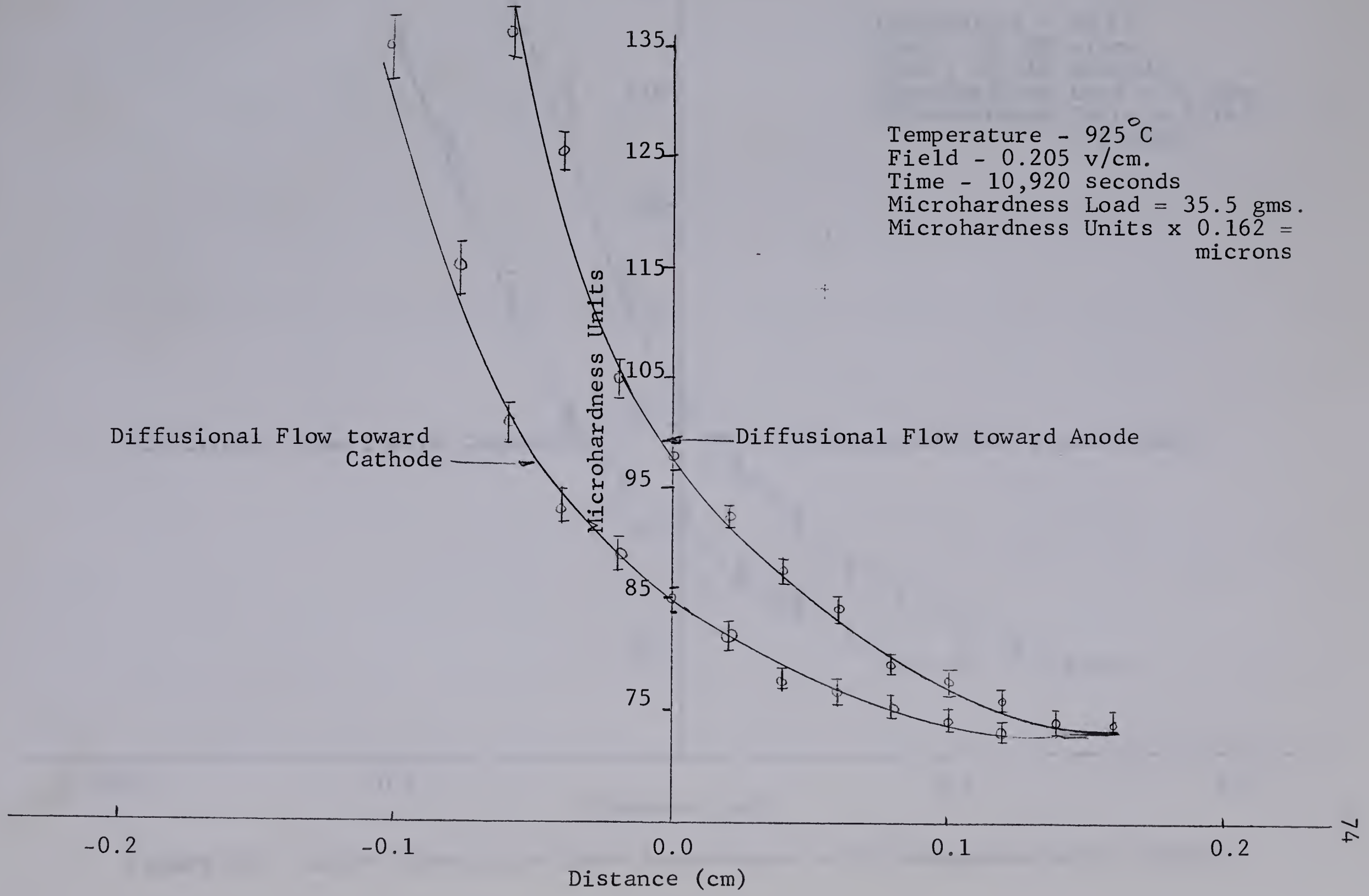

Figure 23. Carbon Penetration Curve Represented in Microhardness Units (925°C)

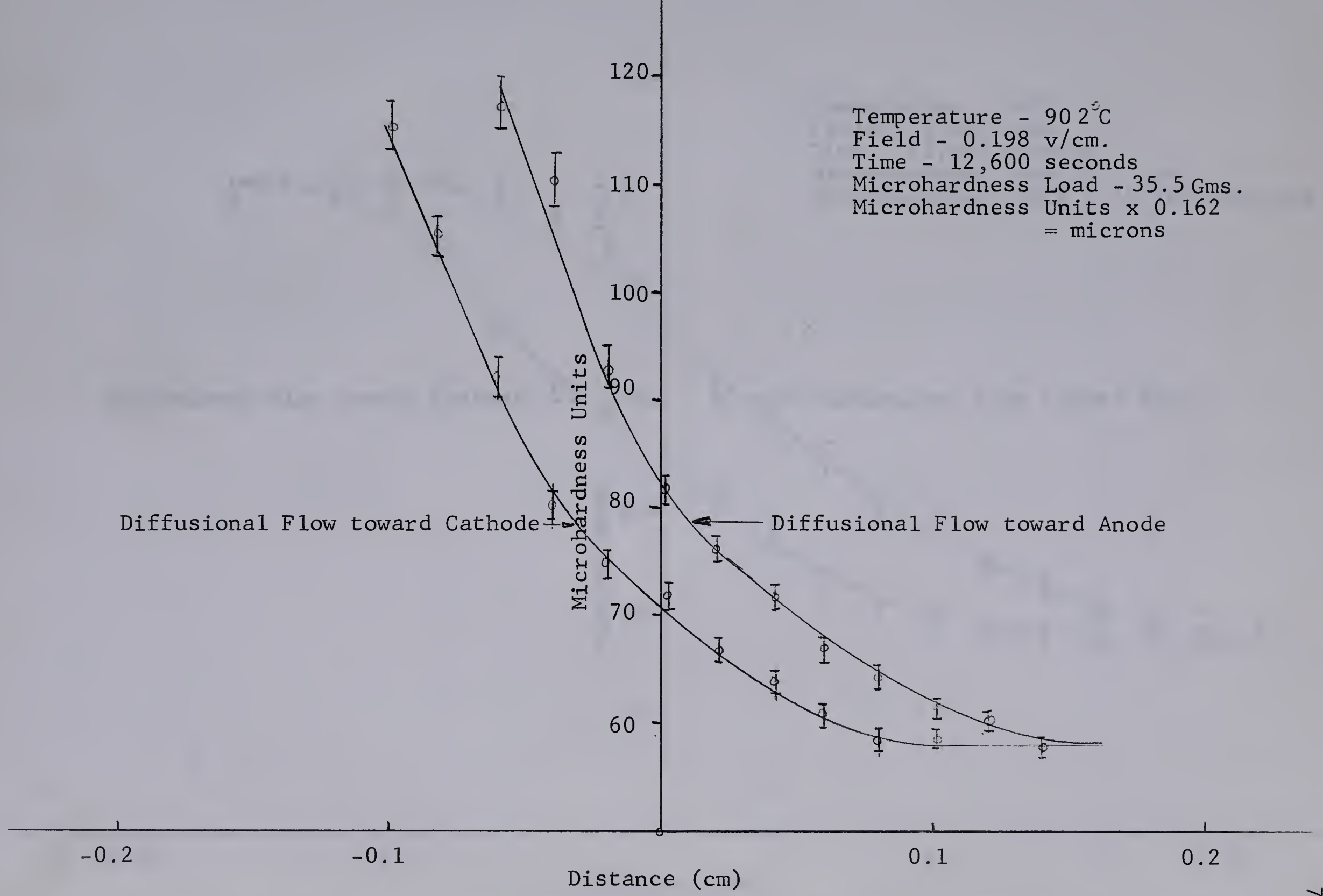

Figure 24. Carbon Penetration Curve Represented in Microhardness Units (902°C)

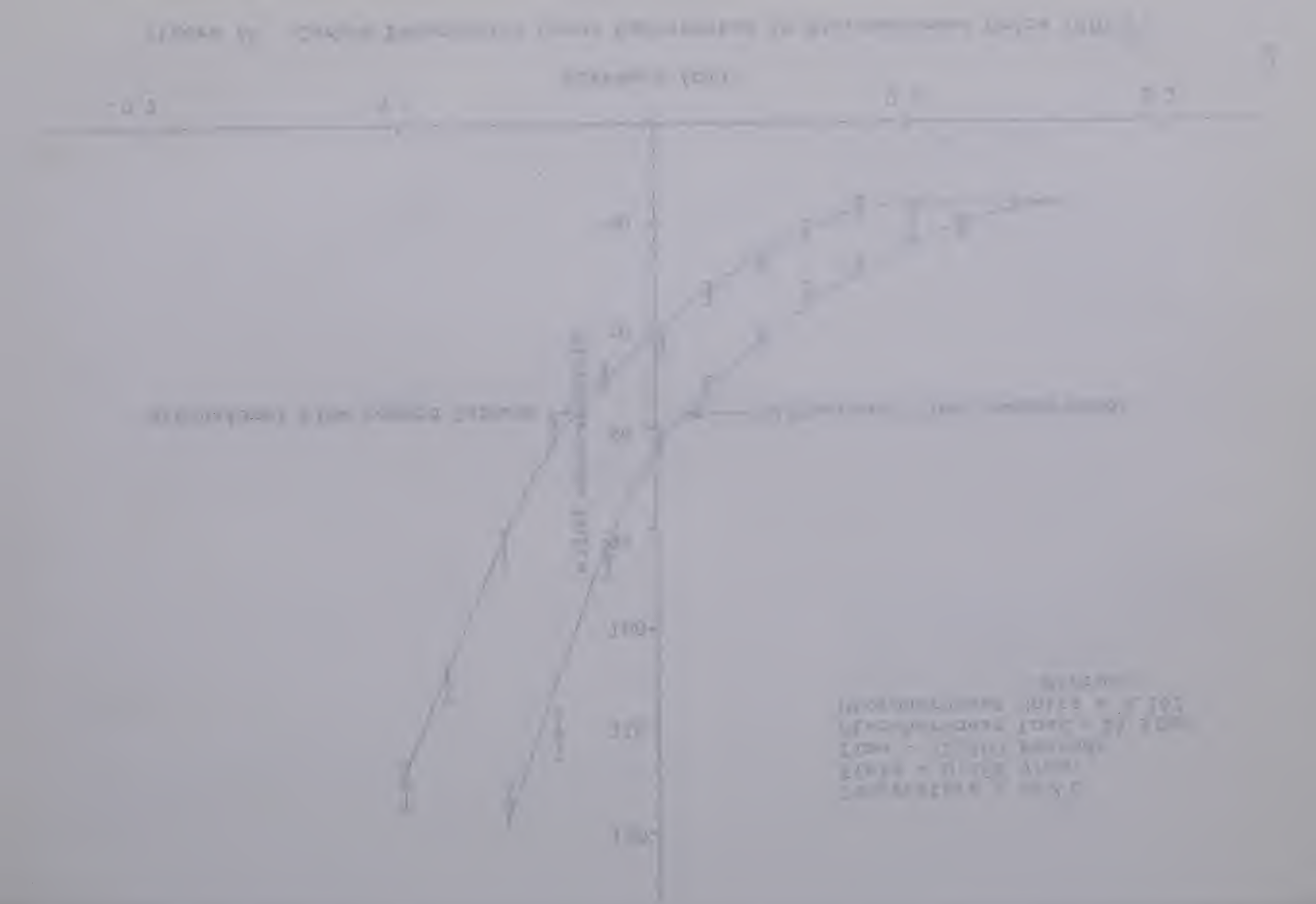

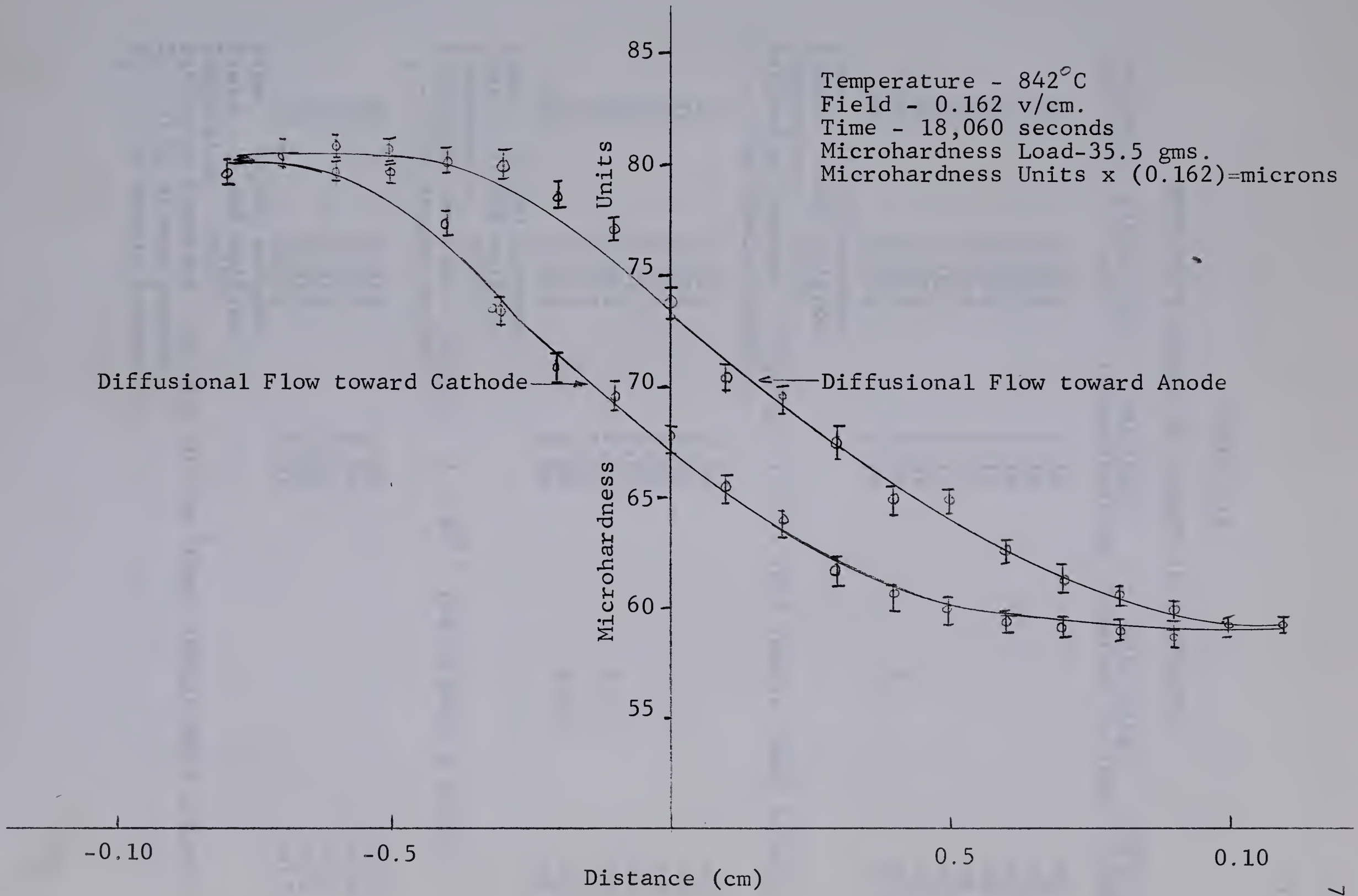

Figure 25. Carbon Penetration Curve Represented in Microhardness Units (842°C)

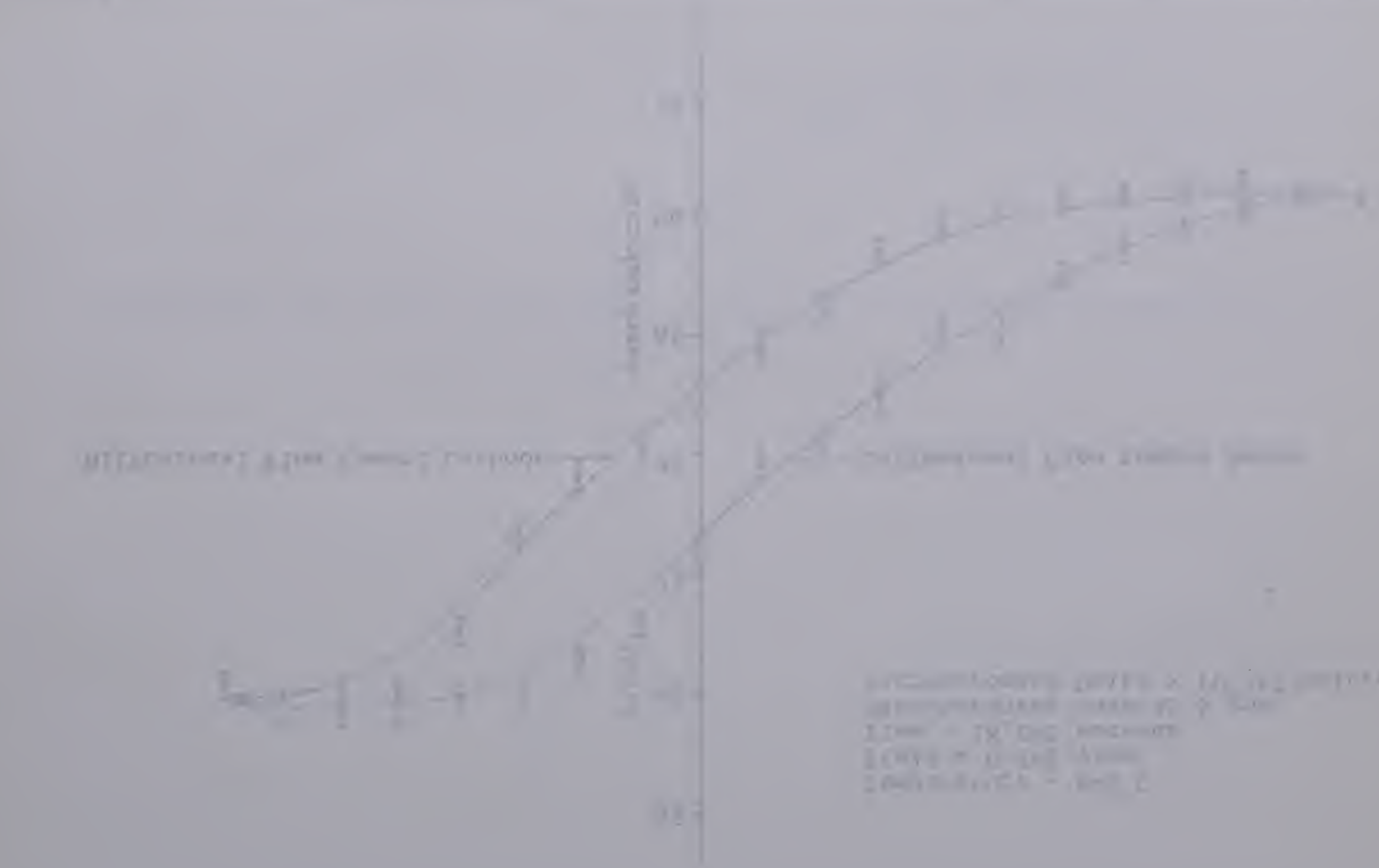

TABLE III

EFFECTIVE CHARGE OF CARBON IN AUSTENITE

HARDNESS DIAG.UNITS	FIELD DIST. cm.	MOBILITY Cm/sec/volt/cm	DIFFUSION Constant cm^2/sec	EFFECTIVE CHARGE
65	0.025	1.11		+8.5
70	0.026	1.16		+8.9
75	0.026	1.16		+8.9
80	0.026	1.16		+8.9
85	0.028	1.25		+9.6
90	0.026	1.16		+8.9
95	0.024	1.07		+8.2
100	0.022	0.99	1.5	+7.6
105	0.022	0.99		+7.6

Time - 10,920 seconds.
Field - 0.205 volt/cm.
Temperature - 925°C.
Diffusion Constant - $D_{925°C}$ - 1.36×10^{-7} (Wells, Mehl & Batz).
C_1 - 2.44 Atomic percent.

65	0.024	0.96		+9.7
70	0.024	0.96		+9.7
75	0.020	0.80		+8.1
80	0.020	0.80		+8.1
85	0.021	0.84	1.1	+8.5
90	0.022	0.88		+8.9
95	0.022	0.88	0.75	+8.9
100	0.022	0.89		+8.9

Time - 12,600 seconds.
Field - 0.198 volt/cm.
Temperature - 902°C.
Diffusion Constant - $D_{902°C}$ - 1×10^{-7} (Wells,Mehl & Batz).
C_1 - 2.44 Atomic percent.

60	0.017	0.58		+14.6
65	0.017	0.58		+14.6
70	0.015	0.51		+12.8
75	0.014	0.48		+12
77.5	0.015	0.51		+17.8

Time - 18,060 seconds.
Field - 0.162 volt/cm.
Temperature - 842°C.
Diffusion Constant - 0.39×10^{-7} $cm.^2$/sec. (Wells,Mehl & Batz).
C_o - 0.82 Atomic percent.
C_1 - 2.44 Atomic percent.

C. HALL FIELD MOBILITY

The boundary shift associated with Hall field electromigration in iron-carbon alloys is shown in Figure 26. Distances were referenced to the copper iron interface in the investigation and are transposed to the centerline in the figure. The original position of the boundary is shown along with the shifted position after a 24-hour anneal. This distance is related to charge through equation 55. The equilibrium concentrations C_{20} and C_{10} were taken from the phase diagram of Darken and Gurry[60] and diffusion constant data obtained from the investigation of Smith.[61] A sample calculation is given in Appendix E.

The results of two such experiments are given in Table IV. Since many measurements can be made from any one anneal, several polishes throughout the couple are reported. The distance migrated is the average of several measurements, usually twenty-five or more. The second run, reported in Table IV, does not contain the accuracy of the first because of the much shorter anneal time.

Figure 27 illustrates the migration shift associated with an iron-nitrogen phase boundary anneal under a Hall field. The results of this and a duplicate run are given in Table V. The equilibrium concentration C_{10} and C_{20} were obtained from the investigation of Paranjpe et al.[62] Diffusion data were selected from the published work of Grieveson.[63]

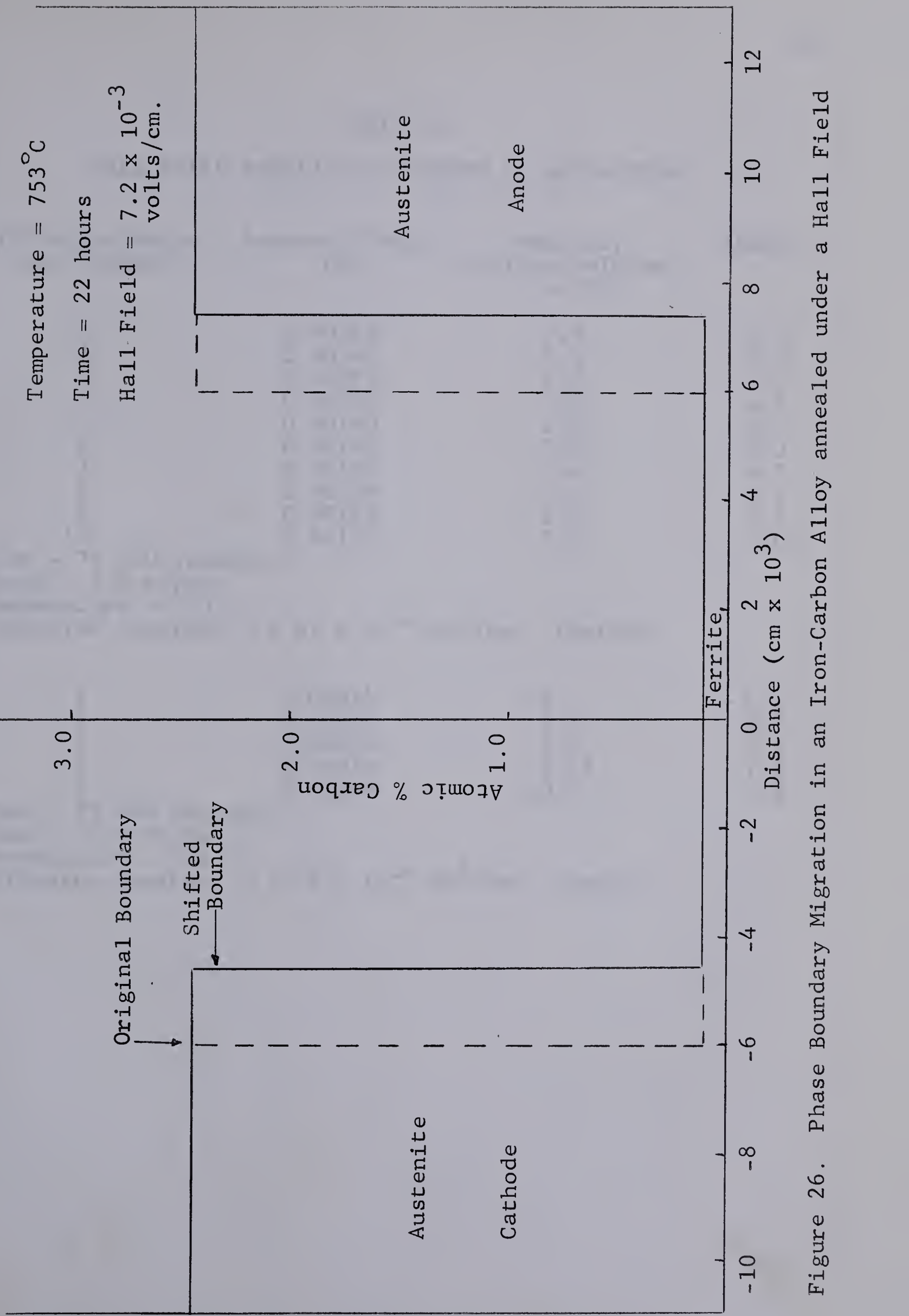

Figure 26. Phase Boundary Migration in an Iron-Carbon Alloy annealed under a Hall Field

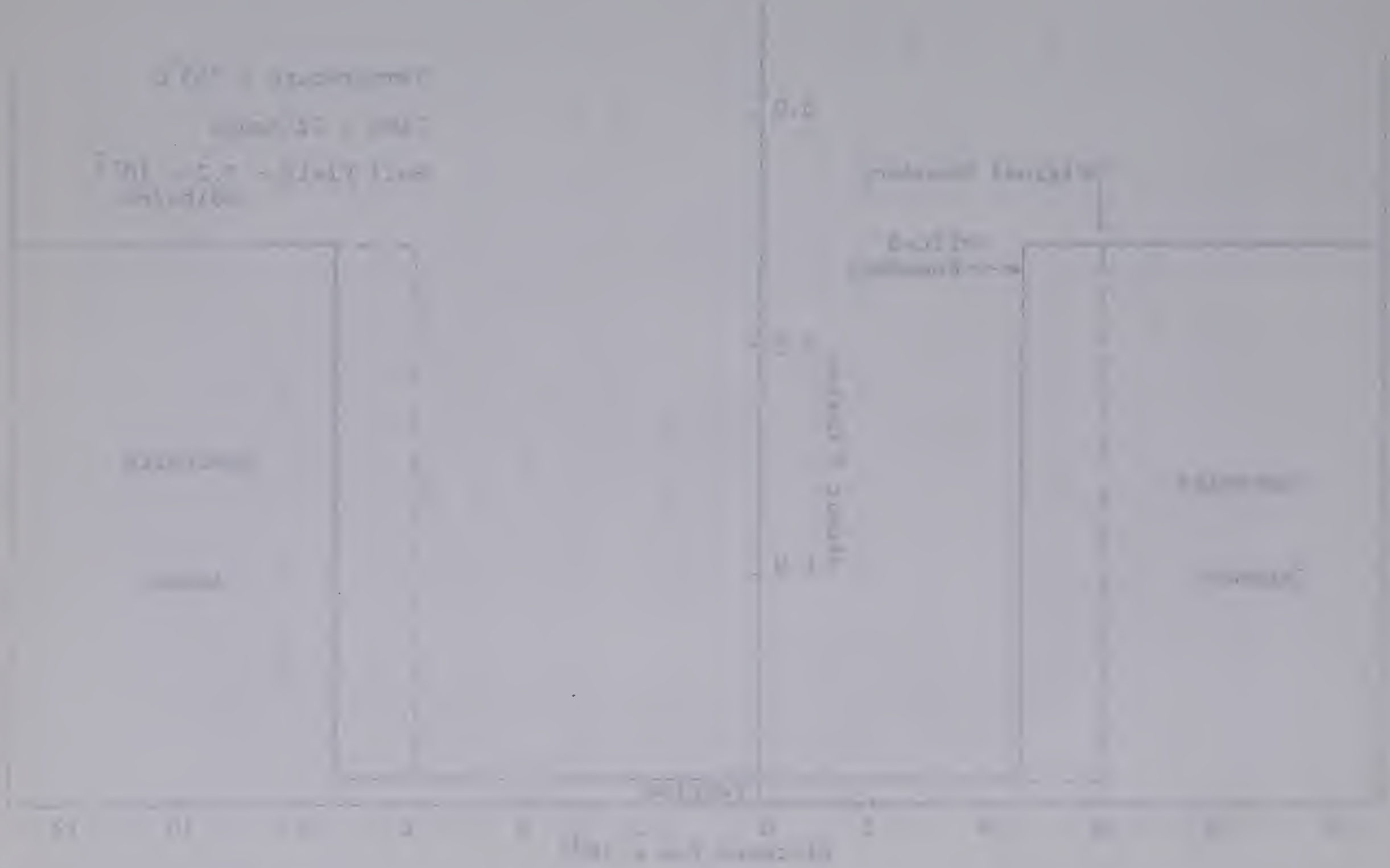

TABLE IV

HALL FIELD MOBILITY OF CARBON IN ALPHA-IRON

Diffusion Couple Layer Number	Boundary Shift Cm.	Mobility Cm/sec/volt/cm. x 10^5	Charge
1	0.00147	7.0	+ 3.9
2	0.00147	8.5	4.7
3	0.00191	9.2	5.1
4	0.00156	7.6	4.2
5	0.00160	7.8	4.3
6	0.00162	7.8	4.3
7	0.00154	7.4	4.1
8	0.00186	7.2	4.9
9	0.00192	8.2	5.1
10	0.00152	7.2	4.0

Time - 79,200 seconds.
Field - 7.2 mv/cm.
Temperature - 753 C.
Diffusion Constant - 1.61×10^{-6} cm^2/sec. (Smith).

1	0.00074	11	+ 6.1
2	0.00037	5.5	3.0
3	0.00050	7.7	4.3
4	0.00015	2.25	1.3
5	0.00069	10.4	5.8

Time - 25,200 seconds.
Field - 7.4 mv/cm.
Temperature - 750 C.
Diffusion Constant - 1.59×10^{-6} cm^2/sec. (Smith).

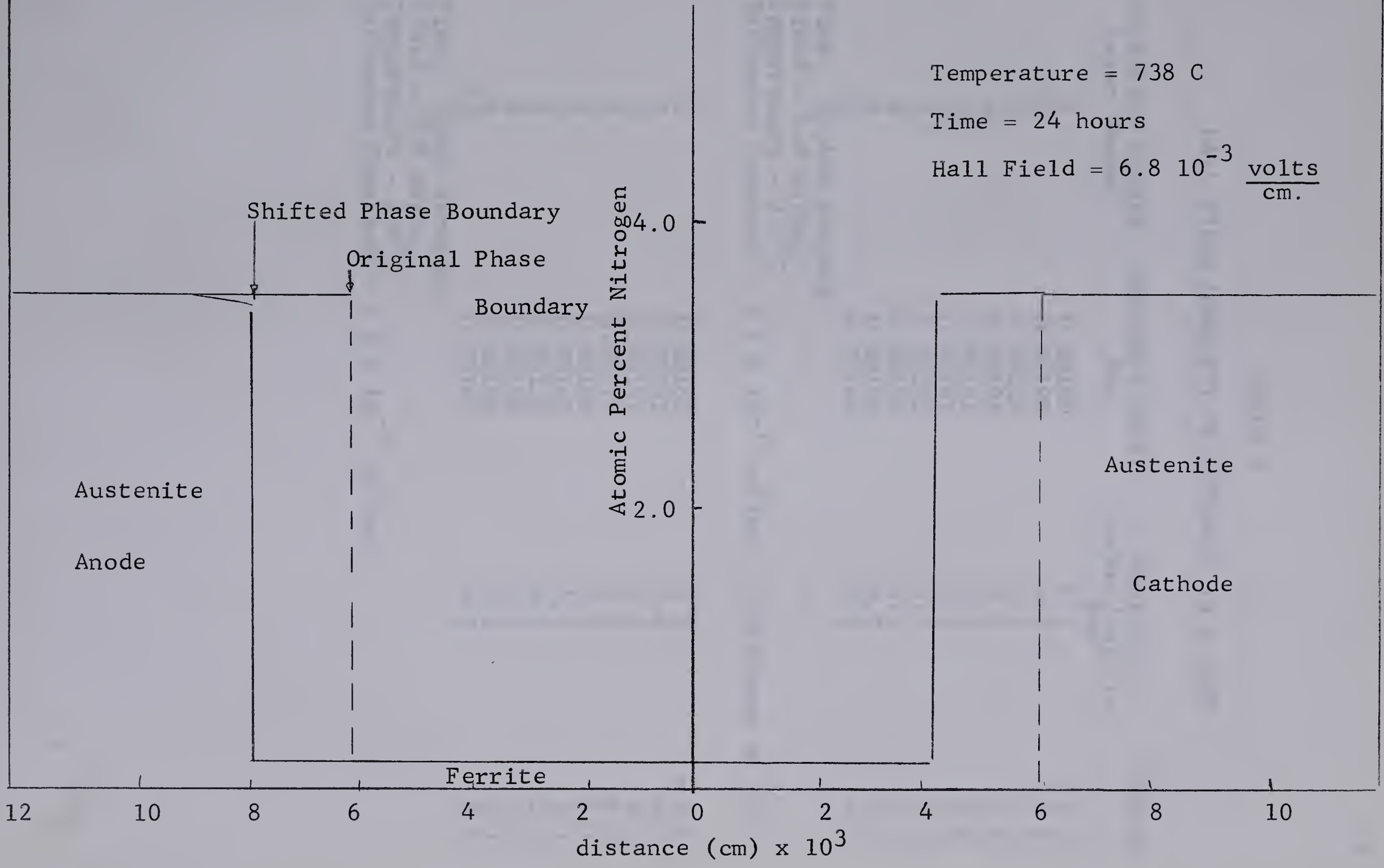

Figure 27. Phase Boundary Migration in an Iron-Nitrogen Alloy annealed under a Hall Field

TABLE V

HALL FIELD MOBILITY OF NITROGEN IN ∝ IRON

Diffusion Couple Layer Number	Boundary Shift Cm.	Mobility Cm/sec/volt/cm. $\times 10^5$	Charge
1	0.00180	4.5	+5.3
2	0.00198	4.9	5.8
3	0.00222	5.7	6.5
4	0.00198	4.9	5.8
5	0.00192	4.8	5.6
6	0.00182	4.5	5.3
7	0.00222	5.7	6.5
8	0.00190	4.7	5.5
9	0.00154	4.0	4.7
10	0.00144	3.8	4.4

Time - 86,400 seconds.
Field - 6.8 mv/cm.
Temperature - 734°C.
Diffusion Constant - 7.1×10^{-7} cm^2/sec. (Turkdogan et al).

1	0.00168	4.9	+5.8
2	0.00192	5.6	6.5
3	0.00192	5.6	6.5
4	0.00178	5.2	6.0
5	0.00196	5.8	6.7
6	0.00142	4.4	5.1
7	0.00150	4.5	5.3
8	0.00108	4.9	5.6
9	0.00196	5.8	6.7
10	0.00160	4.8	5.5

Time - 72,000 seconds.
Field - 6.6 mv/cm.
Temperature - 738°C.
Diffusion Constant - 7.3×10^{-7} cm^2/sec.

D. HALL FIELD MAGNITUDE

The magnitude of the Hall potential impressed on migrating carbon and nitrogen ions was not measured directly but was determined by independent experiments on large samples. The results of these investigations are contained in Table VI. The field intensity in all cases was 18,000 oersteds, and the Hall probes were placed 1 cm. apart. The first alloy iron with 0.03% carbon represents α iron saturated with carbon. Similarly 0.1 wt.% nitrogen represents α iron saturated with nitrogen. High temperature measurements are given for alloys with higher solute concentration.

TABLE VI

HALL FIELD MEASUREMENTS ON IRON ALLOYS

Sample	Temperature °C	Current Density amps/cm^2	Hall Field mv/cm
Iron-0.03 wt.% Carbon	101	680	+0.15
	259	1020	+0.59
	434	1180	+1.60
	529	1365	+2.7
	646	1490	+4.2
	751	1610	+6.8
	794	1650	+2.2
	925	2200	+0.17

H(field intensity) - 18,000 oersteds.
t(thickness of sample) - 0.094 cm.

Iron-0.10 wt.% Nitrogen	122	710	+0.15
	268	980	+0.72
	411	1220	+1.30
	521	1350	+2.60
	647	1480	+4.30
	739	1580	+6.70
	925	1900	+0.14
Iron-0.55 wt.% Nitrogen	925	1820	+0.11
Iron-0.40 wt.% Nitrogen	925	2100	+0.14

H(field intensity) - 18,000 oersteds.
t(thickness of sample) - 0.099 cm.

E. BOUNDARY DIFFUSION RESULTS

Figures 28, 29 and 30 show the extent of migration of the $\alpha \rightarrow \gamma$ phase boundary in iron-carbon alloys over a temperature range from 750°C to 875°C. Figures 28 and 29 show a plot of the measured migration referenced to the original weld interface. They show a $\sqrt{t}$ dependence to a first order approximation, although there are consistent negative curvatures associated with long annealing times. Tabulated $\sqrt{t}$ values may be found in Appendix H. Figure 30 is a concentration profile of a typical phase boundary couple annealed in a two-phase region. Both the theoretical distribution and experimental points measured by the microhardness analytical techniques are shown. The phenomenological theory predicting the amount of migration may be found in Appendix G.

A typical migrating phase boundary is shown metallographically in Figure 31.

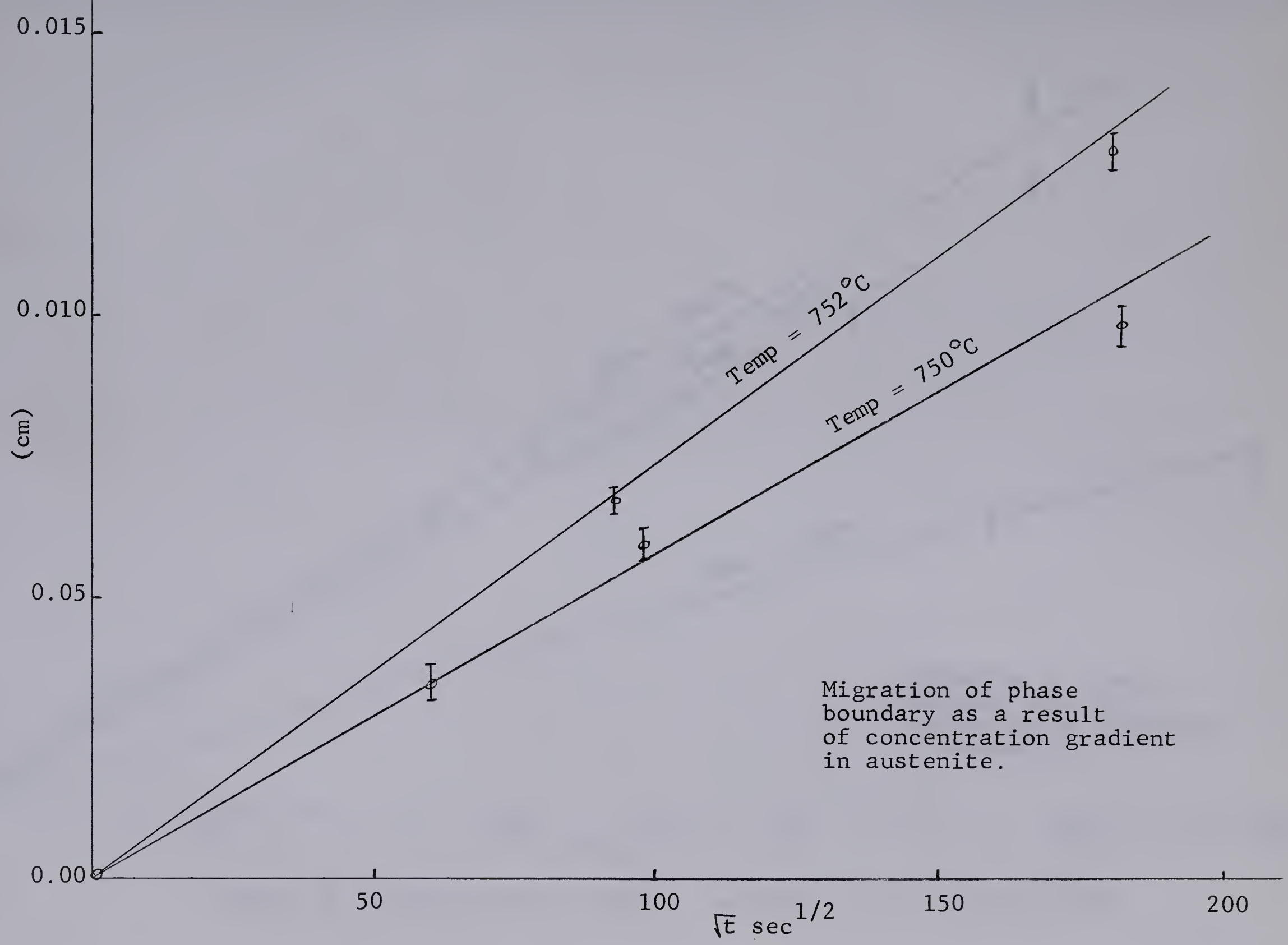

Figure 28. Penetration of Austenite phase boundary as a function of $\sqrt{t}$

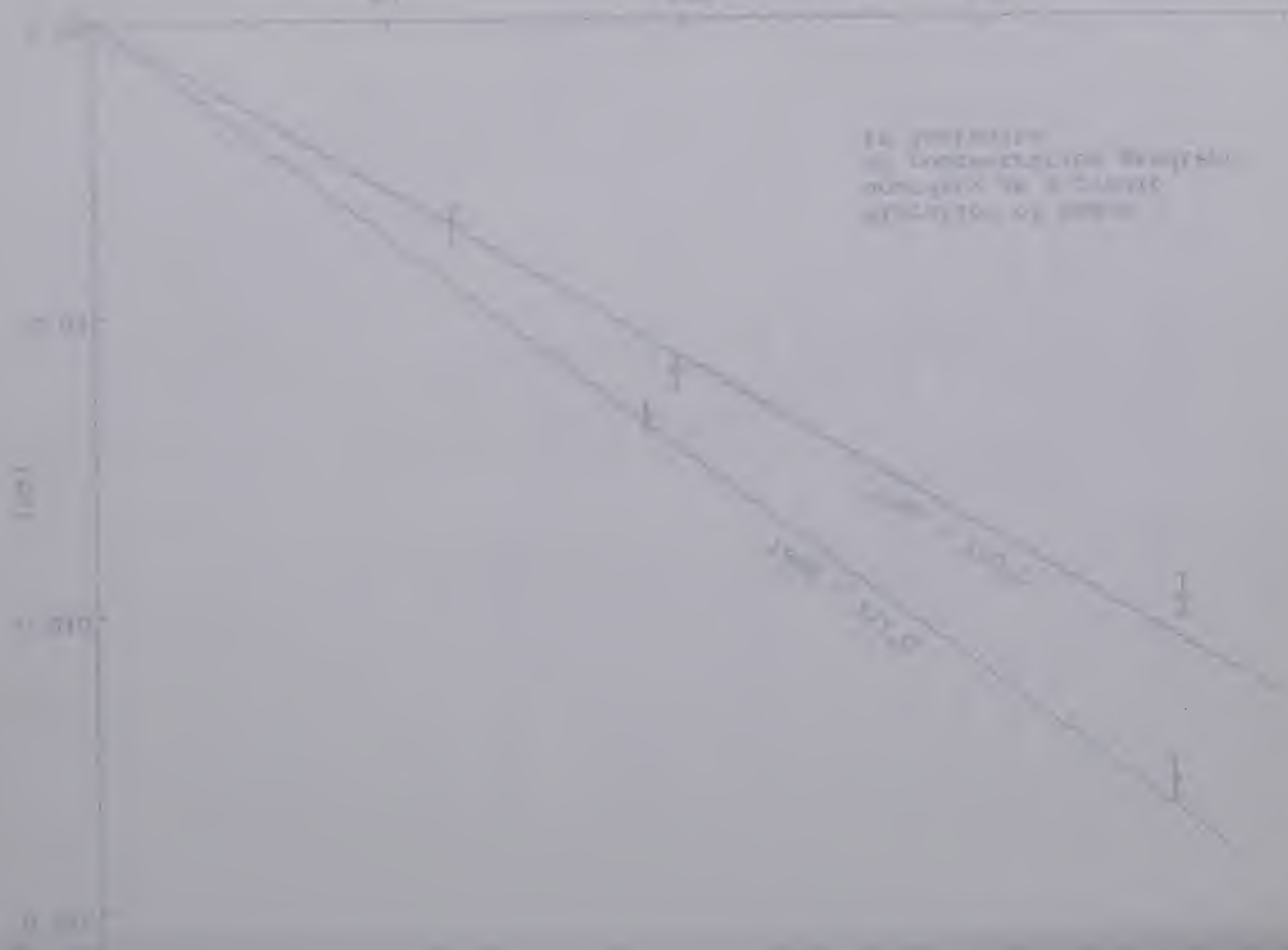

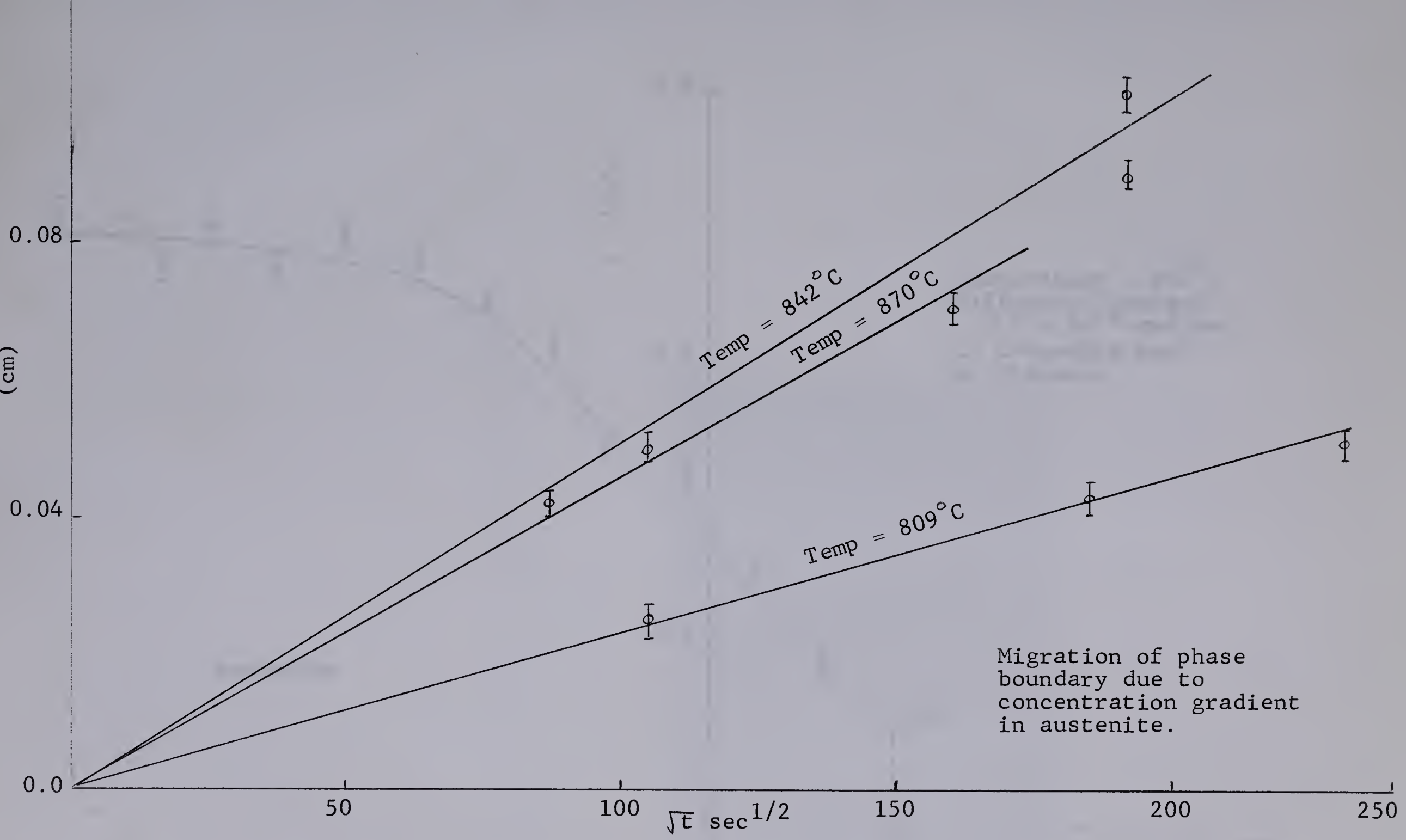

Figure 29. Penetration of Phase boundary as a function of $\sqrt{t}$.

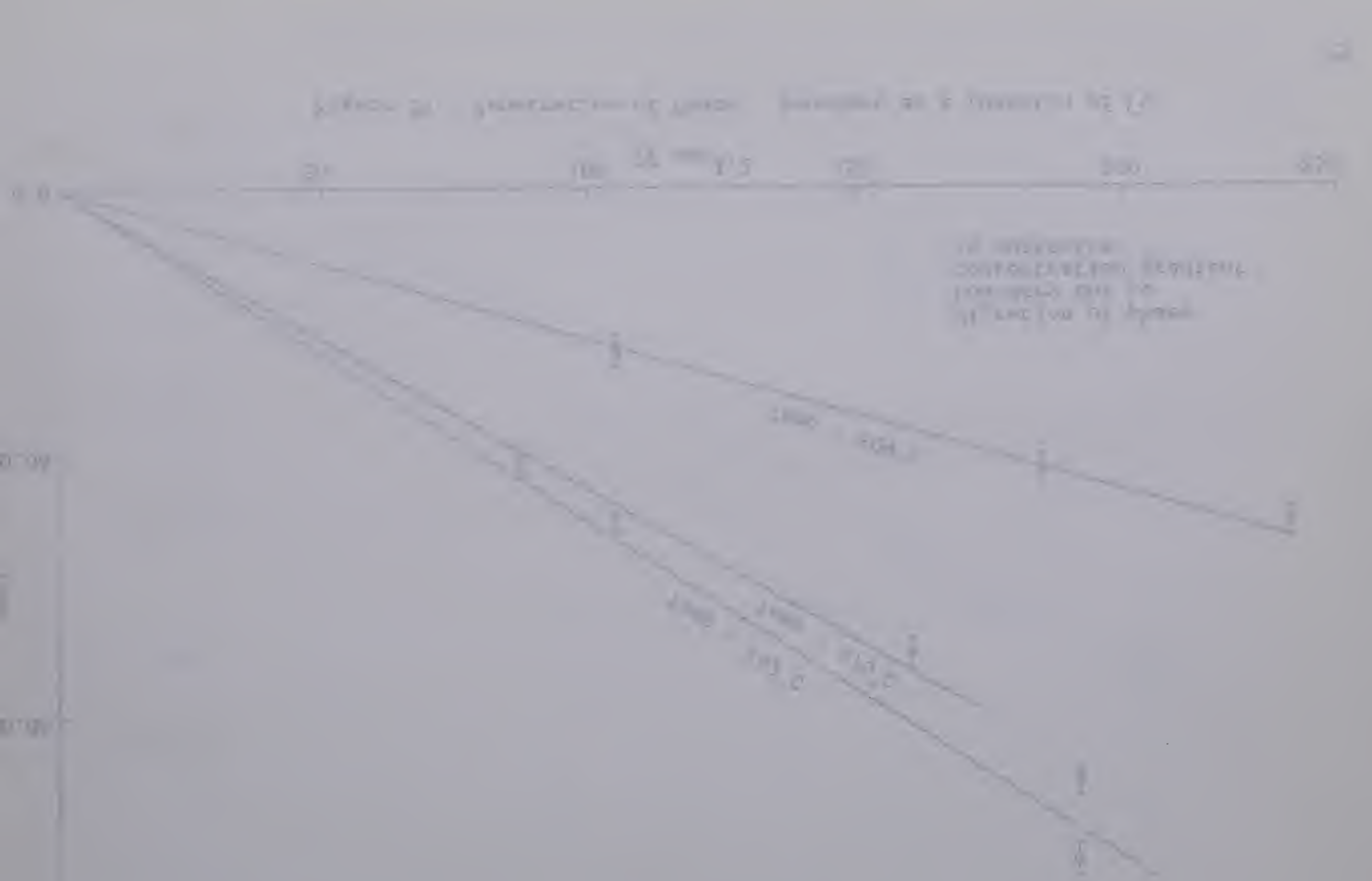

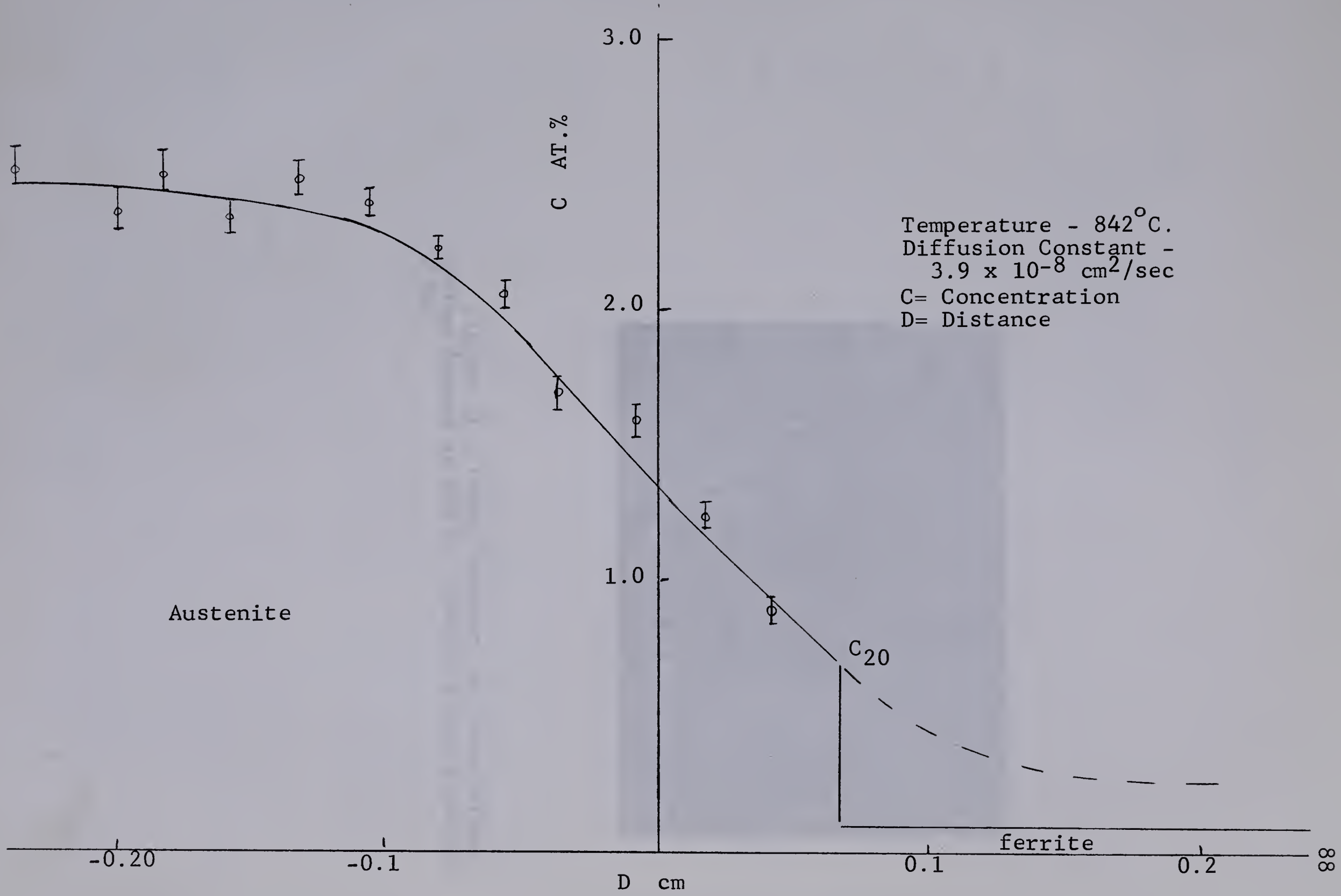

Figure 30. Concentration Profile of Diffusion Couple annealed in two-phase region.

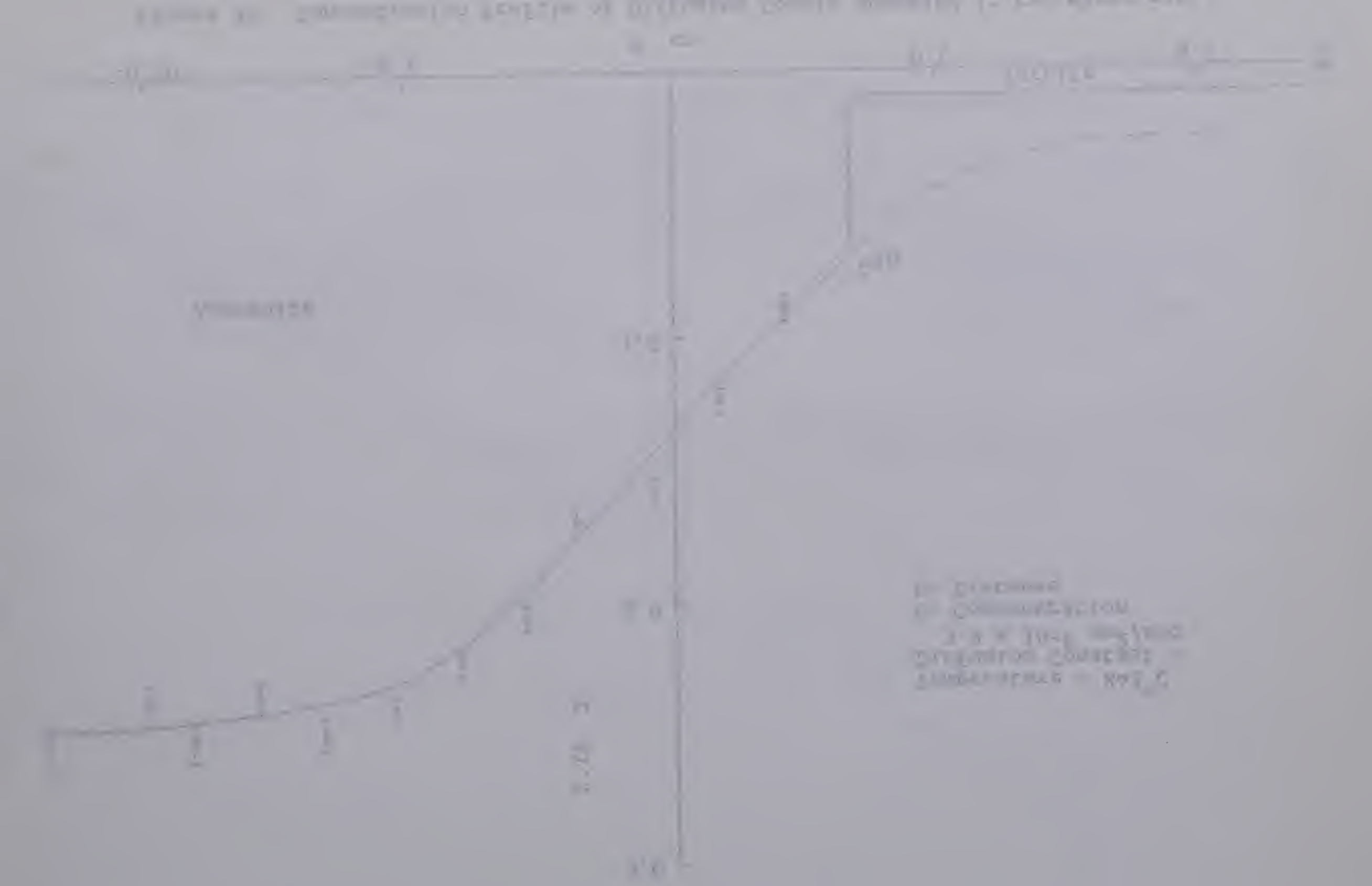

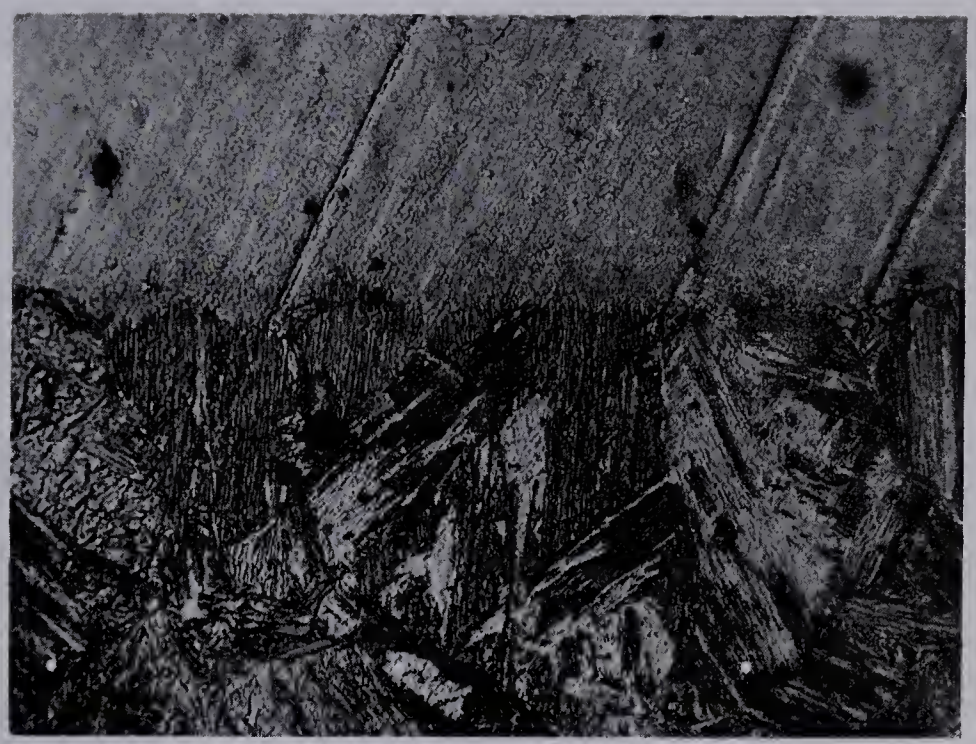

Figure 31 - Phase Boundary in Iron-Carbon system formed at 842°C. Sample water quenched x 500.

DISCUSSION

A. ERRORS

1. Direct Electrodiffusion

Experimental errors in direct electrodiffusion may be separated into two types; those associated with the diffusion coefficient introduced by an error in temperature and those associated with mobility which are incorporated through microhardness measurements and electric field strength. The errors in temperatrue and diffusion constant are estimated from a consideration of the thermocouples employed. The errors in mobility are treated statistically and are reported in terms of 90% confidence limits.

(a) Temperature

A high accuracy in temperature measurement is necessary because temperature appears both in the Einstein equation and in the exponential Arrhenius expression for the diffusion constant. The three-wire chromel-P-alumel-chromel-P thermocouple arrangement of Duwez[55] proved to be highly accurate since the balancing bridge associated with it was very sensitive. The following are some of the factors that lead to erroneous results.

(i) Inhomogeneities: appreciable errors may be introduced in the measured temperature if the thermocouple material contains large mechanical or chemical inhomogeneities. McElroy and Potts[64] have shown that annealing chromel-P wire at 400^{o}C for one-half hour produces a positive shift of about

120μ v while alumel shifts positively approximately 20μ v. This results in an error of approximately one-half degree. There are no results for higher temperatures but it is probable that an error of about the same magnitude would be present. Chemical inhomogeneities may also lead to large errors if located in temperature gradients. The temperature may be in error as much as $\pm$1.5^{o}C from this source.

(ii) Oxidation: the oxidation of chromel and alumel in vacuum and in an inert atmosphere are minimal and errors associated with oxidation are thought to be small.

(iii) Chromium depletion: large changes in the thermocouple e.m.f. can result if there is a carbon source externally available to the thermocouple. Potts and McElroy[64] attribute this to the precipitation of chromium carbide at the grain boundaries and subsequent depletion of chromium from solid solution. In the present investigation care was taken to prevent carbon contamination of the thermocouple wires. The wires were either spot welded to the copper coating separating the thermocouple from the iron-carbon region, or spot welded to the pure ferrite end of the couple, where one might expect very little carbon pick-up. It is assumed, therefore, that thermocouple errors due to carbon contamination are negligible in the present investigation.

Bennett and Rainer[65] have shown that at a very critical oxidation potential chromium could be depleted from solid solution by selective intergranular chromium oxidation.

The vacuum maintained in the present work is well outside the oxidation limits for chromium oxidation to occur.

(iv) Magnetovoltages: Loscoe and Mette[66] found that a field gives rise to extraneous magnetovoltages in portions of the wire subjected to temperature gradients. The principal voltage is due to the Nernst effect and is expressed by

$$E_y = Q_n B_z \, dT/dx,$$

where Q_n is the Nernst coefficient, B_z the magnetic induction and dT/dx a temperature gradient across the wire diameter. This effect is, however, very small causing approximately a $2\mu V/^{o}C$ positive shift at $210^{o}C$ in chromel-P wire and could not be detected in the present experiments. It is safe to assume that the error caused by the magnetic field in the temperature range considered here is less than one-half degree.

(v) Error in balancing the thermocouple bridge circuit: it is difficult to estimate the error introduced through balancing the bridge circuit associated with the three-wire thermocouple arrangement. Balancing was carried out as close to the annealing temperature as possible. Although the temperature is somewhat unsteady when the current is reversed the sensitivity of the balancing circuit near the anneal temperature is a maximum. It was found that the circuit could be balanced with special care to 0.01 mv., but would drift out of balance as much as 0.1 mv. during the experiment. The bridge balance was accordingly checked several times

during the course of the experiment and maintained within $\pm$0.02 mv. This would introduce an error of $\pm$1/2^{o}C.

(vi) Temperature control: the use of the three-wire thermocouple and bridge assembly precluded the use of temperature controllers. This is due to a small d.c. ripple component (not detected on a potentiometer) being transmitted through the circuit to the controller. Sensitive controllers will not operate with any ripple in the power source and therefore, it was necessary to use a power supply with a very sensitive current adjustment. By careful continual adjustment of the current supply the temperature remained within $\pm$2^{o}C of the anneal temperature.

(vii) Temperature variation along the couple: a temperature variation along the diffusion couple length may be expected for two reasons. First, the couple is heated by resistance heating which results in a large gradient from the center of the diffusion couple to the poles, where the temperature is effectively room temperature. To estimate the error involved as a result of this gradient, several thermocouples were placed along the sample and the gradient measured. It was found that in the central region of four-five cm., a gradient of less than 1/2^{o}C/cm. existed. The terminal pieces of the diffusion couple were subject to very steep temperature gradients. Therefore, all mobility experiments were carried out in the central region where a temperature variation of less than 1^{o}C could be expected. Secondly,

a temperature variation arises from the resistance variation corresponding to the concentration gradient in the diffusion zone. Fortunately the variation of resistance with carbon and nitrogen concentration is small i.e. less than 2% for the annealing temperatures and concentration levels used in this investigation. This results in a very small temperature gradient, less than $2^{o}C$ as indicated by weld zone temperature measurements.

Summing up all possible errors in temperature measurement from these considerations an error of $\pm 6^{o}C$ is attributed to temperature measurement. However, these errors are random and represent a considerably larger error than an error with 90% confidence limits. Based on a comparison of thermocouples and on experience $\pm 4^{o}C$ are reasonable temperature limits.

The best diffusion data available in the literature for carbon diffusion in iron are those of Mehl, Wells and Batz.[68] An error of $\pm 4^{o}C$ causes an error of $\pm 6\%$ in the diffusion constant for carbon in iron. Unfortunately, large errors might well be associated with the diffusion of nitrogen in austenite. Grieveson et al[63] report that nitrogen diffuses in austenite according to the equation

$$D_n = 0.91\, e^{-\frac{40,260}{RT}},$$

while Bramely and Turner[69] report

$$D_n = 0.107\, e^{-\frac{34,000}{RT}}.$$

Grozier and Paxton[70], from phase boundary migration experiments, concluded that

$$D_n = 0.02\, e^{-\frac{28,000}{RT}}.$$

These equations give significantly different diffusion constants. In the temperature range considered in this investigation, a difference of an order of magnitude could be obtained by using these equations. However, the equation of Grieveson was used for two reasons. First, Grieveson's results agree reasonably well with the results at lower temperatures of Fast and Verrijp.[71] Secondly, the diffusion constants determined in the present investigation indicated that there was not nearly enough diffusion to obtain the diffusion constants of either Bramely et al[69] or of Paxton et al.[70] An error of about $\pm$6% is attributed to the diffusion constants of Grieveson et al,[63] caused by an error of $\pm 4^{o}C$.

(b) Electric Field Measurement

The electric field was measured by field probes 0.008 cm. in diameter placed approximately 2 cm. apart. With the help of 30x binoculars and a micrometer capable of measuring to 0.001 cm., the distance from probe centers could be determined within $\pm$0.02 cm. Several independent observations were taken for any one field distance and the error in these observations determined. An error of $\pm$0.5% was associated with the measurement of distance between probes.

Some field variation across the diffusion zone might

be expected due to the concentration gradient. Such a gradient gives rise to a variation in the portential drop because of resistance variation with concentration. As in the case of temperature variation this can reasonably be expected to be less than ±2%. Instrument error is negligible compared to the field measurement since the Tinsley potentiometer used measures accurately to 0.005 mv. Taking into consideration the above sources of error, it was estimated that the field measurement was accurate to better than ±2.5%

(c) Errors in Microhardness Analysis

Microhardness determinations have many inherent errors associated with them. Buckle[67] has recently given a comprehensive review of the whole field of microhardness, including a full discussion of the sources of error. He frequently emphasized that comparing the hardness of two materials under similar conditions will cancel most errors to give the best results. Accordingly for analysis purposes a comparison of the indentation diameter under constant load conditions eliminates errors associated with a variation in load. If these indentations are then compared to alloy standards, errors of heat treatment, instrumental errors and errors caused by faulty preparation are reduced since they can all be standardized.

The deviation in hardness for a carbon solute content between 0.1 wt.% and 0.6 wt.% was ±0.4 indentation unit under a load of 35.5 grams. This was determined from several

readings usually 25 or more in the concentration range of interest. The deviation range increased to ±1.2 indentation units for iron containing less than 0.1 wt.% carbon. This is perhaps due to a soaking time insufficient to break up large pearlite colonies and homogenize the structure. At 0.6 wt.%, an error of 0.4 associated with the indentation diameter corresponds to a concentration variation of ±0.01 wt.%, whereas a indentation error of 1.2, in the neighborhood of 0.1 wt.%, results in an error of ±0.005 wt.% solute content. The error limits for the solute nitrogen are very similar to those for carbon. The error associated with indentations in a diffusion penetration series varies from ± 0.01 wt.% at the high concentration end of the couple to ±0.005 wt.% at the low concentration end.

Corresponding to this hardness and concentration variation is an error in the determination of the distance between the penetration curves of a sandwich diffusion couple due to the field. This in turn results in an error in mobility. For example, an error of ±0.4 diagonal unit at a hardness of 70 in Figure 22, corresponds to an error in shift distance of ±0.0025 cm. This results in an error of approximately 6%. An error of ±1.2 indentation unit at a hardness of 120 corresponds to an estimated error of ±2.5%. The calculated mobility values are significant to this degree viz. ±2.5% - 6%.

Taking into account a 6% error associated with the diffusion constant and a $\pm$6% error associated with mobility the error in charge is $\pm$12% based on 90% confidence limits.

2. Estimated Error in Hall Field Charge

From equation 55 the error in charge, determined from boundary migration experiments, is the sum of errors contained in the Hall field E_H, time t, distance x, the temperature T, the diffusion constant D_x and the equilibrium concentration C_{20} and C_{10}. The variables E_H, t, x and T are experimentally determined, treated statistically and reported in terms of 90% confidence limits. The limits of C_{20}, C_{10} and diffusion constants are considered from data in the literature.

(a) Error in E_H

For the most part in the absence of the Ettinghausen voltages, the Hall field obtained by the direct current method is usually very accurate. The main source of error arises in the measurement of specimen dimension. Micrometer measurements of specimen thickness and width allowed an accuracy of about $\pm$1/2%. This gives rise to an error of about $\pm$1% in the current density associated with the measured field. The Hall field contained an error of about $\pm$2% since the distance between the voltage probes could be measured to only 1 cm. $\pm$0.02 cm., and the spot welded leads cover a finite distance. An error of $\pm 4^{\circ}C$ in temperature was estimated which gives rise to an error of about $\pm$2% in the field since the Hall field

is very sensitive to temperature in iron. This estimate is based on observations of many readings at several temperatures. The potentiometer used measured to 0.005 mv. The temperatures of interest in this investigation are those in the neighbourhood of the curie point. In this region a total error of $\pm$4% is reasonably assigned to the Hall potential and an error of $\pm$1% assigned to the current density.

Many extraneous voltages of thermal origin can cause large errors in the measured Hall potentials, such as thermoelectric voltages. Also it is difficult to align the Hall probes perfectly, so that a small potential drop is picked up from the d.c. field. A full account of these errors may be found in Putley[59] and will not be discussed here. These errors are eliminated by reversing the current and measuring the reversed Hall probe potential drop. The magnetic field must also be reversed and two additional readings taken. The average of these four potentials eliminates all errors inherent in Hall potential measurements except that produced by the Ettinghausen effect.

The velocity of electrons due to a potential field is not always equal. The faster electrons are deflected less by the magnetic field than are slower ones which set up a transverse temperature gradient. The Ettinghausen coefficient is defined by the equation

$$\left.\frac{dT}{dy}\right)_y = PB_zI_x \ ,$$

where B_z is magnetic induction in the z direction, I_x is the

current density in the x direction, $\frac{dT}{dy}$ is the temperature gradient in the y direction, and P is the Ettinghausen coefficient. This gives rise to the Ettinghausen - Seebeck field $P\Theta$ where Θ is the thermoelectric power of the solid. This voltage cannot be separated from the Hall voltage. It is, however, generally very small in metals. Measurements in iron by Hall and Campbell[72] show a relatively small Ettinghausen coefficient in iron at 84°C. There have been no investigations at higher temperatures. Nevertheless, the temperature gradient due to the Ettinghausen voltage is no more than a small fraction of one degree and would not affect the temperature-diffusion mobility of the migrating ions. Furthermore, the voltage obtained does not interfere with the results even if it does contain an Ettinghausen contribution since it is still a voltage in the transverse direction where there is no momentum transfer effect.

The measurements made on the higher carbon and nitrogen content alloys at high temperatures were subject to more error. This was a result of the lack of stability within the power supply. At the high current densities used to obtain high temperatures (925°C), Hall fields in the order of 0.15 mv. could only be determined to $\pm$0.08 mv. By obtaining several readings in this temperature range, a probable error of $\pm$20% was calculated.**

The Hall field used in the calculation of solute charge was based on the measured Hall field multiplied by the ratio

**These results were used only for a comparison with the effective austenite charge and not in the ferrite charge calculation.

of the current density used in the mobility experiment to the current density used in the Hall field determination (see Appendix E). The error associated with this procedure involves an error of ±4% in the measured field compounded with ±1% in the current densities used. Therefore, the estimated maximum error associated with the Hall field used in the mobility calculations is ±5%.

(b) Error in Time, Temperature and Migration Distance

The experimental error incorporated in time and temperature as an independent quantity is much less than 1% and therefore negligible. Measured migration distances were treated statistically and found to contain an error of ±7% based on 90% confidence limits.

(c) Errors in C_{10}, C_{20} and D_{α}

The solubility limit of carbon in α iron was taken from the published thermodynamic data of Smith[61]. Although Smith gives no discussion of errors there is good agreement between his work and that of Stanley indicating careful work and a small error. There is about 10% difference between the two investigations; therefore the mean values may be in error as much as ±5%. However, Smith has many results in the neighborhood of 750°C i.e. the temperature of this investigation and hence an error of ±3% is not unreasonable based on 90% confidence limits. The austenite phase field limits C_{20} is taken from the investigation of Wells and Mehl[73] and again a ±3% error is not unreasonable. C_{20} does not appear independently in the charge equation but as $(C_{20} - C_{10})$. However,

$C_{20} \gg C_{10}$ and the error associated with this term is therefore the same as that associated with C_{20} i.e. $\pm$3%.

The diffusion constant data were obtained from the investigation of Smith.[61] These differ from Stanley's[60] determination by a factor of (2). However, the data of Smith were determined by a boundary method similar to the experimental condition used in the present investigation. If the data of Stanley are used, an average charge for carbon in α iron would be +2.1 instead of +4.25 calculated from Smith's diffusion constants. An error of $\pm 4^{o}C$ causes an error of $\pm$5% in the diffusion constant.

(d) Total Error.

From the statistical error treatment of the migration distance and Hall field measurements and from the judgement of the author in estimating the error involved in the diffusion constant and the concentration terms, the error in Hall field charge is $\pm$22%. This error is based on 90% confidence limits.

Nitrogen charge determinations in iron contain errors of about the same magnitude. The concentration terms were obtained from the investigation of Paranjpe et al.[62] The diffusion data were taken from Grieveson et al.[63]

Aside from a consideration of the terms in equation 55 two other sources of error must be considered. If the electric field temperature was not the same as the soaking temperature when making the diffusion couples, some natural diffusion might be expected. The temperature error associated

with this transfer is $\pm 6^{\circ}C$. A temperature error of $6^{\circ}C$ in the neighbourhood of the annealing temperature corresponds to a change in C_{20} of 0.03 wt.%. The boundary migration due to this concentration differential can be calculated as carried out in Appendix F. The results indicate that it could be a very serious error. However, by using a sandwich couple, the error cancels out if conditions on either side of the couple are identical. There is a very good chance that this is indeed so since both sides of the couple were given identical simultaneous carburizing and annealing treatments.

In calculating charge, the flux of carbon to the boundary in γ iron was neglected in equation 55 . Assuming a true charge of +4 or even +6 associated with carbon in γ iron, which corresponds to the maximum possible error, this can also be shown to be negligible (see Appendix F).

B. DIRECT FIELD ELECTROMIGRATION TECHNIQUE

The microhardness technique of determining the penetration curve used in this investigation has many advantages over conventional methods of determining solute mobility. Chemical methods were ruled out since it was necessary to use small specimens to obtain the required high current density. Even then the field effect is small compared to the relatively large chemical diffusion effect. This ruled out as well, microanalytical techniques for carbon analysis.

Some investigators have studied structural changes metallographically and estimated mobility from the observed shift in phases. This method is not very accurate and is at best qualitative. Frantsevich and co-workers[47] have effectively employed radioactive tracer techniques to obtain the small movement associated with electrodiffusion. If, however, the migrating ion exists in solid solution, the method of microhardness has the advantage that hardness or indentation diagonal does not have to be related to solute concentrations. Furthermore, one is able to make an indefinite number of traverses without loss of the sample, which permits a proper statistical analysis of the results. Metallographic examination concurrent with the hardness determinations enables a better control of couple soundness, since defects and defective welds are readily observed. Convenience is also a factor to consider as microhardness measurements are relatively easy to make. One disadvantage of this technique is that a preliminary heat treatment is necessary to standardize the structure. For instance, in this investigation, a soaking and quenching heat treatment was employed. During soaking, considerable diffusion in the diffusion zone may take place. Fortunately, this amount is small compared to the total diffusion and furthermore, cancels out in the calculations for the mobility in sandwich couples. Systems such as Cu-Al studied by Buckle[67] and by Youdelis and Colton[74] are subject to

similar heat treatment disadvantages. Even in iron-silicon which is a solid solution alloy at room temperature, the sample must be in the fully annealed condition.

C. DIRECT FIELD RESULTS

The magnitude of the "effective charge" of carbon in austenite is somewhat smaller in this investigation than that expected from the work of Kalinovich[49] and co-workers. For instance, the effective charge calculated from data by Kalinovich[49] is +8 at 1150°C, increasing to +13.4 at 950°C, while the results of this investigation indicate that the effective charge of carbon in austenite at 925°C is +8.6 $\pm$0.9 increasing to +13.5 $\pm$1.4 at 842°C. Both investigations, however, show that carbon is transferred toward the cathode with a large positive effective charge. Both investigations agree that the effective charge increases with decreasing temperature. The large positive value of charge indicates that there is a hole momentum contribution ($n_h l_h \sigma_h$ - equation 3) superimposed on the direct field force. This is consistent with the Hall measurements of Foner[58] that iron is a hole conductor at room temperature i.e. $n_h > n_e$. The concentration of carriers should not be appreciably affected by small additions of carbon to the lattice since iron contains a high density of carriers in the conduction band. This agrees well with the measurements obtained at 925°C in this investigation which show that iron containing 0.03% carbon and iron containing 4% carbon are both predominantly

hole conductors. Certainly the above results would all seem to confirm the expected behavior of carbon in an iron lattice and indicates that hole momentum transfer is increasingly dominant at lower temperatures.

On the other hand, the effective charge of nitrogen in iron is -8.1 $\pm$0.9 at 1000°C increasing to -14 $\pm$1.4 at 922°C. This indicates that the term $n_e\ l_e\ \sigma_e$ predominates in equation 3. Since the Hall measurements indicate that $n_h > n_e$, then it must be that for iron-nitrogen alloys $l_h\ \sigma_h < l_e\ \sigma_e$. The converse of this must be true in iron-carbon alloys if one adheres strictly to the Fik's model of electrodiffusion. The investigation of Frantsevich[46] on migration of iron is very significant to the present study of electromigration of carbon in iron. The work of Wever[2] indicates that in iron free of carbon, iron atoms migrate toward the cathode. However, in an alloy containing 1 wt.% carbon, Frantsevich found that those iron atoms having a carbon neighbour migrated toward the anode. This suggested that iron receives electrons from the adjoining carbon atom and becomes negatively charged with the result that the carbon atom becomes positively charged. These results were substantiated by the independent investigation of Gertsriken[75] and co-workers.

If the acceptor-donor relationship is accepted, then the substitution of nitrogen for carbon in the lattice might well change the zone structure in the neighbourhood of the impurity ion, so that while $l_h\ \sigma_h > l_e\ \sigma_e$ for iron-carbon

alloys, $l_h \sigma_h < l_e \sigma_e$ for iron-nitrogen alloys. Such a change would mean that nitrogen donates more electrons than carbon to the 3d band while carbon donates more electrons correspondingly to the 4s band.

Although the experiments conducted in this investigation were not designed to determine a diffusion mechanism change, it is not unreasonable to postulate such a possibility. Two factors contribute to diffusion mobility viz. distortion of the lattice by activated ions and an electronic contribution due to the charge distribution of the activated state of the ion. The existence of an external field could tend to polarize the internal field surrounding the carbon ion, creating accelerated diffusion migration along the field direction. Such a diffusion mechanism modification is consistent with the acceptor-donor concept. It is not too difficult to imagine a rotation mechanism enhanced by the external field whereby a positively charged carbon ion and a negatively charged iron atom exchange positions to constitute a field enhanced jump process. Such a process would result in high D values and in turn give anomalous high charges as calculated from the Einstein equation. This hypothesis could be experimentally verified by a very accurate determination of the diffusivity in the field. The diffusion constants determined in this investigation do not possess the necessary accuracy to test the hypothesis.

D. PHASE BOUNDARY TECHNIQUE

The method of migrating phase boundaries offer a convenient and sensitive method of measuring the charge of a migrating solute ion. It has the advantage that chemical analysis is unnecessary if an accurate phase diagram for the system is available from which equilibrium concentrations can be obtained. It has a further advantage in that very small fluxes such as those generated by low fields are detectible if the boundary is well defined as, for instance, in the case of iron carbon alloys. The analysis is also non-destructive making possible any desired number of measurements. Usually it is possible to make diffusion couples by equilibrating the two phases involved by annealing. These couples do not suffer from weld defects characteristic of conventional couples.

A major disadvantage of this method is that there are, in general, two flux terms controlling the boundary motion which are usually independent. The flux rates differ in the two phases as a result of different solute ion charges and diffusion constants. Diffusion constants are frequently available in the literature; however, the charge in one of the phases must still be determined independently of the other phase before the phase boundary method can be used. In the case of the solutes, carbon and nitrogen in iron, the flux term in austenite is negligible compared to the flux term in the ferrite phase and phase boundary

motion is almost exclusively electromigration in ferrite. This method can be applied only to systems whose phase boundaries are well known and where there exists a two phase region in the temperature range of interest. There must also be accurate diffusion data for the impurity ion in both phases.

Although the chemical potential of the two phases is equal and there is no driving force, there is an entropy of mixing such as that encountered in self diffusion. Thus, left for long lengths of time, the two phases should mix. As the metallography indicates in these experiments mixing was small and the boundary remained very sharp.

E. HALL FIELD RESULTS

Considering a maximum error of $\pm 22\%$ in the Hall field values, the average charge of activated carbon in iron is $+4.25 \pm 0.9$ which is significantly close to the chemical valence of carbon +4. This is also the metallic valence assigned by Pauling.[77] Similarly, the charge of $+5.9 \pm 1.2$ obtained for nitrogen in α iron suggests a charge of +5 might be associated with nitrogen in α iron. Again, it must be emphasized that this charge refers to the activated state of the ion, which may not necessarily be that of the natural ion. The charge of +4.25 for carbon in α iron is far less than Babikova's[51] value of +49 obtained for the "effective charge" of migrating ions in α iron. This can be attributed to the absence of hole momentum transfer in

these experiments.

The diffusivity of carbon and nitrogen in iron is very similar, both the activation energy and D_o. A large difference in electronic structure and ionic size is, then, not to be expected. The completely ionized size of the +4 carbon ion is 0.2A while the +5 nitrogen ion is 0.15A based on the Pauling Scheme. A large negative charge associated with nitrogen as indicated by the high "effective charge" of nitrogen in austenite would result in an ion ($-N^{-3}$ is 1.71A) of large dimension and hence much slower diffusion. There are also a number of other properties that are probably related to the charge state of the ion. For instance, Yensen,[78] found that small additions of carbon to α iron reduced the maximum permeability by some 350% when the carbon content was increased from 0.0015 wt.% to 0.008 wt.%. Similar changes were found in the hysteresis loss increasing from 505 ergs/cm^3/cycle to 1700 ergs/cm^3/cycle and in coercive force increasing from 0.17 to 0.58 oersteds. On the donor -acceptor basis, one might expect such a change in magnetic properties since donor electrons probably are accepted by the iron 3d shell. Nitrogen is found to have similar effects to that of carbon.[79]

The high charge state of carbon and nitrogen in α iron suggests a strong interaction of these solutes with the iron lattice. Since iron is not a particularly good acceptor of electrons and the energy required to ionize carbon is high

such interaction is not to be expected. However, there is only about 1 carbon atom in the lattice for every 1000 iron atoms. Thus, most carbon atoms in α iron have only iron neighbours. They have 4 near neighbours and 4 second near neighbours very close to the first near neighbours. Thus, several iron acceptors are available to the carbon donor. Also, the donor electrons are not necessarily removed entirely but only to the electron atmosphere between the carbon and iron. This would not require nearly as much energy as removing electrons entirely from carbon.

The results are consistent with other investigations. Yu Miller[32] showed that carbon in α iron was charged, as found in experiments in which C^{14} migrated toward the cathode under a Hall field. Bass and Lazarus[76] concluded that carbon is ionized in α iron from their experiments on the effect of pressure on the diffusion of carbon. They found pressure to have very little effect on the diffusion of carbon whereas, if carbon were a neutral atom, pressure should have reduced the amount of diffusion. The results of this investigation agrees with the work of Frantsevich et al[49] who found carbon to be charge to a +3.7 level in austenite. This treatment is based on direct electromigration results, and on the temperature and concentration dependence of conductivity.

Since there are facts to support the results obtained in this investigation and other facts which appear to contradict the results, further experiments are required to provide

additional information. One such experiment that might be considered for a direct measure of internal magnetic field of an atom is the Mossbauer effect, which relates to a recoilless resonance fluorescence phenomenon of the atom. The theoretical and experimental aspects of this phenomenon are considered by Frauenfelder in a comprehensive review of material up to 1962.[80] One of the consequences of a Mossbauer experiment is a measure of the magnetic field associated with the electronic configuration of the atom. For instance, Hanna et al[81] have found that the internal magnetic field in iron 57 is 331 kilooersteds. If carbon interacts with the iron nucleus on an acceptor-doner basis, the field of some iron-atoms would no doubt be modified extensively. Therefore, measuring the modified field of Fe^{57} with carbon in the lattice might give some information of the interaction.

SUGGESTIONS FOR FURTHER WORK

1. A severe limitation of the electrodiffusion Hall field technique is the very small Hall fields generated in metals. This necessitates very sensitive methods of detecting the ion's velocity and in general, makes the experimental procedure difficult. To increase the generated Hall field either the magnetic field must be increased or the current density increased. Alternatively an alloy system with a high Hall coefficient can be employed such as a semiconducting system. However the carrier density in such systems are low and direct field momentum transfer is small. Thus direct field measurements often indicate the charge state of the migrating ion. Very high magnetic fields have been generated in superconducting magnets operating at low temperature where the wire windings become superconducting. However, maintaining high temperature electrodiffusion samples in such a field would be very difficult.

The current density in the present investigation was limited by the resistive heating of the sample. It was found that the current density could be increased by a factor of about 4 times by maintaining the sample in a helium atmosphere. By immersing the sample in a molten salt bath the current density could probably be increased many times and reasonable working Hall fields established. The salt bath would also eliminate the necessity of the vacuum system used in this investigation.

2. Vacancy centers are regions of high negative charge and are instrumental in the diffusion of many alloy components. The magnitude of the mobility of vacancies is usually detected by the displacement of the matano interface i.e. the Kirkendall shift. By measuring the difference between the field and no-field Kirkendall shift some idea of the magnitude of the charge of vacancies might be obtained. Darken's analysis of interdiffusion would have to be modified to take into account the added mobility of alloy components and of the vacancies. This would probably be somewhat involved but might prove to be illuminating in the mechanism of substitutional alloy diffusion.

SUMMARY AND CONCLUSIONS

1. Microhardness measurements are shown to be an effective way of analyzing for carbon and nitrogen in iron. The method requires a standardized heat treatment to bring the alloy to a martensite condition. Microhardness sensitivity is high in the low solute concentration range and decreases at higher concentrations.

2. A method involving microhardness measurements across a diffusion zone, diffusion-annealed under an electric field, is shown to be an effective means of determining solute ion charge. Difficult analytical procedures are eliminated by this method since only the distances from the weld to points of equal microhardness in a sandwich diffusion couple are required to find the field velocity of the solute ions.

3(a) The "effective charge" of carbon in iron measured under a direct electric field of .2 $\frac{v.}{cm.}$ increases from +8.6 $\pm$0.9 at 925°C to +13.5 $\pm$1.4 at 842°C. This implies that hole momentum transfer increases with decreasing temperature.

(b) The effective charge of nitrogen in iron measured under a direct electric field increases from -8.1 at 1000°C to -14.0 at 922°C. This implies increased electron momentum transfer as the temperature decreases.

(c) Positive Hall coefficients at 925°C are found for both systems showing that both systems are hole conductors.

4. The results indicate that $l_e \sigma_e < l_h \sigma_h$ for iron-carbon alloys, whereas $l_e \sigma_e > l_h \sigma_h$ for iron-nitrogen alloys.

Alternatively, the results could be explained by postulating a field affected diffusion mechanism resulting in a field diffusivity differing from the normal diffusion constant.

5. The phenomenological diffusion theory controlling phase boundary migration by an impressed electric field is presented. It is shown that under limited circumstances the amount of migration is related to the charge of the solute ion and is very sensitive to small impressed fields (for example, Hall fields).

6. A method of designing phase boundary diffusion couples by carburizing and annealing in a two phase region is presented. This method has the advantage that no weld zone exists and couples are thus free of weld defects.

7(a) By placing a Hall field across a sandwich couple, a Hall field charge of $+4.3 \pm 0.9$ is found for carbon in α iron and $+5.9 \pm 1.3$ for nitrogen in α iron.

(b) Such measurements indicate that carbon and nitrogen migrate as highly charged ions consistant with the conclusion of Frantsevich et al[46] for carbon in γ iron.

(c) The results agree with the conclusion of Bass and Lazarus in their investigation of diffusion under high pressure.

BIBLIOGRAPHY

1. Wever, H., The Physical Chemistry of Metallic Solutions and Intermetallic Compounds, Vol. I, paper 26, 1959, London,(H.M. Stationary Office)

2. Wever, H., Z.Elektrochem., 1956, Vol. 60, p. 1170.

3. Grone, A.R., J. Phys. Chem. Solids, 1961, Vol. 20, p. 88.

4. Dayal, P. and Darken, L., Trans. AIME, 1950, Vol. 88, p. 1156.

5. Seith, W. and Daur, Th., Z. Elektrochem., 1934, Vol. 40, p. 829.

6. Jost, W., Diffusion in Solids, Liquids and Gases, 1952, Academic Press.

7. Lodding, A., Z. Naturforsch, 1955 (A), Vol. 10, p. 924.

8. Verhoeven, J., Metallurgical Reviews, 1963, Vol. 8, No. 31, p. 311.

9. Einstein, A., Ann. Physik., 1905, Vol. 17, p. 549.

10. Frenkel, J., Kinetic Theory of Solids, 1955, New York (Dover Publications).

11. Kalinovich, D.F., Soviet Physics-Solid State, 1961, Vol. 3, p. 812.

12. Kuz'menko, P.P., Ukrain., Fiz. Zhur, 1962, Vol. 17, p.117.

13. Fiks, V.B., Soviet Physics-Solid State, 1959, Vol.1, p.14.

14. Glinchuk, M.D., Ukrain., Fiz. Zhur, 1959, Vol. 4, p. 684.

15. Smolin, M.D. and Frantsevich, I.N., Soviet Physics-Solid State, 1961, Vol. 3, No. 7, p. 1536.

16. Brown, S. and Barnett, S.J., Phys. Rev., 1952, Vol. 87, p. 601.

17. Klemm, A., Z. Naturforsch, 1954 (A), Vol. 9, p. 1031.

18. Fiks, V.B., Soviet Physics-Solid State, 1964, Vol. 6, No. 8, p. 1828.

19. Mott, N.F. and Jones, H., "The Theory of the Properties of Metals and Alloys," 1936, Oxford (Clarendon Press).

20. Dekker, A.J., Solid State Physics, 1957, Englewood Cliffs,(Prentice-Hall Inc.)

21. Seitz, F., The Modern Theory of Solids, 1940, New York and London, (McGraw Hill Inc.)

22. Skaupy, F., Z. Physik Chem., 1907, Vol. 58, p. 560.

23. Schwarz, K., Elektrolytische Wanderung in flussigen und festen Metallen. Leipzig, 1940, (Johann Ambrosuis Barth)

24. Wagner, C., A. Physik Chem., 1932, B15, p.347.

25. Schwarz, K., Z. Physik Chem., 1933 (A), Vol. 165, p. 223.

26. Klemm, A., Z. Naturforsch, 1953 (A), Vol. 8, p.397.

27. Klemm, A., ibid, 1954 (A), Vol. 9, p.1031.

28. Mangelsdorf, P.C., J. Chem. Physics., 1960, Vol.33,p.1151.

29. Boltaks, B.I., Diffusion in Semiconductors, 1963, New York, (Academic Press).

30. Miller, Yu., Soviet Physics-Solid State, 1962, Vol. 3, No. 8, p. 1728.

31. Fiks, V.B., Soviet Physics-Solid State, 1963, Vol. 4, No. 7, p.1366.

32. Miller, Yu. C. and Gurov, K.P., Soviet Physics-Solid State, 1962, Vol. 3, p. 2096.

33. Van Horn, D.D., Transaction ASM, 1959, Vol. 51, p. 185.

34. Kirkaldy, J.S. and Purdy, G., Trans. AIME, 1963, Vol.227 p. 1255.

35. Grozier, J.D., Paxton, H.W. and Mullins, W.W., Trans. AIME, 1965, Vol. 233, p. 130.

36. Smith, R.P., Trans. AIME, 1962, Vol. 224, p. 105.

37. Kuz'menko, P.P. and Khar'kov, E.I., Ukrain. Fiz. Zhur, 1959, Vol. 4, p. 537.

38. Kuz'menko, P.P. and Khar'kov, E.I., Ukrain. Fiz. Zhur, 1960, Vol. 5, p. 428.

39. Seith, W. and Wever, H., Z. Elektrochem. 1963, Vol.57,p.791.

40. Claisse, F. and Koenig, H.P., Acta. Met., 1956, Vol. 4, p. 650.

41. DeBoer, J.H. and Fast, J.D., Rec. Trav. Chem., 1940, Vol. 59, p. 161.

42. Wagner, C. and Heller, G., Z. Physikal Chem., 1940 (B), Vol. 46, p. 242.

43. Seith, W. and Kubaschevski, O., Z. Elektrochem., 1935, Vol. 41, p. 551.

44. Lebedev, T.A., Mettalurgia, 1940, No. 11-12, Vol. 61

45. Dayal, P. and Darken, L.S., Trans. Indian Institute of Metals, 1956, Vol. 27, p.41.

46. Frantsevich, I.N., Kalinovich, D.F., Kovenski, I.I., Physics of Metals and Meallography, 1959, Vol. 8, No. 4, p. 93.

47. Frantsevich, I.N., Kalinovich, D.F., Kovenski, I.I., and Smolin, M.D., Soviet Physics-Solid State, 1959, Vol. 1, p.58.

48. Kalinovich, D.F., Soviet Physics-Solid State, 1961, Vol. 3, p. 812.

49. Hume-Rothery W., Journal, Iron and Steel Institute, 1957, Vol. 188, Pt. 2, p. 255.

50. Smolin, M.D. and Frantsevich, I.N., Soviet Physics-Solid State, Vol. 3, No. 7, p. 1536.

51. Babikova, Iv.F. and Gruzin, Al., Physics of Metals and Metallography, 1957, Vol. 5, Pt. 2, p. 57.

52. Seith, W. and Daur, Th., Z. Elektrochem., 1938, Vol. 44, p. 242.

53. Shewman, P.G., "Diffusion in Solids," 1963, New York, (McGraw Hill Inc.)

54. Gray, A.G., "Modern Electroplating," 1953, New York, (John Wiley).

55. Boekter, O.A. and Duwez, P., Report No. 3 to O.N.R. C.I.T., (Pasadena), March, 1962.

56. "Microhardness,- Its Theory and Practice with the Reichert Microhardness Tester," (an instruction manual issued by C. Reichert) Opt ische Werke Wien, Austria.

57. Fitzgerald, A.E. and Higginbotham, D.E., "Basic Electrical Engineering," New York, Toronto, London, (McGraw Hill).

58. Foner, S. and Pugh, E.M., Phys. Rev., Vol. 91, p. 20.

59. Putley E.H., "The Hall Effect and Related Phenomena," 1960, London (Butterworths).

60. Darken, L.S. and Gury, R.W., "Physical Chemistry of Metals," 1953, New York, Toronto, London, (McGraw Hill).

61. Smith, R.P., Trans. AIME, 1962, Vol. 224, p. 105.

62. Paranjpe, V.G., Cohen, M., Bever, M.B. and Floe, C.F., Trans. AIME, 1950, Vol. 188, p. 26.

63. Grieveson, A. and Turkdogan, E.T., Trans. AIME, 1964, Vol. 230, p. 1608.

64. Potts, J.F. and McElroy, D.L., in "Temperature, -Its Measurement and Control in Science and Industry," 1962, New York, (Reinhold Publishing Co.,)

65. Bennett, R.L. and Rainey, W.T., ibid, p. 289.

66. Loscoe, C. and Mette, H., ibid, p. 283.

67. Buckle, H., Met. Rev., 1959, Vol. 4, p. 49.

68. Wells, C., Batz, W. and Mehl, F., Trans. AIME, 1952, Vol. 188, p. 553.

69. Bramely, A. and Turner, G., Journal of Iron and Steel Inst., 1928, Vol. 17, p. 23.

70. Grozier, J.D., Paxton, H.W. and Mullins, W.W., Trans. AIME, 1965, Vol. 233, p. 130.

71. Fast, J.D. and Verrijp, M.B.,Journal of Iron and Steel Institute, 1954, Vol. 176, p. 24.

72. Hall, E.H. and Campbell, L.L., Proc. Am. Acad. Arts and Science, 1910, Vol. 46, p. 625.

73. Mehl, R.F. and Wells, C., Trans. AIME 1937, Vol. 125, p. 429.

74. Youdelis, W.V. and Colton, D., Canadian Journal of Physics, 1964, Vol. 42, p. 2217.

75. Gertsriken, S.D., Dekhtyar. I,Ya., Mikhalenkov, V.S. and Fal'chenko, V.M., Ukrain, Fiz. Zhur, 1961, Vol. 6, p. 129.

76. Bass, J. and Lazarus, D., Phys. and Chem. of Solids, Vol. 23, p. 1820.

77. Pauling, L., Journal of Amer. Chem. Soc., (1947), Vol. 69, p. 542.

78. Yensen, T.D. and Ziegler, N.A., Trans. Am. Soc. Metals, (1935), Vol. 23, p. 556.

79. Yensen, T.D., Phys. Rev., 1932, Vol. 39, p. 358.

80. Frauenfelder, H., "The Mossbauer Effect," W.A. Benjamin Inc. Publishers.

81. Hanna, S.S., Preston, R.S. and Heberle, J., from "The Mossbauer Effect," Proceedings of Second International Conference on the Mossbauer Effect, 1962 New York, (John Wiley).

APPENDIX A

ANALYSIS OF ARMCO IRON

The following analysis was obtained from Chicago Spectro Analysis Incorporated for residual impurities in Armco Iron.

	Weight %
Chromium	0.01
Copper	0.07
Manganese	0.03
Nickel	0.05
Oxygen	0.108
Phosphorus	0.010
Silicon	0.005
Sulphur	0.014

APPENDIX B

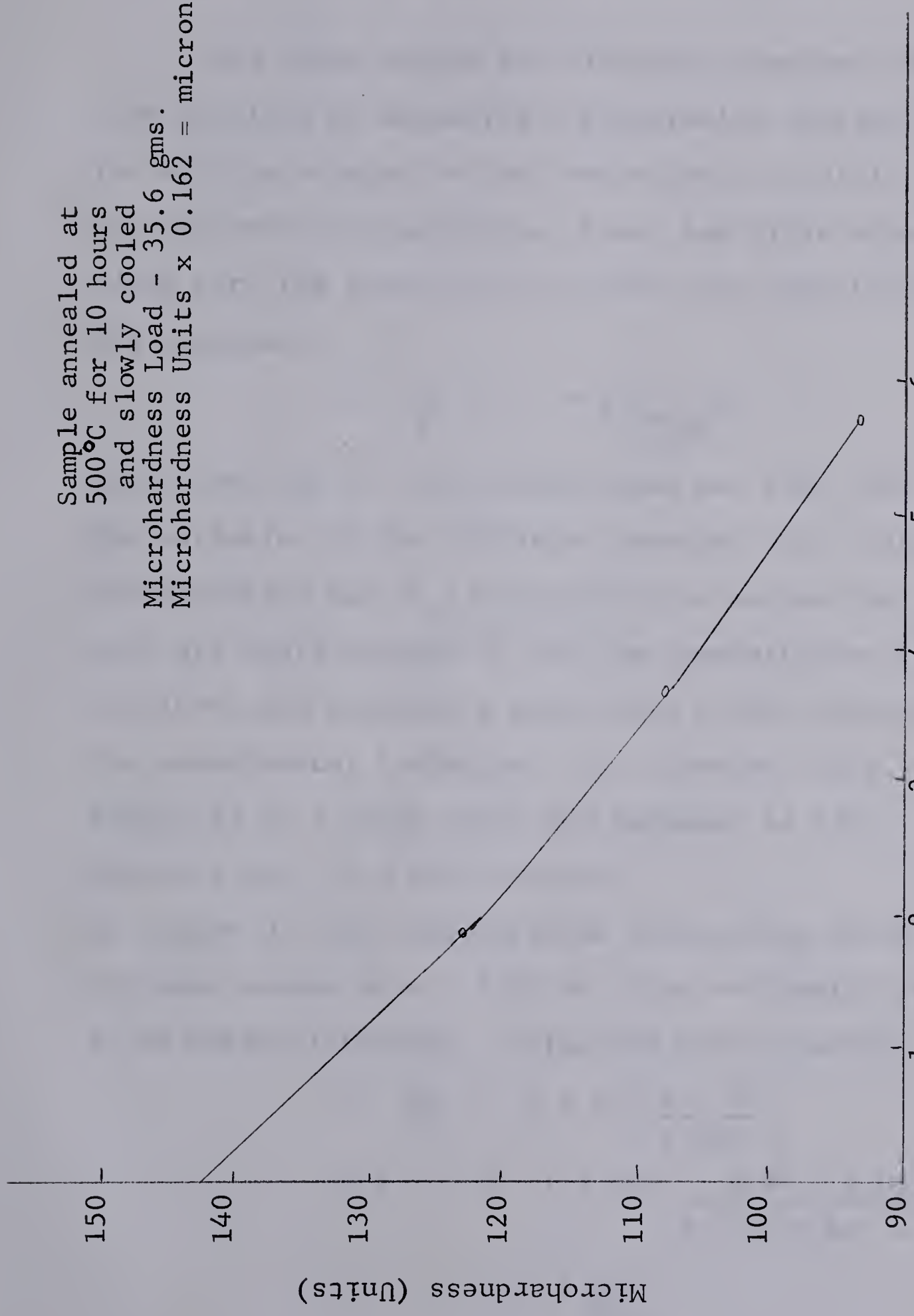

Figure 32. Effect of Silicon on Microhardness of Annealed Iron

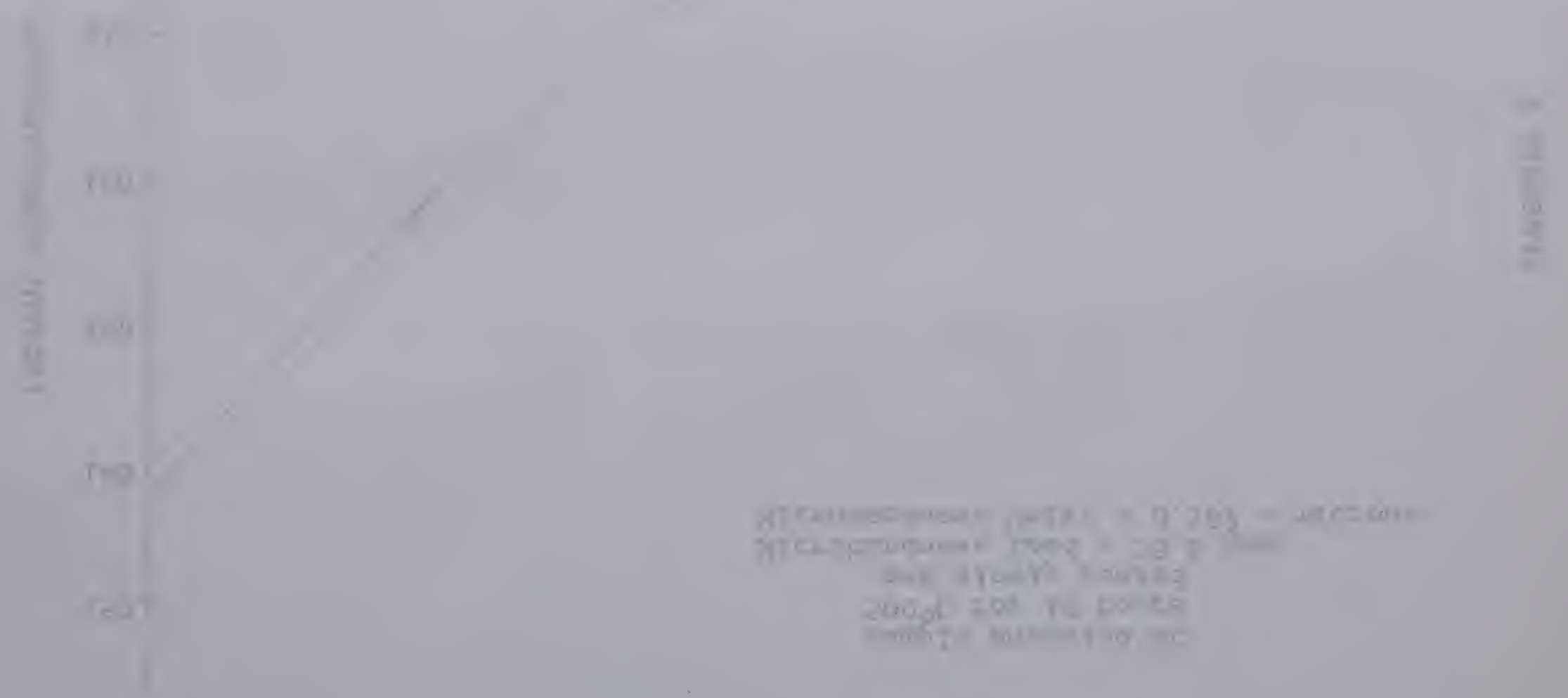

APPENDIX C

GRUBE METHOD FOR DIFFUSION CONSTANT ANALYSIS

The Grube method for diffusion constant determination consists of measuring a penetration distance from the weld to a point on the concentration profile. The concentration at that point, time, ion field velocity along with the penetration distance are substituted into the equation,

$$C = \frac{Co}{2} \left\{ 1 - \text{erf} \frac{x - vt}{2\sqrt{Dt}} \right\},$$

and solved for D. This method does not take into account the variation of the diffusion constant with solute concentration but it is reasonable to assume that errors here are small because of the low concentration range involved, and provides a good check on the accuracy of the experimental technique. To illustrate this, consider Figure 33 at a point where the hardness is 110.

Hardness 110 - 0.5 AT% nitrogen.

On Figure 33, the concentration penetration curve 0.5 AT% nitrogen occurs at x - 0.09 cm. from weld which is assumed to be Matano interface. Using the Grube equation

$$C = \frac{Co}{2} \left\{ 1 + \text{erf} \frac{x - vt}{2\sqrt{Dt}} \right\}$$

$$0.5 = 1.46 \quad 1 + \text{erf} \frac{0.09 - 0.032}{2\sqrt{(D)(1.626 \times 10^4)}}$$

$$D = 1.3 \times 10^{-7} \frac{cm^2}{sec}$$

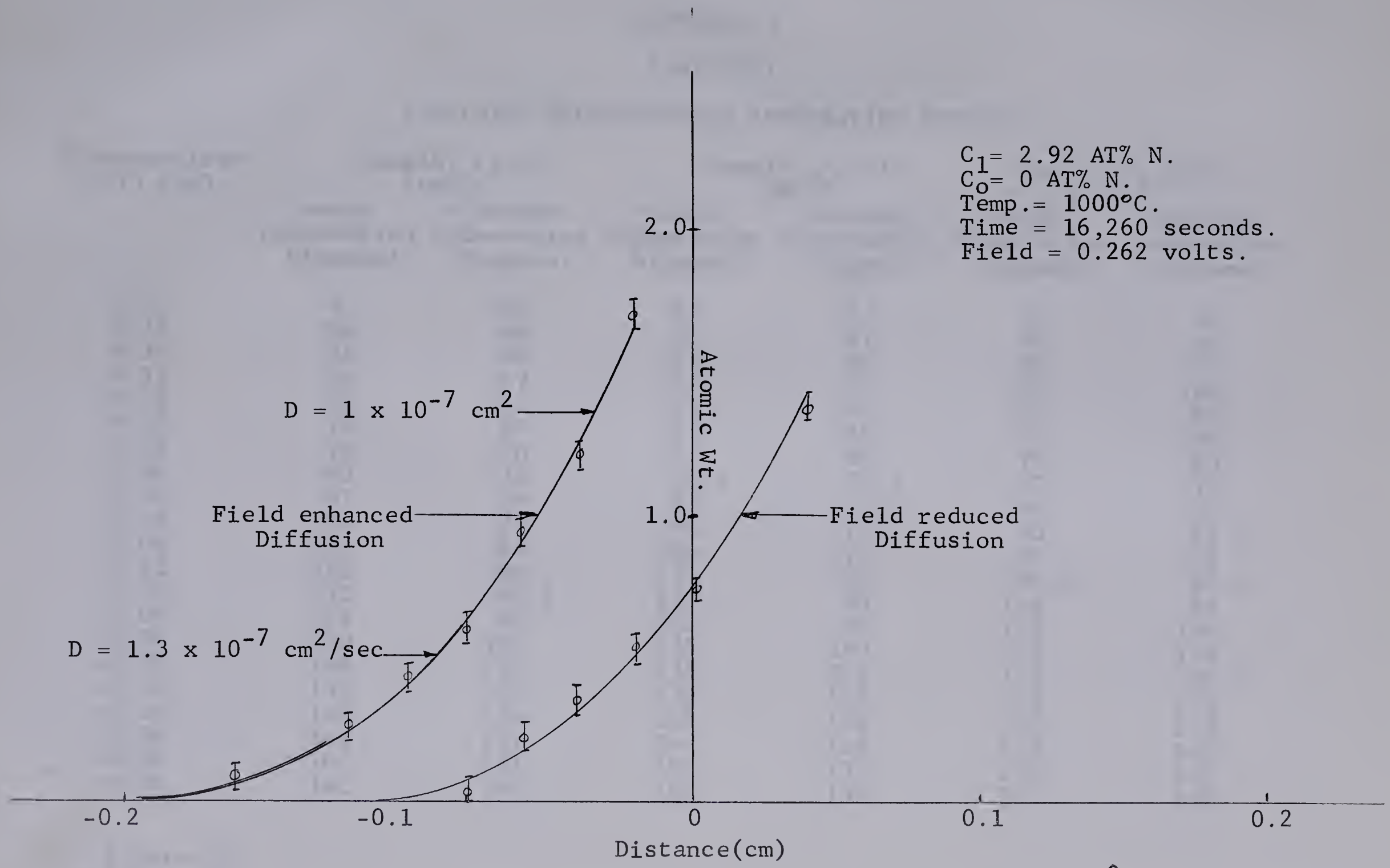

Figure 33. Nitrogen Concentration Penetration Curve (1000°C)

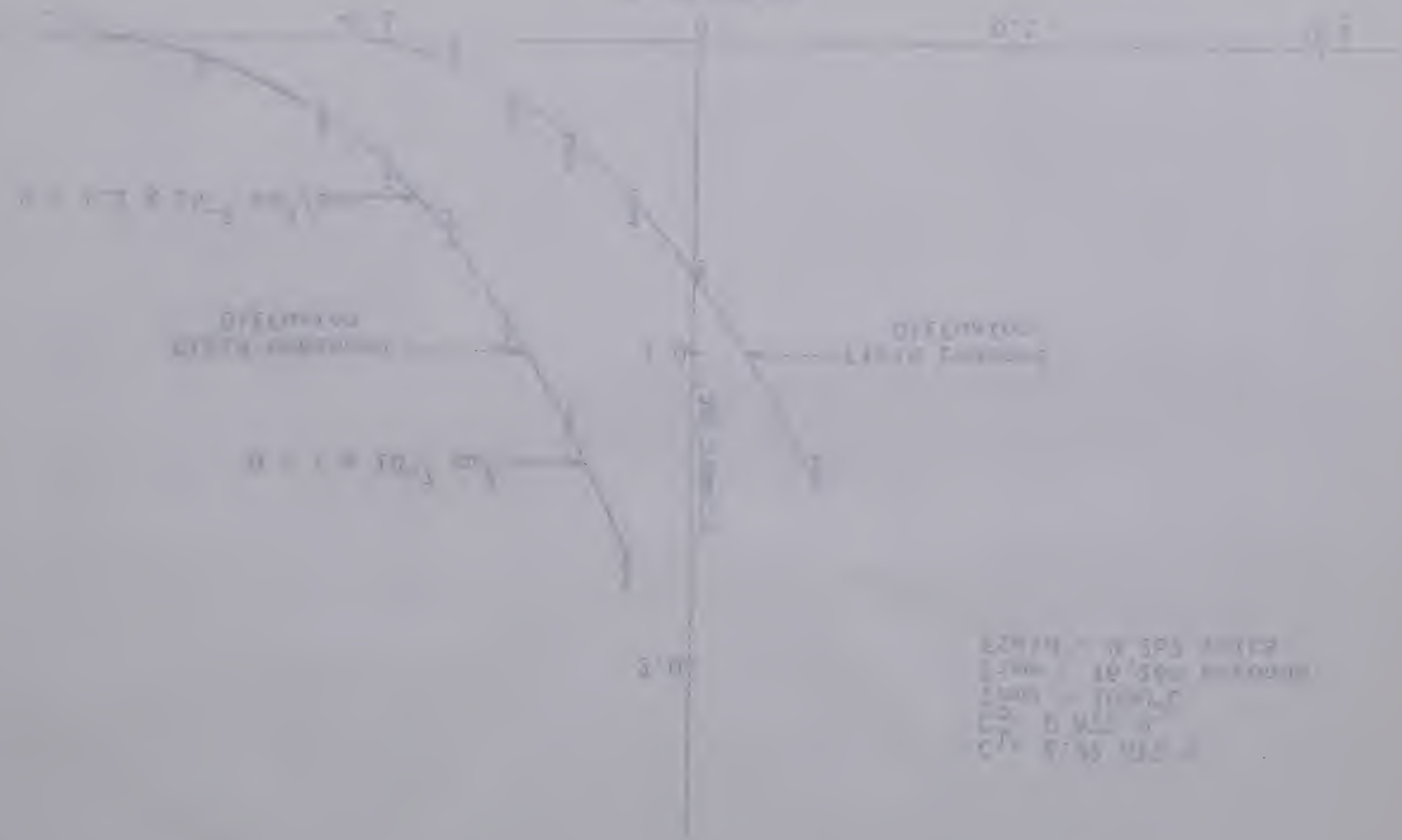

APPENDIX D

TABLE VII

TABULATED MICROHARDNESS PENETRATION RESULTS

Distance from Weld (cm)	Sample: F_e-N* 1000 °C		Sample: F_e-N** 962 °C		Sample: F_e-N*** 922 °C	
	Anode Indentation Diagonal	Cathode Indentation Diagonal	Anode Indentation Diagonal	Cathode Indentation Diagonal	Anode Indentation Diagonal	Cathode Indentation Diagonal
0.20	67	66	67	67	67	66
0.18	66	68	68	67	68	67
0.16	68	66	71	66	65	67
0.14	69	67	72	67	66	66
0.12	73	67	73	68	65	65
0.10	75	68	75	68	70	66
0.08	78	70	77	69	70	65
0.06	83	72	82.5	70.5	77	71
0.04	87	74	87	71.5	80	72
0.02	94	76	96	73.5	90	69.5
0.00	101	80	106	77	97	78
-0.02	108	84	111	82	104.5	85.5
-0.04	112	90.5	118	86	114	97
-0.06	118	96	123	92	121	104
-0.08	130	104	130	100	125	114
-0.10	136	113	135	111	137	120.5
-0.12	142	120	138	116	142	125
-0.14	142	124	139	121	142	133
-0.16	142	131	140	126	142	142
-0.18	142	131	142	131	142	142
-0.20	142	142	142	138	142	142

* Figure 20.
** Figure 21.
*** Figure 22.

TABLE VIII

TABULATED MICROHARDNESS PENETRATION RESULTS

Distance from Weld (cm)	Sample: F_e-C* 925°C		Sample: F_e-C** 902°C		Sample: F_e-C*** 842°C	
	Anode Indentation Diagonal	Cathode Indentation Diagonal	Anode Indentation Diagonal	Cathode Indentation Diagonal	Anode Indentation Diagonal	Cathode Indentation Diagonal
0.16	59	58	59	59		
0.14	60	59	58	58		
0.12	60.5	58	60	59		
0.10	62.5	58	62	58	59.5	59.5
0.08	65.5	60	64.5	59	59	59.5
0.06	68	62	67	61	62.5	59
0.04	72.5	63.5	71	63.5	65	61
0.02	77	66.5	76	66.5	68.5	64
0.00	83	70	80.5	71	74	67
-0.02	89	74	92	75.5	78.5	71.5
-0.04	110	79	128	80.5	80	77
-0.06	122	86	142	93	79	80
-0.08	133	100	142	107	80	80
-0.10	142	122	142	115		
-0.12	142	138	142	124		
-0.14	142	142	142	142		
-0.16	142	142	142	142		

* Figure 23.
** Figure 24.
*** Figure 25.

APPENDIX E

By measuring the distance a phase boundary has migrated under a Hall field the charge of the carbon and nitrogen migrating in an iron lattice is related to the boundary shift by equation 55, viz.

$$q = \left[\frac{C_{20} - C_{10}}{C_{10}}\right] \frac{xkT}{eED\ t} \quad .$$

From Table IV, Run number 1

$x = 14.7$

$D = 1.6 \times 10^{-6} \frac{cm^2}{sec}$ (Smith et al)

$T = 1026$ K

$C_{20} = 2.45$ Atomic Percent (Darken and Gurry)

$C_{10} = 0.90$ Atomic Percent (Darken and Gurry)

$t = 79{,}200$ seconds

From Table V, the Hall field is 6.8 under a current density 1610 $\frac{amps.}{cm^2}$. The current density in this experiment was 1710 $\frac{amps.}{cm^2}$.

$$E_H = 6.8 \times \frac{1710}{1610} = 7.2$$

Substituting the above quantities into the expression for charge gives $q = +3.9$.

APPENDIX F

Calculation showing that error of $\pm 6^{\circ}C$ produces negligible error in migration measurement.

From iron-carbon diagram

(1) The ΔC_{20} corresponding to $6^{\circ}C$ is 0.015 wt.% in the neighbourhood of $750^{\circ}C$.

(2) $C_{20} = 0.55$ wt.% (Darken and Gurry)

Thus at maximum

$$(C_2 - C_{20}) = 0.015 \text{ wt.\%}$$

$$\frac{C_2 - C_{20}}{C_{20} - C_0} = 0.023$$

(3) From equation 57, $\frac{\xi}{2\sqrt{Dt}} = 0.023$

(4) Considering typical experimental time of 24 hours = 8.64×10^4 seconds.

D_c $2.1 \times 10^{-9} \frac{cm^2}{sec}$ (Wells, Batz and Mehl)

$2\sqrt{Dt} = 0.027$

(5) Thus, $\frac{\xi}{2\sqrt{Dt}} = 0.023 = \frac{\xi}{0.027}$

$= 6 \times 10^{-4}$ cm.

The migration due to the field was 18×10^{-4} cm. This constitutes an appreciable amount of the migration but cancels out in the migration measurement since the couple is a sandwich couple and approximately the same amount of diffusional migration will appear on either side of the couple. Subtracting the two distances eliminates that

migration due to chemical diffusion.

(b) Error Introduced by Neglecting the Austenite Boundary Flux

If nitrogen in γ iron had, say, a maximum charge of +7, the velocity

$$v = 4 \times 10^{-10} \frac{cm}{sec}$$

obtained by the Einstein equation, would result in a movement

$$C_{20}x = C_{20}vt$$

$$x = (4 \times 10^{-10})(8.64 \times 10^{4})$$

$$x = 34 \times 10^{-6} \text{ cm.}$$

However, the boundary actually moved 18×10^{-4} cm.

$$\% \text{error} = \frac{34}{18} \sim 2\%.$$

Thus, the error introduced by neglecting the γ flux is negligible.

APPENDIX G

PHASE BOUNDARY DIFFUSION

Consider an iron-carbon alloy diffusion couple with the composition relationships shown in the phase and profile diagrams below.

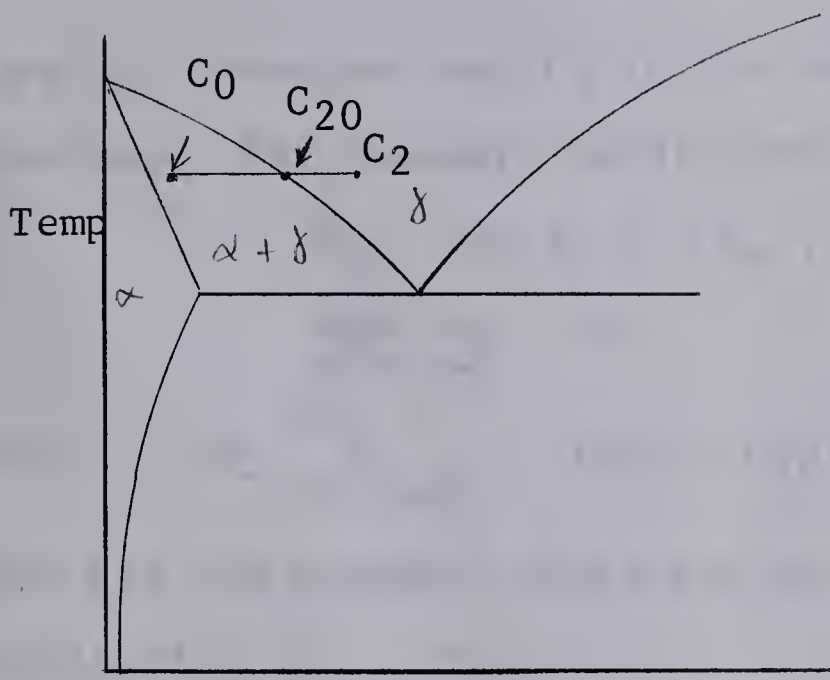

Figure 34(a) Iron-carbon Phase Diagram

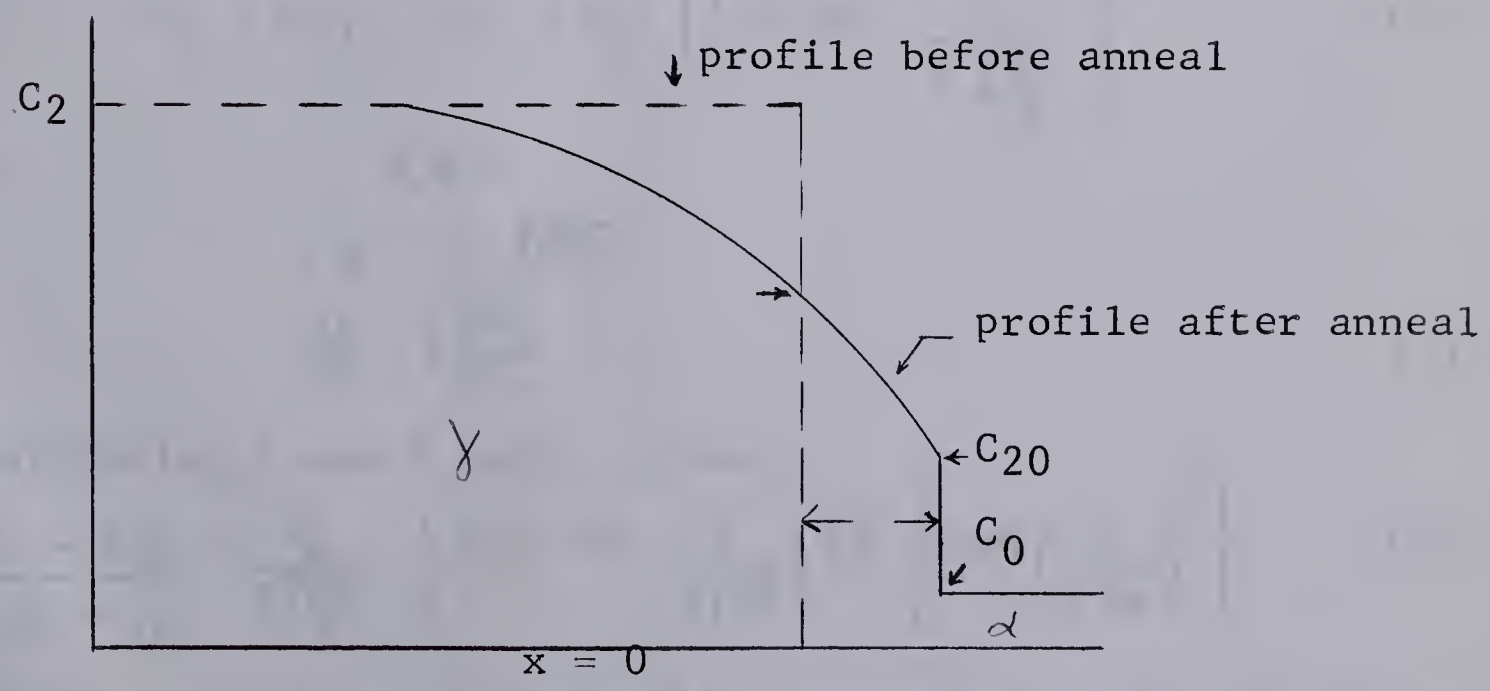

Figure 34(b) Concentration Profile of Iron-Carbon alloy annealed in two phase region

If the distance $= k\sqrt{t}$ (determined experimentally), then the single phase composition curve can be considered to be the same as that for a diffusion couple of infinte extent. The composition is given by

$$C = k_2 - (C_2 - k_2) \operatorname{erf} \frac{x}{\sqrt{4D_2 t}} , \qquad (1)$$

where k_2 = constant and C_2 is the concentration at the weld interface. The boundary conditions are

$$C_2 = C_{20} \text{ at } x = x_o ,$$

$$\lim_{x \to -\infty} c_2 = C_2 ,$$

also
$$-D_2 \frac{\partial c_2}{\partial x}_{x=\xi} = (C_{20} - C_{10}) \frac{d\xi}{dt} , \qquad (2)$$

where ξ is the boundary migration distance.

Substituting no. 1 into no. 2

$$-D_2 \; -(c_2 - k_2) \frac{2}{\sqrt{\pi}} \left[\exp - \left(\frac{\xi}{2\sqrt{D_2 t}} \right)^2 \right] \frac{1}{2\sqrt{D_2 t}} = (C_{20} - C_{10}) \frac{d\xi}{dt} \qquad (3)$$

$$C_{20} = k_2 - (c_2 - k_2) \operatorname{erf} \frac{\xi}{2\sqrt{Dt}}$$

$$C_2 - C_{20} = (c_2 - k_2) \left[1 + \operatorname{erf} \frac{\xi}{2\sqrt{D_2 t}} \right] \qquad (4)$$

but
$$\xi \propto t$$

$$\xi = 2\gamma\sqrt{D_2 t}$$

$$\frac{d\xi}{dt} = \gamma \sqrt{\frac{D_2}{t}} \qquad (5)$$

Substituting 4 and 5 into 3 gives:

$$\frac{c_2 - C_{20}}{C_{20} - C_{10}} = \frac{\xi}{2\sqrt{D_2 t}} \left[1 + \operatorname{erf} \frac{\xi}{2\sqrt{Dt}} \right] \sqrt{\pi} \left[\exp \left(\frac{\xi}{2\,Dt} \right)^2 \right], \qquad (6)$$

where the migration distance ξ is determined metallographically and the concentration terms are obtained from the phase

diagram. From equation 6, the diffusion constant may be calculated or alternatively, from a knowledge of the diffusion constant, the boundary shift can be determined.

APPENDIX H

TABLE IX

DIFFUSION PHASE BOUNDARY MIGRATION DISTANCES

Run	Temperature	Time(secs)	$\sqrt{t}$	Boundary Migration(cm.)
#1B	750°C		0	0.0000
		3600	60	0.0034
		9540	97.5	0.0060
		33180	182	0.0097
#2B	752°C	0.00	0	0.0000
		9540	97.5	0.0095
		33180	182	0.0156
#3B	809°C	0	0	0
		10800	104	0.0240
		36000	189	0.0430
		54000	232	0.0540
#4B	842°C	0	0	0
		11040	105	0.0498
		36540	191	0.0950
#5B	870°C	0	0	0
		7320	85.5	0.043
		25440	160	0.072